UNIVERSITY OF CALIFORNIA
RIVERSIDE

Thermal Conductivity Enhancement of High Temperature Phase Change Materials for Concentrating Solar Power Plant Applications

A Dissertation submitted in partial satisfaction
of the requirements for the degree of

Doctor of Philosophy

in

Mechanical Engineering

by

Melina N. Roshandell

June 2013

Dissertation Committee:

Professor Reza Abbaschian, Chairperson
Professor Cengiz Ozkan
Professor Javier Garay

The Dissertation of Melina N. Roshandell is approved:

Committee Chairperson

University of California, Riverside

Acknowledgements

This dissertation would not have been possible without the help of so many people in so many ways. I would like to express my deep appreciation and gratitude to my advisor, Prof. Abbaschian for the patient guidance and mentorship he provided to me over the course of my research. His intellectual heft is matched only by his genuinely good nature and down-to earth humility, and I am truly fortunate to have had the opportunity to work with him.

I would also like to thank my committee members, Prof. Ozkan, and Prof. Garay for all the enlightening and instructive discussions throughout the course of my research and for carefully reading my thesis and examining my results.

Additionally, I would like to thank Anoop Mathur and Rajan Kasetty from Terrafore Company, who let me to be a part of their experimental team and financially supported my research. I would like to thank Prof. Garay again for letting me use his lab to conduct some of my experiments.

I would like to thank all my friends and colleagues, specially Shaahin Amini, and Haamun Kalaantari, and Sam Pournazeri, who as good friends were always willing to help. It would have been a lonely Lab without you.

I would like to acknowledge the mechanical engineering department staff, Eilene Montoya, Roseanna Barron-Lopez, Katie Dell, Sarah Nosce, Paul Talavera, Becki Jo Ray, and Terry Traver for their help and support through these years.

I also like to thank my parents Akram and Fareed, my sisters Melika and Mobina, and other family members Nahid, Cyrus, Amirhossein, and Saeed for their support, encouragement, and understanding.

Finally, I would like to thank my husband, Ali Zand, for his immeasurable sacrifices and support while I pursued this final degree.

Dedicated to

Earth and its future residents

ABSTRACT OF THE DISSERTATION

Thermal Conductivity Enhancement of High Temperature Phase Change Materials for Concentrating Solar Power Plant Applications

by

Melina N. Roshandell

Doctor of Philosophy, Graduate Program in Mechanical Engineering
University of California, Riverside, June 2013
Professor Reza Abbaschian, Chairperson

Phase change materials (PCMs) can be used in latent heat storage systems to store or release heat by going through phase transformation. In the present work, an in-depth survey of PCMs thermal properties are investigated. It was concluded that Alkali nitrate salts are suitable PCM candidates for the medium temperature heat storages because of their moderate latent heat of fusion (100-300 KJ/Kg), low cost, and good phase-change properties such as no-phase segregation and supercooling. However similar to most other PCM candidates, Alkali nitrate salts exhibit very low thermal conductivity (<1 W/K.m), which limits their use, unless their effective thermal conductivities are enhanced.

In this research, first thermal conductivities of potassium nitrate and sodium nitrate were measured in the temperature range of 25-400°C, using transient hot wire method. It was found the thermal conductivities of potassium and sodium

nitrate to be 0.62 W/K.m, and 0.57 W/K.m at 25°C, respectively. In addition, it was observed that thermal conductivity of sodium nitrate is approximately constant in the temperature range of 25-400°C while that of potassium nitrate decreases with an increase of temperature beyond 140°C. A DSC analysis indicated that this decrease is because of the orthorhombic to rhombohedral crystal transformation of potassium nitrate at 140°C.

To improve the thermal conductivities of potassium and sodium nitrate, PCM composites consisting of aluminum and copper foams and the salts were prepared and investigated. The effective thermal conductivities of aluminum-PCM composites were found to be in the range of 1.7-7.2 W/K.m while the effective thermal conductivities of copper-PCM composites were in the range of 6.3- 19.5 W/K.m. The measurements of effective thermal conductivity of the composite at molten state exhibited no changes for Al- $NaNO_3$ and Cu- $NaNO_3$ composites. However those of Al- KNO_3 and Cu- KNO_3 decreased by about 25%.

The effect of graphite flakes on aluminum-PCM and copper-PCM composites was studied to further increase their conductivities as well as improving their latent heat storage capacities. The effective thermal conductivities of Al-PCM-C composites were found to be in the range of 3.1-13.3 W/K.m while the effective thermal conductivities of Cu-PCM-C were measured to be in the range of 11.9-78.1W/K.m.

Contents

List of Figure

List of Tables

Chapter 1

Introduction

The development of clean and renewable energy technologies and their rapid implementations (e.g; solar, wind, biofuel, and geothermal) are in the rise because of the limited resources of fossil fuels and global warming affects. Recent advances on deployment of solar energy to generate electricity shows potential for the lower cost and cleaner source of energy. Different types of solar power plants have been designed and developed around the world. Among the concentrating solar power plants (CSPP) are Solar Two in California and GemaSolar in Spain [1]. In these power plants, vast fields of collector mirrors, Figure.1.1, focus and send solar radiation to a receiver tower. In the receiver tower, the collected solar radiation heats up the heat transfer fluid (HTF) which would carry the heat to thermal energy storage (TES). Then a secondary HTF would transfer the heat from the heat storage to heat exchanger in energy conversion device to generate electricity.

Fig. 1.1. GemaSolar power plants near Seville Spain [2].

Figure 1.2 presents a concentrating solar power plants proposed by Anoop et al.. [3] to supply heat to a boiler for brayton turbine. In this plant, focused solar radiation heats up the heat transfer fluid (Hitec salt) in a central receiver tower to 1050°F (565°C), then the heat transfer fluid goes through a heat exchanger and heats up the PCM to 1025°F (551°C) and stores heat by melting the PCM. The stored heat is then released by the solidification of PCM and transferred to a secondary heat exchanger used to generate a high temperature (537°C) steam for the steam turbine to generate electricity.

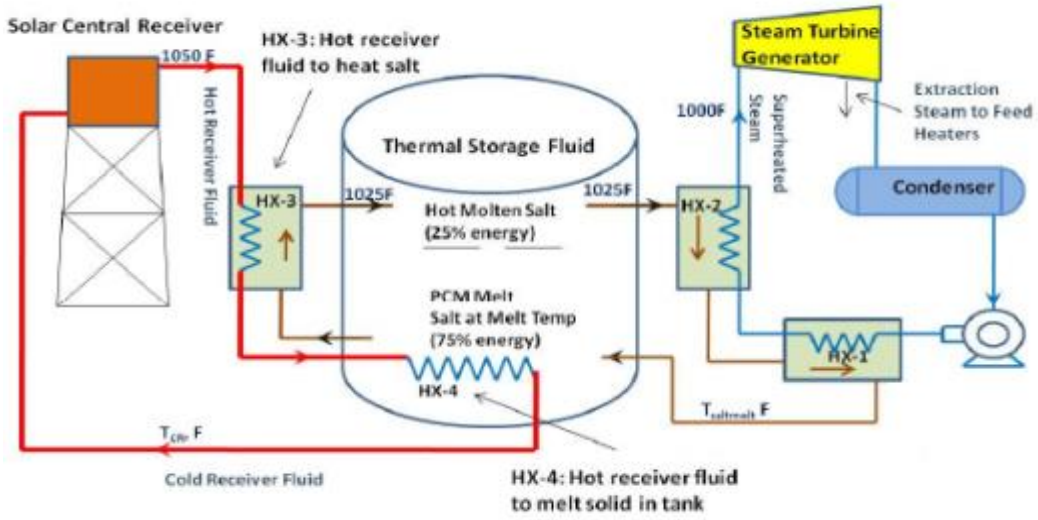

Fig. 1.2. Solar power plant operation [3].

Use of thermal storage in concentrating solar power plants is necessary to store the solar energy for night and cloudy days that sunshine is not available. A survey by Baylin et al.. [4] indicated that storing solar energy in the form of heat is more desirable because of ease of harvesting and reduction of cost compared to electrical storages.

Mills [1] reported that one of the main approaches to achieve a cost effective and efficient solar thermal electricity generator is a medium- to high-temperature (T>300°C) heat storage that can operate almost continuously at high temperatures. Furthermore, he divided the heat storage modes into two categories of medium temperature (300-500°C) heat storages that can operate with Stirling engines at 42% efficiency and lower temperature Brayton micro-turbines at 25-33% efficiency, and high temperature (500-900°C) heat storages

that can operate with larger Brayton turbines at 40% efficiency. Consequently, the qualified PCMs for concentrating solar power plants applications have to have a melting temperature of 300°C or higher to be able to provide enough heat for Stirling or Bryton turbines.

In last couple of decades, solar energy has been recognized as a great source of renewable energy and caused much attention and research to be drawn into design and development of high-temperature heat storages that can be used as heat sources for steam turbines. Mainly three approaches have been considered for solar thermal energy storages. These are thermo-chemical heat storages, sensible heat storage and latent heat storage [4].

Thermo-Chemical Energy Storage:

When a chemical reaction takes places, there is a difference between the enthalpy of the substances present at the end of the reaction and the enthalpy of the substances at the start of the reaction. This enthalpy difference is known as the heat of reaction. If the reaction is endothermic, it will absorb heat when reaction takes place; if the reaction is exothermic, it will release heat. Therefore, a chemical reaction with high heat of reaction can be used for thermal energy storage if the products of the reaction can be stored and if the heat stored during the reaction can be released when the reverse reaction takes place.

Even though this method sounds promising, currently there is no thermo-chemical thermal storage that has been commercialized. Moreover, according to Sharma [5], there are many chemical processes such as hydration/dehydration of materials or adsorption/desorption of gases that can be used as a possible thermo chemical energy storing, but there are not sufficient studies to predict the long-term reversibility of these reactions.

Sensible Heat Storage

Sensible heat storage (SHS) system utilizes the heat by the change in temperature of the material during the process of charging and discharging. As such, thermal energy is stored by raising the temperature of a solid or liquid. The amount of heat stored depends on the specific heat of the medium, the temperature change and the amount of storage material, shown in equation 1.1.

$$Q = \int_{T_i}^{T_m} mC_p dT = mC_p (T_f - T_i) \qquad (1.1)$$

where Q is the amount of stored heat, m is the mass of heat storage material, C_p is specific heat of storage material, T_f is final temperature, and T_i is initial temperature.

Sensible heat storage is often used with solids like stone or brick, or liquids such as water, as storage material. Gases have very low volumetric heat capacity and therefore are not good candidates for sensible heat storage [6]. The specific heat of some selected solid and liquid materials is shown in Table 1.1. Among the

presented materials, water appears to be the best SHS liquid available for temperatures below 100° C, because it is inexpensive and has a high specific heat. However for higher temperature application, oils, molten salts and liquid metals are better candidates because of their higher melting and boiling temperatures compared to water.

Table 1.1. A list of selected solid and liquid materials for sensible heat storage [5].

Material	Operating Temperature Range (°C)	Density (Kg/m3)	Specific Heat (KJ/Kg)
Brick	--	1600	840
Rock	--	2560	874
Concrete	--	1900-2300	880
Engine Oil	Up to 160	888	1880
Isopentanol	Up to 148	831	2200
Ethanol	Up to 78	790	2400
Buthanol	Up to 118	809	2400
Octane	Up to 126	704	2400
Proponal	Up to 97	800	2500
Isotunaol	Up to 100	808	3000
Water	0-100	1000	4190

Latent Heat storage

The solid-liquid phase change or melting and solidification can store large amounts of heat. During melting, while heat is being transferred to the storage material, the material still keeps its temperature constant at the melting temperature, also called the phase change temperature as shown in Figure 1.3.

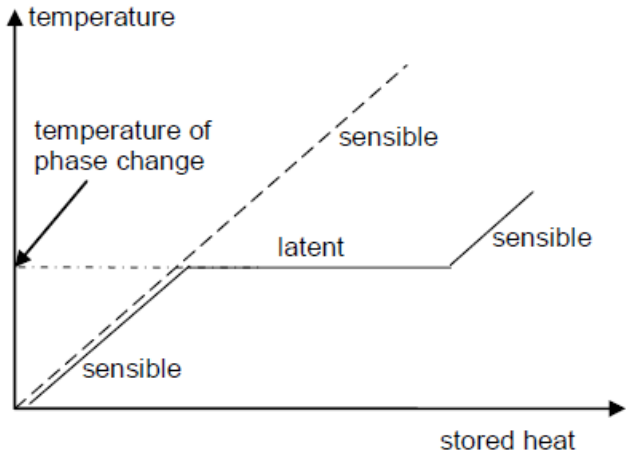

Fig. 1.3. Heat storage as latent heat for the case of solid-liquid phase change [6].

If the melting is completed, further transfer of heat results again in sensible heat storage. The storage of the heat of melting cannot be detected from the temperature, because the melting proceeds at a constant temperature. The heat supplied upon melting is therefore called latent heat and the process is called latent heat storage [5].

Materials with a solid-liquid phase change, which are suitable for heat storage, are commonly referred to as latent heat storage material or simply phase change material (PCM). The latent heat stored during the phase change process, is then calculated from the enthalpy difference Δh between the solid and the liquid phase. In the case of solid-liquid phase change, it is called melting enthalpy Δh_m or heat of fusion, as seen in equation 1.2.

$$Q = m a_m \Delta h_m \qquad (1.2)$$

where Q is the amount of stored heat, m is mass of heat storage medium; a_m is melted fraction, and Δh_m is heat of fusion per unit mass.

PCMs are able to store large amounts of heat or cold at comparatively small temperature change. A summary by Hauer [7] compares the energy storage densities achieved with different methods is presented in Table1.2.

Table 1.2. Comparison of Typical Storage Densities of Different Energy Storage Methods

Storage Method	Material	MJ/m3	KJ/Kg
SHS	Granite	50	17
	Water	84	84
LHS	Water	306	330
	Paraffins	180	200
	Hydrate salts	300	200
	Alkali Salts	600-1500	300-700
Battery	Zinc/Manganese oxide battery	--	180
	Lead Battery	--	70-180

As presented in Table 1.2. PCM can store about 3 to 4 times more heat per volume than is stored as sensible heat in solids or liquids in a temperature interval of 20 °C. Because currently a big part of the energy is delivered to the end user as electricity, a comparison with the storage of electrical energy was also presented. Batteries show smaller or comparable storage densities as in latent heat storage. Therefore, latent heat storages seem to be better method to store heat compared to sensible and electrical storages, because they can store more

energy per unit weight and volume. Another additional benefit of latent heat storages for concentrating solar power plant application is their constant operating temperature, which can supply energy at constant rate to a turbine running at optimal efficiency [8].

The efficiency of latent heat storages mainly depends on PCMs thermal properties, such as latent heat and thermal conductivity. As shown in equation 1.2 the amount of latent of PCM has direct effect on the heat storage capacity. Furthermore, the thermal conductivity of PCMs plays an important role in charging and discharging cycle time and efficiency of the latent heat storage. In most of latent heat storages, the PCMs are stored in large shell and tube heat exchangers as a bulk material, therefore sufficient thermal conductivity is required to transfer heat in and out of PCMs.

A suitable phase change temperature and significant latent heat are two obvious requirements for phase-change material. However, there are other requirements based on the PCM applications. These requirements are summarized from several literature surveys on concentrating solar power plants presented by Hoshi [9], Mills [1], Anoop [3], and others [5-11] which can be listed as:

- Melting temperature range of (300-500°C) to provide sufficient heat for high temperature Stirling engines which operates at 42% efficiency.

- High latent heat that leads to higher heat capacity therefore decreases the storage size. The latent heat for most common PCMs used for CSPP are in the range of (100-300 KJ/Kg).

- Good thermal conductivity to store or release the latent heat in a given volume of the storage material in a short time.
- No supercooling to assure that melting and solidification can proceed in a narrow temperature range. Supercooling is the effect that a temperature significantly below the melting temperature has to be reached, until a material begins to solidify and release heat. If that temperature is not reached, the PCM will not solidify at all and only sensible heat will be stored. Also when nucleation starts in suppercooled fluid, the crystal growth is very fast and uncontrolled, which leads to instant PCM solidification.
- Thermal stability to assure a long lifetime of PCM if exposed to high temperature.

- Complete phase-change reversibility to use the storage material for as many as 5000 cycles (once a day for 15 years) [3].

- Low toxicity and corrosion to make storage material selection easier and more economical.

- Low cost to be competitive with other methods of electricity power generators.

In the present work, an in-depth review of PCMs categories, characteristics, and their thermal properties is conducted to select an appropriate PCM under the above criteria.

1.1. **Phase Change Material**

There are a wide variety of PCMs available that melt and solidify at a broad range of temperatures and are utilized in many applications. One of the most widely used low temperature PCMs is paraffin wax, which is inexpensive compared to other PCM categories and has moderate thermal conductivity values. Salts are higher temperature PCMs with higher volumetric energy density and thermal conductivity. Other materials that have been studied in the past are fatty acids and eutectic mixtures of organic and various inorganic materials.

In 1983, Abhat [12] presented a useful classification of the PCMs used for thermal energy storages. In that classification, PCMs were divided into three major categories: organic, inorganic, and eutectic PCMs. Among others who have studied and used the same PCMs categories are Lane [14], Dincer and Rosen [15]. Figure 1.4 represents the PCM classification that is a combination of the Abhat and Sharma arrangement [5, 12].

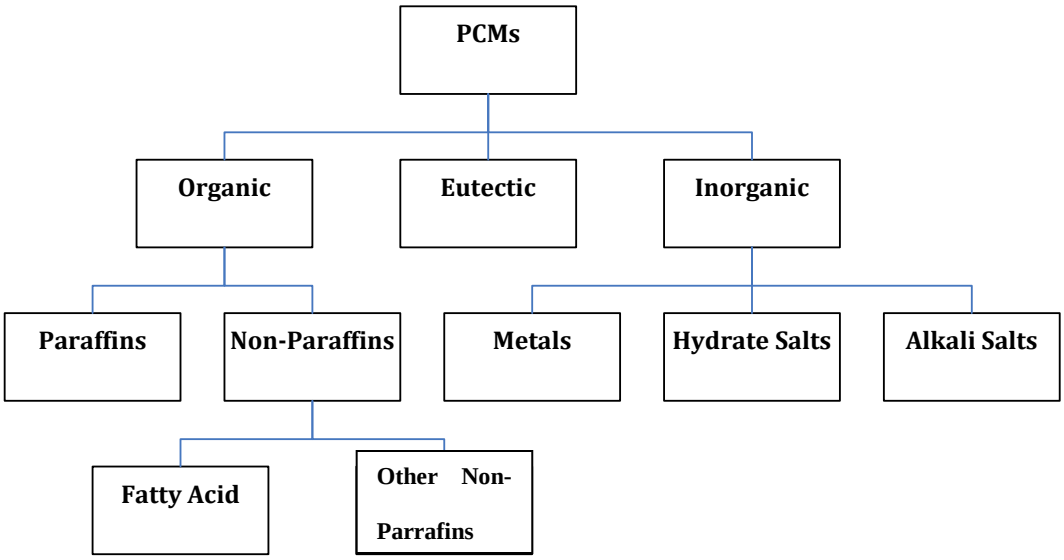

Fig. 1.4. PCM classification.

As shown in above diagram, PCMs have been divided into three major categories of organic, inorganic, and eutectic materials. Comparing the three categories, inorganic compounds have almost double volumetric latent heat storage capacity (250–400 kg/dm3) compared to the organic compounds (128–200 kg/dm3) [16]. The differences in thermal behavior of these materials necessitated to collect and review the thermal properties and physical characteristic of each PCM's subgroup presented throughout literature since 1981.

1.1.1. **Organic PCMs**

Organic PCMs are divided into two subcategories: paraffins and non-parafins. These material classes cover the temperature range between 0 °C and about 200 °C. Because of the covalent bonds in organic materials, most of them are not

stable to higher temperatures. In most cases, the density of organic PCM is lower than 1000 kg/m3 and thus smaller than the density of most inorganic materials such as water and salt hydrates. The most commonly used organic PCMs are parafiins. Paraffin is a technical name for an alkane, but often it is specifically used for linear alkanes with the general formula C_2H_{2n+2}.

Paraffins are suitable candidates for PCMs because of their very broad range of melting temperature. In these materials, the rise of numbers of C atoms increase the chain length and has a direct effect on the latent heat of fusion and the melting point. The longer the chain, the higher latent heat and melting point [12, 17]. Some selected paraffins, based on their number of atoms, melting point, and latent heat are shown in Table 1.3, which exhibits several paraffins with chain lengths from 14 C atoms to 30 C atoms, with melting point changing from 5.5°C to 65.4°C and latent heat of fusion from 228 KJ/Kg to 251KJ/Kg.

Table 1.3. Melting Point and Latent Heat of Fusion of Paraffins Base on Their Number of Atoms or Chain Length [5]

No of Carbon atom in paraffin	Melting Point (°C)	Latent Heat (KJ/Kg)
14	5.5	228
15	10	205
16	16.7	237.1
17	21.7	213
18	28	244
19	32	222
20	36.7	246
21	40.2	200
22	44	249
23	47.5	232
24	50.6	255
25	49.4	238
26	56.3	256
27	58.8	236
28	61.6	253
29	63.4	240
30	65.4	251

Paraffins are safe, reliable, predictable, and non-corrosive. They are chemically inert and stable below 500°C, melt congruently, show little volume changes on melting and have low vapor pressure in the molten phase. However, only technical grade paraffins may be used as PCMs in latent-heat storage systems because of cost consideration. Table 1.4 lists some technical grade paraffins, in 42-68°C melting rang and latent heat of 189-210 KJ/Kg. These paraffin mixtures are not completely refined oil, thus they exhibit lower latent heat of fusion compared to pure paraffins in Table1.3.[18-19].

Table 1.4. Physical Properties of Some Paraffins [11]

Paraffin Type	Melting Point (°C)	Latent Heat (KJ/Kg)
6160	42-44	189
P116	45-48	210
5338	48-50	189
6035	58-60	189
6403	62-64	189
6499	66-68	189

Apart from some several favorable characteristic of paraffins, Sharma et al.. [5] have reported that the systems that are using paraffins usually have very long freeze–melt cycles because of poor thermal conductivity [4, 20-21]. Among the other undesirable properties of paraffins are non-compatibility with plastic containers, and moderate flammability. All these undesirable effects can be partly mitigated by modifying the wax and the storage unit.

Furthermore, the non-paraffin organic materials are divided into fatty acids and other non-paraffin organic. All fatty acids are described by a general formula of CH3(CH2)2nCOOH. Table1.5 lists some of the most common saturated fatty acids. Their latent heat is similar to that of paraffins, and their melting temperature increases with the length of the molecule. Because fatty acids consist of one component, they are stable upon cycling. Like paraffins, fatty acids also show little or no supercooling. However, fatty acids are flammable and should not be exposed to excessively high temperatures, flames, or oxidizing agents. They also exhibit low thermal conductivity, low flash points, have varying level of toxicity,

and are instable at high temperatures. Also they cost 2–2.5 times more than the technical grade paraffins [22, 23].

Table 1.5. Latent Heat of Fusion and Melting Temperature of Some Fatty Acids [5]

Material	Melting Point (°C)	Latent Heat (KJ/Kg)
Acetic acid	16.7	184
Polyethylene glycol	20-25	146
Capric acid	36	152
Eladic acid	47	218
Lauric acid	49	178
Pentadecanoic acid	52.5	178
Tristearin	56	191
Myristic acid	58	199
Plamatic acid	55	163
Stearic acid	69.4	199
Acetamide	81	241
Methyl fumarate	102	242

Among the other non-paraffins organic PCMs are sugar alcohols and polyethylen glycol (PEG). Table 1.6 presents example of sugar alcohols; their melting temperatures are in the range of 90 °C to 200 °C, and they have very high latent heat per unit volume. In contrast to many other organic materials, melting temperature of sugar alcohols are comparatively high in most cases. [6]

Table 1.6. Latent Heat of Fusion and Melting Temperature of Some Sugar Alcohols [6]

Material	Melting Point (°C)	Latent Heat (KJ/Kg)
$C_5H_7(OH)_5$/Xylitol	94	263
$C_6H_8(OH)_6$/D-Sorbitol	97	185
$C_4H_6(OH)_4$/Erythritol	120	340
$C_6H_8(OH)_6$/D-Mannitol	167	316
$C_6H_8(OH)_6$/Galictitol	188	351

Polyethylen glycol (PEG) is a polymer with the general formula C2nH4n+2On+1. It is produced from ethylene glycol $C_{2H}H_4(OH)_2$. The base unit of a linear PEG chain is made up of the monomers of -CH2-CH2-O-. The monomers have a molecular weight of 44 g/mole. Polyethylene glycols are available in a molecular weight range from about 200 to 35000 [6]. Table.1.7 lists some properties of PEGs. PEGs with an average molecular weight between 200 and 400 are liquids at room temperature; PEG 600 melts at 17 – 22 °C. The melting temperature of all PEGs with a molecular weight exceeding 4000 g/mol is around 58 – 65 °C.

Table 1.7. Examples of PEG Materials and Their Properties [6]

Material	Melting Point (°C)	Latent Heat (KJ/Kg)
PEG400	8	100
PEG600	17-22	127
PEG1000	35-40	-
PEG3000	52-56	-
PEG6000	55-66	190
PEG10000	55-60	-

In summary, most organic PCMs exhibit high-latent heat of fusion and melt congruently. However, their low melting points (7-60°C) make them not suitable for CSPP. In addition, they exhibit low thermal conductivity and supercooling, which lead to longer charging and discharging cycles and wider operating temperature.

1.1.2. **Inorganic PCMs**

Inorganic PCMs can be categorized into three major groups: alkali salts, hydrate salts, and low (Tm < 300°C) melting temperature metals. Inorganic PCMs are better candidates for medium- to high-temperature (T>300°C) heat storages because of their higher melting point compared to organic PCMs. They also are non-flammable; however, they are corrosive to most metals and suffer from decomposition and suppercooling, which can affect their phase change properties such as melting temperature and heat storage capacity [16].

1.1.2.1. Hydrate Salts

Hydrate salts with the general formula of $AB-nH_2O$ can be considered as a mixture of inorganic salts and water forming a crystalline solid. These salts usually melt to either a hydrate salt with fewer moles of water or to its anhydrous form, therefore the solid–liquid transformation of hydrate salts actually are dehydration of the salt. Table 1.8 presents several hydrate salts and their thermal properties. Although hydrate salts are attractive materials for use

in thermal energy storage because of their high latent heat (100-200 KJ/Kg) and low cost. But because hydrate salts consist of several components, at least one salt and water, they can potentially separate into different phases and thus show problems with cycling stability. In addition to their supercooling problem, some of them by as much as 80 °C, their low melting temperatures (T<100°C) make them unqualified to be used at high temperature heating storages.

Table 1.8. Melting Point and Latent Heat of Fusion: Salt Hydrates [4]

Material	Melting Point (°C)	Latent Heat (KJ/Kg)
$K_2HPO_4.6H_2O$	14	109
FeBr3.6H2O	21	105
$Mn(NO_3)_2.6H_2O$	25.5	148
$FeBr_3.6H_2O$	27	105
$CaCl_2.12H_2O$	29.8	174
$LiNO_3.2H_2O$	30	296
$LiNO_3.3H_2O$	30	189
$NaCO_2.10H_2O$	32	267
$NaSO_4.10H_2O$	32.4	241
$KFe(SO_4)_2.10H_2O$	33	173
$CaBr_2.6H_2O$	34	138
$LiBr_2.2H_2O$	34	124
$Zn(NO_3).6H_2O$	36.1	134
$FeCl_3.6H_2O$	37	223
$Mn(NO_3).4H_2O$	37.1	115
$Na_2HPO_4.12H_2O$	40	279
$CoSO_4.7H_2O$	40.7	170
$KF.2H_2O$	42	162
$MgI_2.8H_2O$	42	133
$CaI_2.6H_2O$	42	162
$K_2HPO_4.7H_2O$	45	145
$Zn(NO_3)_2.4H_2O$	45	110
$MgNO_3.7H_2O$	47	142
$CaNO_3.4H_2O$	47	153
$Fe(NO_3)_2.9H_2O$	47	155
$Na_2SiO_3.4H_2O$	48	168
$K_2HPO_4.3H_2O$	48	99
$Na_2S_2O_3.5H_2O$	48.5	210
$MgSO_4.7H_2O$	48.5	202
$Ca(NO_3)_2.3H_2O$	51	104

Overall, hydrate salts can be identified with three types of melting behavior: congruent, incongruent, and semi-congruent. Congruent melting occurs when the anhydrous salt is completely soluble in its water of hydration at the melting temperature, for instance $K_2HPO_4.6H_2O$ which melts congruently at 14°C. Incongruent melting occurs when the salt is not entirely soluble in its water of hydration at the melting point, such as $Ca(NO_3)_2.3H_2O$ which melts at 51°C to water and solid $Ca(NO_3)_2$. Semi-congruent melting occurs when the liquid and solid phases have different compositions because of conversion of the hydrate to a lower-hydrate. $Na_2S_2O_3.5H_2O$ is an example of materials that can be transformed into other hydrate forms before either complete melting or freezing occurs, resulting in a broadened melting point range.

The major problem in using hydrate salt is the incongruent melting. As n moles of water of hydration are not sufficient to dissolve one mole of salt, the result is supersaturated solution at the melting temperature. The extra salts from the supersaturated solution settle down at the bottom of the container and are unavailable for recombination with water during the reverse freezing process. This phenomena cause an irreversible melt–freeze process which increase by every discharge cycle.

Various methods are proposed to resolve the incongruent melting of hydrate salts. Among them are mechanical stirring [26-27], encapsulating the PCM to reduce separation [28-30], adding thickening agents to prevent salt segregation by holding it suspended [27, 31-32], and use of excess water to prevent supersaturated solution [33-34].

Although addition of water prevents formation of heavy anhydrous salts and makes the system stable, but it reduces the storage density because of increase of water's weight fraction [33]. The use of some thickening agent, such as Bentonite clay has been suggested to overcome the problem of phase segregation. However, this will reduce the rates of crystallization and heat transfer to the salt because of the lower thermal conductivity of the mixture.

Another common obstacle with hydrate salts is the supercooling. Because the rate of nucleation is very low at the fusion temperature, the material has to be cooled below its melting temperature, usually about 15-30°C below their melting temperature, to start the solidification process. Consequently, energy, instead of being discharged at the melting temperatures, is discharged at much lower temperatures, which leads to wider operating temperature range [3].

To overcome the salt segregation and the supercooling of hydrate salts, the use of a nucleating agent, such as Borax has been suggested [31]. However, this requires some thickening agent to prevent settling of the high density Borax. Herrick et al.

[27] have shown the effect of mechanical mixing with the use of rolling cylinders. They have observed complete phase transformations, uniform freezing, and repeatable performance over 200 cycles.

To overcome the above-mentioned problems associated with the application of hydrated salts in non-agitated thermal storage systems, scientists [35-37] have put significant efforts in developing nucleating agents and stabilizers for some of the hydrated salts. One approach has been to encapsulate PCMs in spherical plastic; for example, calcium chloride encapsulated in plastic [16]. The products have been tested for a large number of cycles and have been found to be stable. The reported latent heat for the commercial $CaCl_2.6H_2o$ is 267 MJ/m^3 [35], which is lower than that of the pure salt because of the extra water and the nucleating and thickening agents used. The volumetric storage density based on 1 m^3 of a tank is 160 J. Although calcium chloride has lower latent heat compared to other hydrate salts, but it was selected for encapsulation because it was easier to stabilize, and had minimum phase segregation[16]. Ryu et al. [36] have also performed extensive study on suitable thickening and nucleating agents, which can be used for a number of hydrated salts. Table.1.9 summarizes their important findings, showing a significant reduction in the degree of supercooling by applying suitable nucleating and thickening agents.

Table 1.9. The Effect of Thickening Agents on Supercooling of Several PCMs [37]

PCM	Tm (°C)	Nucleating Agent	Supercooling (°C) W/O Nucleator	Supercooling (°C) W/Nucleator
$Na_2SO_4.10H_2O$	32	Borax	15-18	3-4
$Na_2HPO_4.12H_2O$	36	Borax	20	6-9
$Na_2HPO_4.12H_2O$	36	Carbon	20	0-1
$Na_2HPO_4.12H_2O$	36	TiO_2	20	0-1
$Na_2HPO_4.12H_2O$	36	Copper	20	0.5-1
$Na_2HPO_4.12H_2O$	36	Aluminum	20	3-10
$CH_3COONa.3H_2O$	46	Na_2SO_3	20	4-6
$CH_3COONa.3H_2O$	46	$SrSO_4$	20	0-2
$CH_3COONa.3H_2O$	46	Carbon	20	4-7
$Na_2S_2O_3.5H_2O$	57	K_2SO_4	30	0-3
$Na_2S_2O_3.5H_2O$	57	$Na_2P_2O_7.10H_2O$	30	0-2

1.1.2.2. Alkali Salts

Alkali or alkaline salts are formed from a base or hydroxide by the partial replacement of its hydrogen by a negative or acid element or radical. These salts are attractive as latent heat thermal energy storage materials for medium to high temperature (300°C- 870°C) applications on the basis of their desirable thermo-physical properties such as high latent heat (> 200 KJ/Kg), good endurance-stability at high temperatures, and low-volume expansion (<10%). Table 1.10 shows a selection of widely used alkali salts. The main drawbacks of these salts are the low thermal conductivity, which has a direct effect on the charging and discharging cycle time and the efficiency of the heat storage. Therefore, the

thermal conductivity enhancement of these types of PCMs are necessary [38-39]. The improvement of thermal conductivity has been studied extensively, and various methods have been reported. Among these are the additions of fin structure, increasing the surface area with encapsulation methods, adding particles with high thermal conductivity, and using porous metal structures, which will be explained and discussed thoroughly in the next chapter.

Table 1.10. Example of Alkali Salts for PCM Applications [11]

PCM	Melting Point °C	Latent Heat (KJ/Kg)
$LiNO_3$	224	360
$NaNO_3$	307	172
KNO_3	333	266
$MgCl_2$	714	452
$NaCl$	800	492
Na_2CO_3	854	276
K_2CO_3	897	236

1.1.2.3. Metals

This category of PCMs includes low melting metals and metal eutectics. Metals and their alloys are not the best candidates because of their very high density, which leads to storage's design complications and higher cost. However, they are attractive candidates for low volume applications because of their high heat of fusion per unit

volume. The best characteristic of metals is their high thermal conductivities, which eliminates extra design and modification in heat exchangers for efficient heat extraction. A list of most common used low melting temperature metals and alloys' PCMs is given in Table.1.11.

Table 1.11. Melting Point and Latent Heat of Fusion of Metals

Material	Melting Point (°C)	Latent Heat (KJ/Kg)
Gallium	30	80.3
Tin	232	59
Bismuth	271	51.9
Bi-Cd-In Eutectic	61	25
Bi-Pb-In Eutectic	70	29
Bi-In Eutectic	72	25
Bi-Pb-Sn Eutectic	96	--
Bi-Pb Eutectic	125	--
Lead	327	23

1.1.3. **Eutectic PCMs**

A eutectic composition is a mixture of two or more components that yields the lowest possible melting point in an alloy system. The main advantage of eutectics compared to other PCM candidates is the complete melting and freezing at a single temperature. These materials almost always melt and freeze without segregation, because they freeze to an intimate mixture of crystals, leaving little opportunity for the components to segregate. The eutectic mixture may consists of organic-organic, organic-inorganic, and inorganic-inorganic materials. An example is shown in Figure 1.5 for binary mixture of Sodium nitrate-Sodium

Chloride, which indicates a eutectic temperature at 298 °C at the 93.3% KCl-6.7% $NaNO_3$ composition.

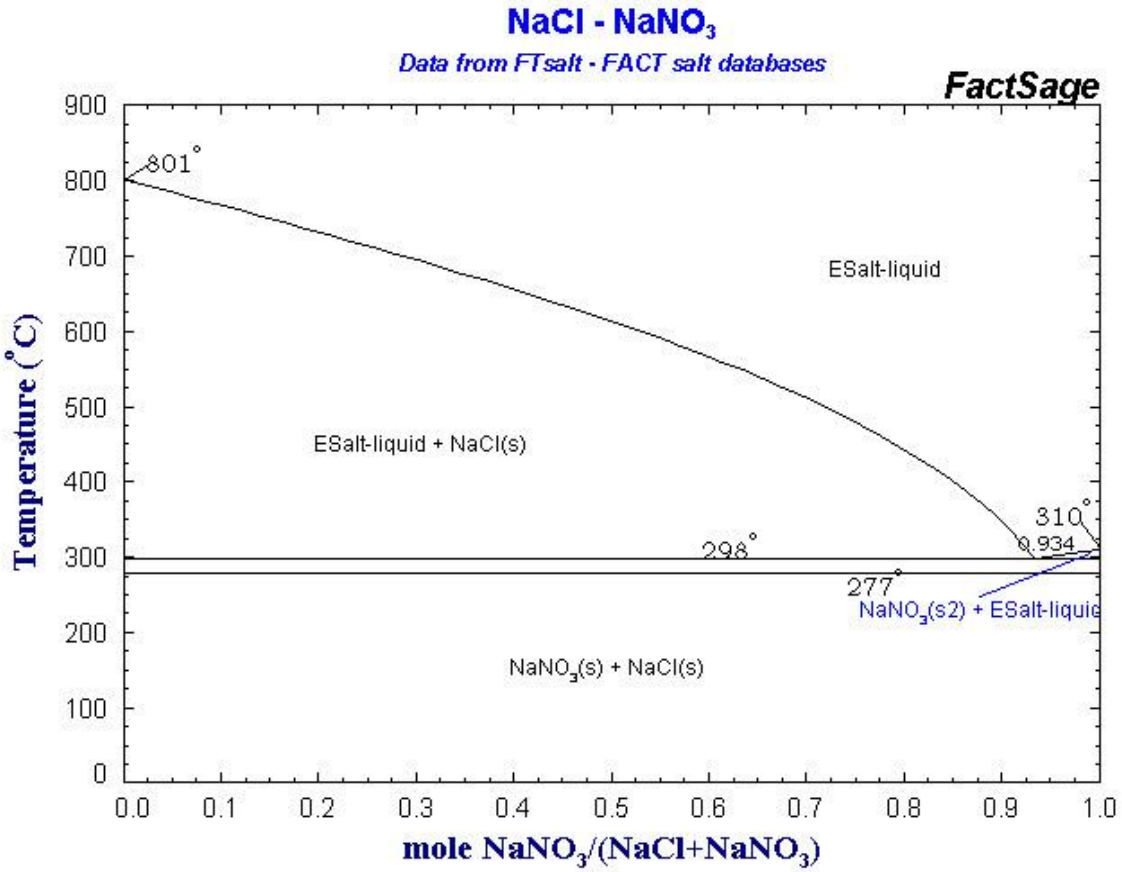

Fig. 1.5. Sodium nitrate-Sodium chloride phase diagram [41].

Binary or ternary eutectic mixtures of nitrate salts are suitable candidates for PCM because of their high latent heat, low cost, and low vapor pressure. Table. 1.12 presents a few of the widely used inorganic eutectic mixtures. One of the most popular eutectic mixtures for solar thermal heat storages is the “solar salt”

consisting of 51% $NaNO_3$ and 49% KNO_3 with melting temperature of 223°C, as presented in Figure.1.6. The eutectic has been used as a heat transfer fluid and thermal energy storage medium in the solar heat storages such as the Solar Two Concentrating Solar Power pilot plant since 1980 [36-37,40]. This binary mixture of $NaNO_3$ and KNO_3 is also used in the 2-tank direct system of the Archimedes project in Italy [42] and the Gemasolar Thermosolar Plant (Gemasolar) in Spain [43].The solar salt has the highest thermal stability, the lowest cost and the highest melting point.

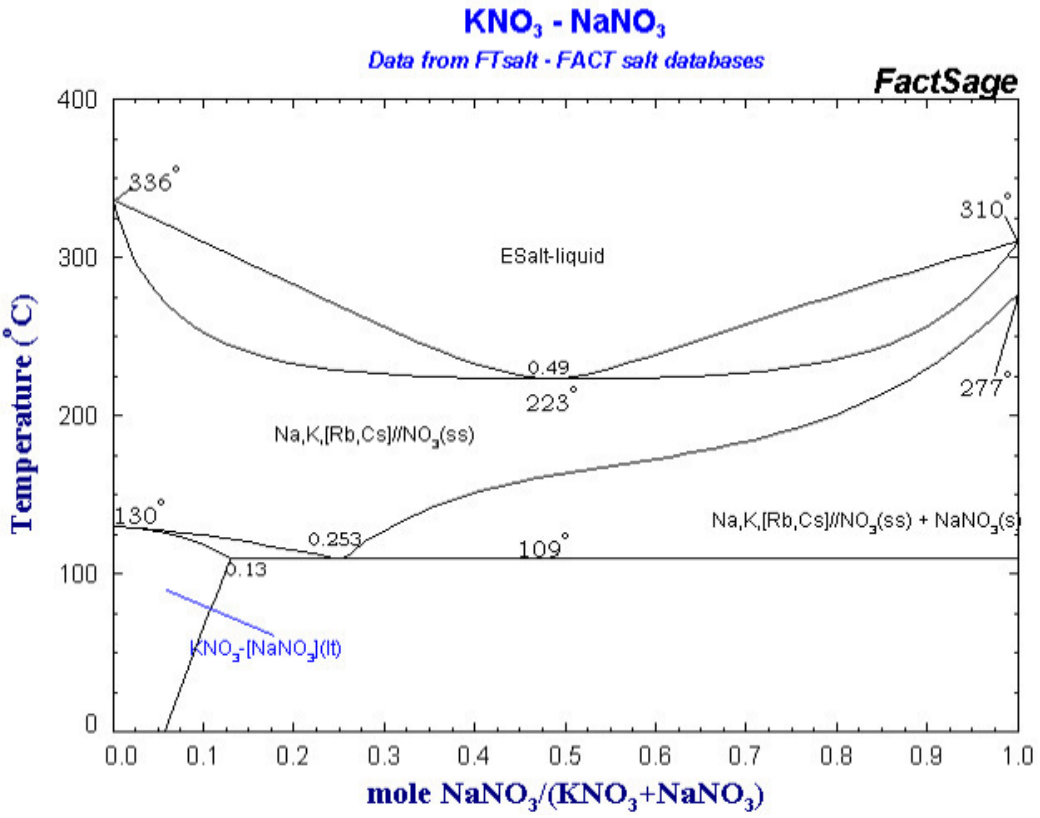

Fig. 1.6. Sodium nitrate-Potassium nitrate phase diagram [41].

Other well-known eutectic mixtures are the Hitec and HitecXL salts. Hitec salt consists of a ternary mixture of 53wt% KNO_3, 40wt% NaNO2, and 7wt% $NaNO_3$ with a melting temperature of 142°C, and the HitecXL formed from a ternary mixture of 48wt% Ca(NO3)2, 45wt% KNO_3, and7wt% $NaNO_3$ with a melting temperature of 133°C [44]. The thermal stability of Hitec salt can reach up to 454 °C and could be used up to 538°C for a short period of time with use of nitrogen blanket to prevent the slow conversion of the nitrate components to nitrite.

Table 1.12. Melting point and heat of fusion of some inorganic eutectic mixtures.

Material composition Wt%	Melting Point (°C)	Latent Heat (KJ/Kg)	Cost ($/Kg)
60% NaNO3-40% KNO3	221	161	1.25
53% KNO3- 40% NaNO2- 7%	142	83.7	2.85
48% Ca(NO3)2, 45% KNO3-7% NaNO3	133	91.2	3.9
14%LiNO3+86%Mg(NO3)2.6H2O	72	180	--
53% Mg(NO3)2.6H2O+47%Al(NO3)2.9H2O	61	148	--
58.7%Mg(NO3)2.6H2O+41.3% MgCl2.6H2O	59	132	--

Although PCMs have appropriate properties that make them attractive for storage applications, they also have different drawbacks. Among these are, low thermal conductivity, high-cost, supercooling, phase segregation, volumetric expansion, or poor stability at extended temperature cycling [16]. The following section is a brief summary of the PCMs thermal conductivity enhancement methods.

1.2. **PCMs Thermal Conductivity**

Since PCMs store large amounts of heat, and because it is necessary to transfer this heat to the outside of the storage to use it, the low thermal conductivity, potentially in the solid state can increase the charging and discharging (melt/freeze) cycle time significantly.

A study by Hoshi et al. [8] compared the charging cycle times of a thermal storage with use of two PCMs with different thermal conductivities. First, they used KNO_3 with thermal conductivity of 0.5 W/K.m as a phase change material and second Pb with thermal conductivity of 31 W/K.m. They assumed the heat storage was charged to 100MJ/m3 and their numerical model results indicated that the time required for Pb and KNO_3 to charge the heat storage are 250 min and 2000 min, respectively. Although KNO_3 is one of the most promising PCMs for CSPP application, its low thermal conductivity makes it an unsuitable candidate, unless thermal conductivity enhancement techniques are used to reduce the charging and discharging cycle times.

While a wide range of PCMs have been studied and categorized and most of their thermal properties (e.g; latent heat, specific heat, and melting temperature) and phase change behaviors have been evaluated throughout the literature, only a few studies focused on the thermal conductivity of these materials. Table.1.10 presents some of PCMs' thermal conductivities presented in literature.

Table 1.13. Thermal Conductivity of PCMs

PCMs	Melting Point (°C)	Latent Heat (KJ/Kg)	Thermal Conductivity (W/K.m)
$C_{14}H_{30}$	6	230	0.21
$C_{18}H_{38}$	28	245	0.36
$CH_3(CH_2)_6COOH$	16	149	0.15
$CH_3(CH_2)_{12}COOH$	58	186	0.17
$C_4H_6(OH)_4$	120	340	0.32-0.73
PEG600	17-22	127	0.19
$LiNO_3$	254	360	0.59
$NaNO_3$	307	172	0.51
KNO_3	333	266	0.5

As presented in above table one major issue of most PCMs is their unacceptably low thermal conductivity. To improve the heat transfer rate through these materials two main techniques can be used. First, increasing the heat transfer surface area; this can be done by micro or macro encapsulation of PCMs or using fins. Second, increasing the thermal conductivity by adding higher thermally conductive particles, such as metal shavings or graphite flakes. Among widely studied methods in literature are, use of metallic fillers, metal matrix structures, finned tubes, and the addition of aluminum shavings or graphite matrix [43-52].

A technique through which heat transfer area can be increased, while accommodating volume change, and protecting the PCM from the heat transfer fluid is encapsulating the PCM. Encapsulations are usually classified by their size into macro- and microencapsulation. Macroencapsulation means filling the PCM in a macroscopic containment that fit amounts from several ml up to several liters. These are often containers and bags made of metal or plastic [6].

Macroencapsulation is very common because such containers or bags are available in a large variety. Microencapsulation, on the other hand, is the encapsulation of solid or liquid particles of 1 μm to 1000 μm diameter with a solid shells. Physical processes used for microencapsulation include spray drying, centrifugal and fluidized bed processes, or coating processes. The main advantages of microencapsulation regarding PCM are the improvement of heat transfer to the surroundings because of the large surface-to-volume ratio of the capsules, and the improvement in cycling stability, because phase separation is restricted to microscopic distances. Furthermore, it is also possible to integrate microencapsulated PCM into other materials, such as building insulations, or food containers [5-6].

Lane et al. [53] identified several potential phase-change, heat storage materials suitable for encapsulation. He also assessed the technical and economical feasibility of using encapsulated PCMs for thermal energy storage in solar driven residential heating applications. His studies showed microencapsulation of $CaCl_2.6H_2O$ in polyester resin was particularly successful for development of wall and floor panels with heat storage abilities. Also, macroencapsulation of $CaCl_2.6H_2O$ in plastic film containers reported to be another promising method for heat transfer enhancement in heating systems using air as the heat transfer medium [54].

Although use of PCMs encapsulated in plastic spheres has shown significant improvement of thermal conductivity in packed bed storage application, the high pressure drop through the bed and its initial costs are major drawbacks of this technique [55-56].

In air-based systems, the heat transfer coefficients of both air and PCM are low. Therefore, to improve the performance of phase change storage units, Farid has suggested the use of more than one PCM with different melting temperatures in a thin flat container [16]. The same idea was applied later by Kanzawa for a unit consisting of vertical tubes filled with three types of waxes having different melting temperatures. During heat charging cycle, the air flows first across the PCM with the highest melting temperature to insure continuous melting of most of the PCMs. The direction of the air must be reversed during heat discharge. Both the theoretical and experimental measurements showed an improvement in the performance of the phase-change storage units using this type of arrangement [57].

Other scientists have tested the idea of using finned tubes in which the PCM was placed between the fins. Although a significant improvement in heat transfer rate was found, the high cost of the finned tubes may make their use uneconomical [58-59]. It is to be noted that such arrangements may improve heat transfer rates significantly only when a liquid is used as a heat transfer fluid.

Velraj et al. [42] reviewed attempts that have been made on heat transfer enhancement. They also tested different methods of heat transfer enhancement, which included the use of longitudinal internal finned tubes in a shell and tube heat exchanger unit, dispersing the PCM with high thermal conductivity particles, and using metallic packing such as leasing rings placed inside tubes containing the PCM. Figure.1.7 presents the leasing rings used to enhance the thermal conductivity of paraffin by factor of 10 when reducing the volume fraction of paraffin by 20%. Velraj et al. also had studied the effect of using inner fins in the tubes containing the PCM, as shown in Figure 1.8. The overall thermal conductivity was improved, and the charging and discharging cycles' time were reduced by about 70% [60].

Fig. 1.7. Leasing ring used by Valraj et al. to improve thermal conductivity of Paraffin [42].

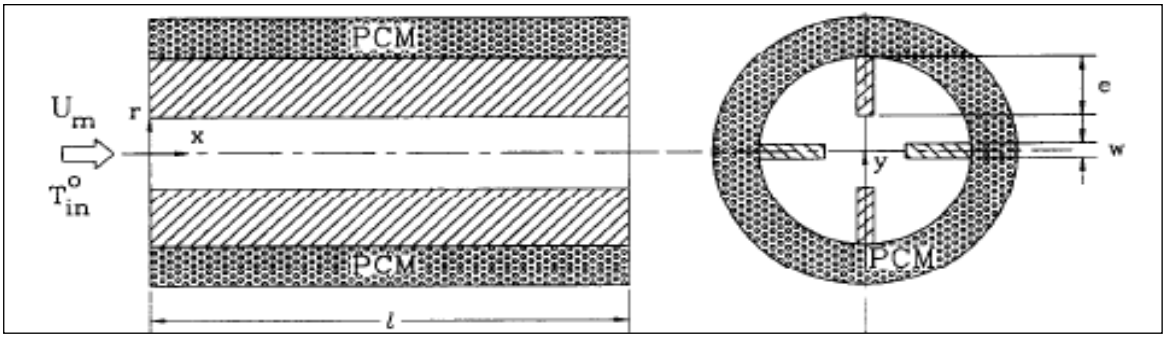

Fig. 1.8. Internal fin tubes for thermal conductivity enhancement [60].

Ageynim et al. [59] also studied heat transfer enhancement by using axial fins on the external tube immersed vertically in a PCM, which is called a longitudinal fin, as presented in Figure.1.9. Their experimental measurements and theoretical

predictions showed that the use of fins enhances the heat transfer rate significantly and decreases the charging and discharging cycle times from 31 hrs to 8 hrs.

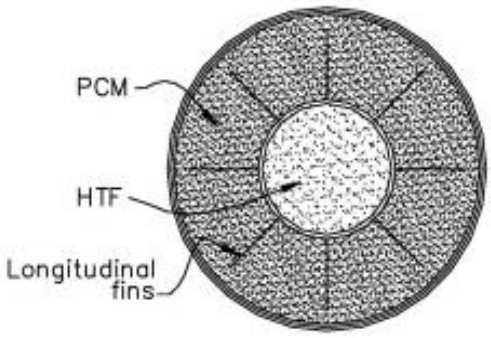

Fig. 1.9. Longitudinal fin PCM system [59].

Although there are a wide range of PCMs, and there have been extensive research on their property improvement, only a few of them have been commercialized. In the fallowing section some of PCMs' applications and prospected applications other than concentrating solar power plants have been presented.

1.3. **Alternative PCMs' Applications**

There are many applications for heat storage and thermal protection that can operate with PCM technology. Among them are building insulators, water heaters, thermal protection for electronics, spacecrafts, and solar power plants. Table.1.14 presents some of the different applications of PCMs found in the literature.

Table 1.14. A list of the most common PCMs' applications

Application	References
Thermal Storage for Solar Energy	[14, 61-65]
Building application	[63, 67-69]
Ice bank	[70-73]
Heating and sanitary hot water, Off-peak rate and adopting unloading curves	[74-77]
Temperature control for electronic room	[78]
Food storage for transportation, hotel trade, etc.	[75, 79-81]
Thermal protection of electronic device	[75, 80-81]
Medical application	[75,79]
Spacecraft thermal systems	[82]
Solar Power plants	[83,84]

1.3.1. **Building Application**

The use of PCMs for thermal storage in buildings was one of the first applications studied, together with typical storage tanks. The first application of PCMs described in the literature was in their use for heating and cooling systems in buildings, by Telkes in 1975, and Lane in 1986 [14, 61]. The use of building structural components for thermal storage was pointed out by Barkmann and Wessling in 1975 around the same time [67], and later by other authors [66, 85-86].

The advancement in lightweight building materials has made a great impact in the safety and cost of construction of buildings, but simultaneously affects the thermal properties because of low thermal mass. The lower thermal mass would cause high temperature fluctuations which could result in a high heating and cooling demands. Therefore the application of PCMs in building materials to smooth temperature variations has attracted lots of attention [87-89]. An interesting possibility in building applications is the impregnation of PCMs into porous construction materials, such as plasterboard, to increase thermal mass [68, 89]. The use of PCMs for air-conditioning applications have been developed, as such, during night and cooler temperature, PCM solidifies and release the heat, while during the hot hours, it absorbs the heat by going through melting phase transformation. This process is known as free-cooling [70-72].

Another application of PCMs in buildings is thermoelectric refrigeration. Omer et al. have integrated a phase change material in the thermal diode to improve effectiveness of the heat sink [90-91]. Ismail et al. studied the possibility of using a window with a PCM curtain to generate heat absorption during cold hours. They designed a double-sheeted window with a gap filled with PCM. During the cold hours, the PCM would freeze and release heat to prevent the temperature of the internal ambient from decreasing [92-93]. Similarly, Merker et al. developed a new PCM-shading system to avoid overheating around the window area [94-95].

One very important subject in applications of PCMs in buildings is the safety which was studied by Salyer [96]. He studied four different groups of PCMs base on their response to fire. Among the four PCM types, the most suitable candidates for building applications are the paraffin PCMs whose origins were from the polymerization of ethylene or as a by-product of petroleum.

1.3.2. **Satellite Technology**

Revanka et al. [97] has proposed to replace the conventional batteries by PCM for satellite power testing. He suggested placing a series of metal cells containing PCM that is liquid under high temperature in satellites, which then freezes during hours of cold darkness and releases its latent heat. The heat released can then generate electricity by driving thermoelectric units. Because the systems generate at least three times more power than batteries of comparable size, they are seen as a possible alternative to conventional satellite solar power systems that rely on batteries.

1.3.3. **Solar Water Heater**

Solar water heater is becoming more popular because they are relatively inexpensive and simple to fabricate and maintain. Esen et al. [98] have theoretically studied the effects of various thermal and geometric parameters on the PCM melting time for several PCMs and tank configurations. They studied the parallel fluid flow through cylindrical PCM storage, shell-tube heat exchanger

where the PCMs were stored in shell, and loose encapsulated spherical PCMs in water tank. Among these techniques, shell-tube heat exchanger exhibit the highest heat storage capacity, while the loose encapsulated spherical PCMs presented shorter discharging cycle time [74, 99].

Prakesh et al. [100] analyzed a built-in, storage-type water heater containing a layer of PCM filled at the bottom. He reported this system may not be effective because of the poor heat transfer between PCM and water. Also, Cassedy et al. [101] claimed that today PCMs do not offer economic savings for thermal storage at low temperatures (50-100°C), since these systems (paraffin) cost about the double of the cost of hot water systems. He does, however, point out the advantages associated with materials like paraffin, such as low corrosion, and chemical stability. Mehling et al. studied the possibility of including a PCM-module at the top of a stratified water tank. Their results indicated increase of energy storage and a better performance of the tank [102, 103].

1.4. **Summary**

A brief survey on thermal- and phase-change properties of PCMs was performed to find a suitable PCM for concentrating solar power plants' heat-storage applications. The main requirements for these heat storages are as follows: operating temperature of 300°C or higher to provide sufficient heat to Stirling or Brayton steam turbine, moderate to high heat of fusion for smaller storage space, good thermal conductivity

to store or release the latent heat in a given volume of the storage material in a short time, no supercooling or phase segregation to store and release maximum latent heat at operating temperature, low toxicity to ease the design of storage and heat exchangers, and low cost.

Overall, PCMs have been categorized into three main categories: organic, inorganic, and eutectic mixtures. Organic material such as paraffin, fatty acids, and sugar alcohols cover the melting temperature up to about 200°C. Because of the covalent bonds in organic materials, most of them are not stable at higher temperatures. The result is that, with the exception of sugar alcohols, organic materials usually have smaller melting enthalpies per volume than inorganic materials.

Inorganic materials cover a wide temperature range. Compared to organic materials, inorganic materials usually have similar melting enthalpies per mass, but higher ones per volume because of their high density. Their main disadvantage is material incompatibility with metals, because severe corrosion can be developed in some PCM-metal combinations. Inorganic PCMs have been divided into three subcategories of hydrate salts, alkali salts, and metals. Hydrate salt's melting temperature is in the range of 0-150 C, and it consists of a salt and water in a discrete mixing ratio. Because salt hydrates consist of several components, at least one salt and water, they can potentially separate into different phases and thus show problems with cycling stability. In fact, phase separation is a common problem with salt hydrates. Alkali salts

have higher melting temperature and latent heat compared with hydrate salts. Many of these salts are chemically stable; however, carbonates and nitrates can decompose under unsuitable conditions.

Metals and their alloys are not the best candidates for PCM application because of their very high density, which leads to storage's design complications and higher costs. However, they are the best candidates for low volume application because of their high heat of fusion per unit volume.

None of the PCM groups presented could fulfill all the requirements for high-temperature heat storages. However, Alkali salts covered most of the requirements, such as operating temperature (T>300 C), high heat of fusion (>200), no supercooling, low toxicity, and low cost. The only weakness of this group was their very low (K<1 W/K.m) thermal conductivities. Nevertheless it is possible to use these materials as PCMs for high temperature heat storage if thermal conductivity enhancement strategies are employed to decrease charging/discharging cycle times.

Chapter 2

Measurment of Thermal Conductivity of PCMs

Among the important factors that have to be considered in PCM selection is the desired operating temperature, its ability to melt and freeze at preferred temperature for many cycles without becoming thermally unstable. The other two thermal properties that have to be considered are the latent heat of fusion and thermal conductivity.

2.1. **Medium to High Temperature PCMs**

According to Mills et al. [1] medium melting temperature (300-500°C) PCMs can be used at low pressure turbines such as Stirling engines, while high-temperature (>500°C) PCMs can be used for large high temperature Brayton steam turbine. In this section, the thermal properties of several medium to high (300-900°C) temperature PCMs that can be used in concentrated solar power plants was reviewed and studied. The thermal properties of several alkali salts, and some metals have been gathered from the literature [104-108]. Figure .2.1 shows the results for the most common PCM with the melting point of 300°C to 900°C. This plot presents the melting point and latent heat of several salts, and a few lower melting metals. The plot indicates that latent heat increases respectively in the order of metal, nitrates, carbonate, hydroxide, and chloride with the exception of lithium nitrate, which exhibits a very high latent heat compared to other nitrates.

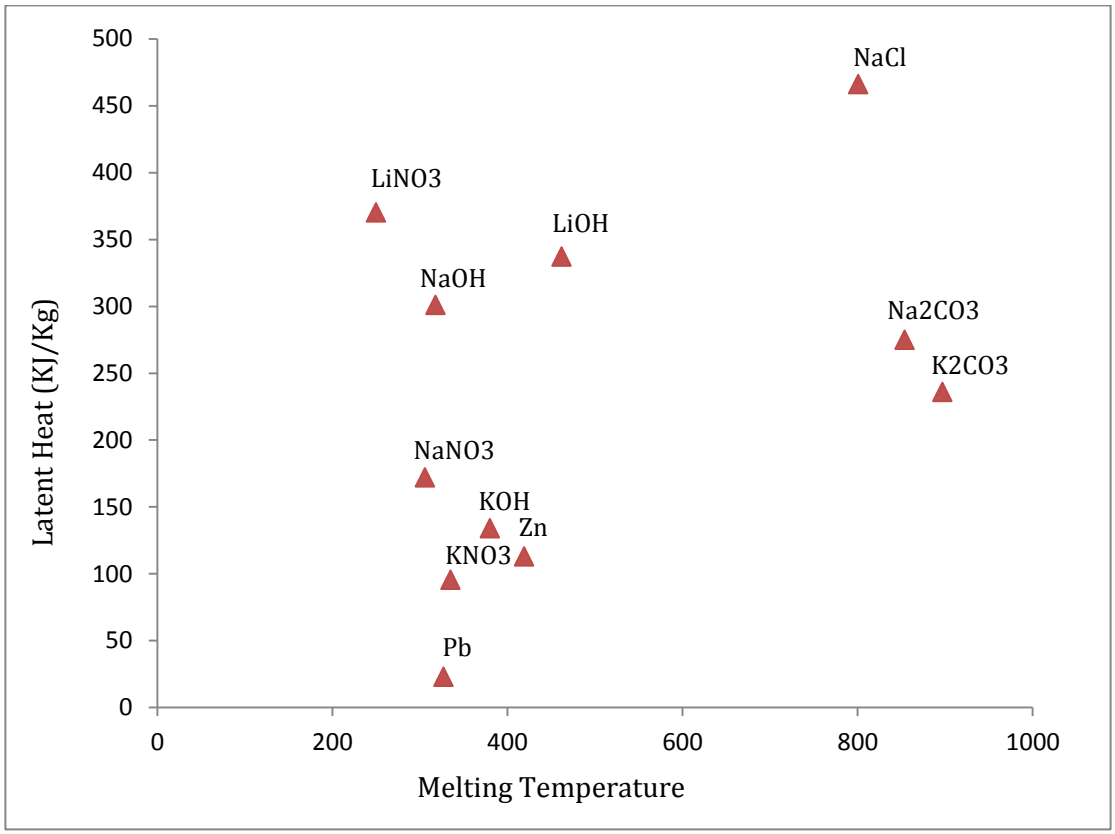

Fig. 2.1 Latent heat of high temperature phase change materials.

Some of the heat storages are designed to store sensible heat as well as latent heat, therefore the amount of specific heat can play an important role in heat storage capacity. Figure 2.2 presents the melting point and specific heat of several PCM candidates with medium to high melting temperatures (300-900°C). The results indicate that nitrate and carbonate salts exhibit a moderate (1-2 KJ/Kg.K) specific heat compared to metals and chloride salts. Once again, lithium salts show higher specific heat compared to others, making them a better

candidate for PCM based on their latent and specific heat. However, lithium salts are much more expensive compared to other presented candidates, and their application in latent heat thermal energy storage might not be very cost effective.

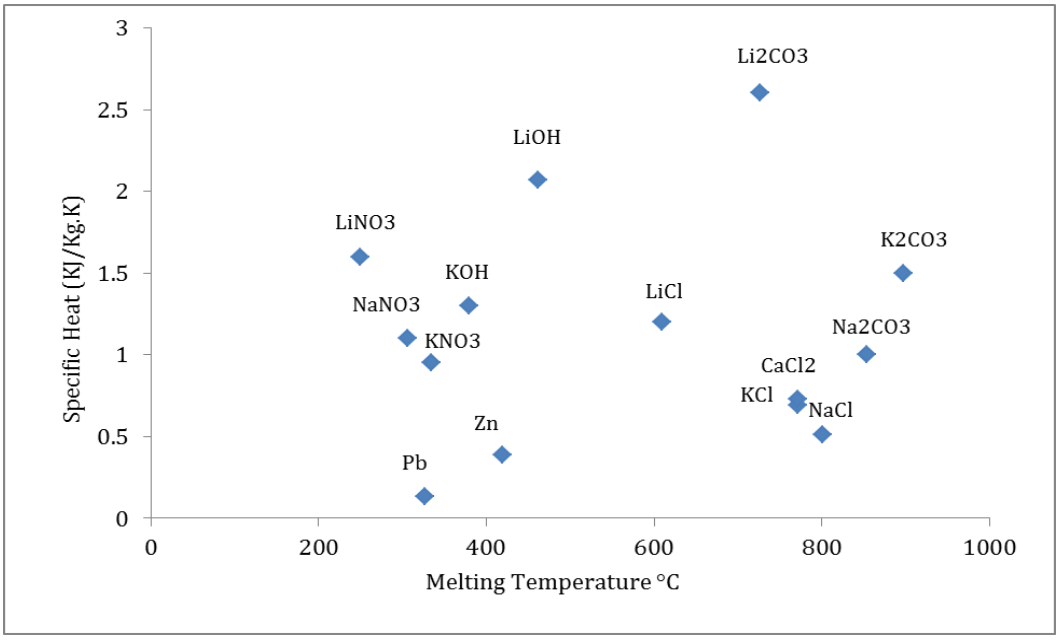

Fig.2.2. Specific heat of high temperature phase change materials.

Nevertheless, the best PCM for high temperature latent heat storage applications should fulfill thermal stability and thermal conductivity. Thermal stability is important to assure the long lifetime of the PCM when exposed to high temperature or radiation, and moderate thermal conductivity is desired to be able to store and release the latent heat from large volume of PCMs in a feasible time period.

In most of the latent heat storage units, the heat would be transferred in and out of the storage with the use of heat transfer fluid (HTF), as shown in Figure.2.3, the HTF would pass through the pipes or paths that have been placed in PCM.

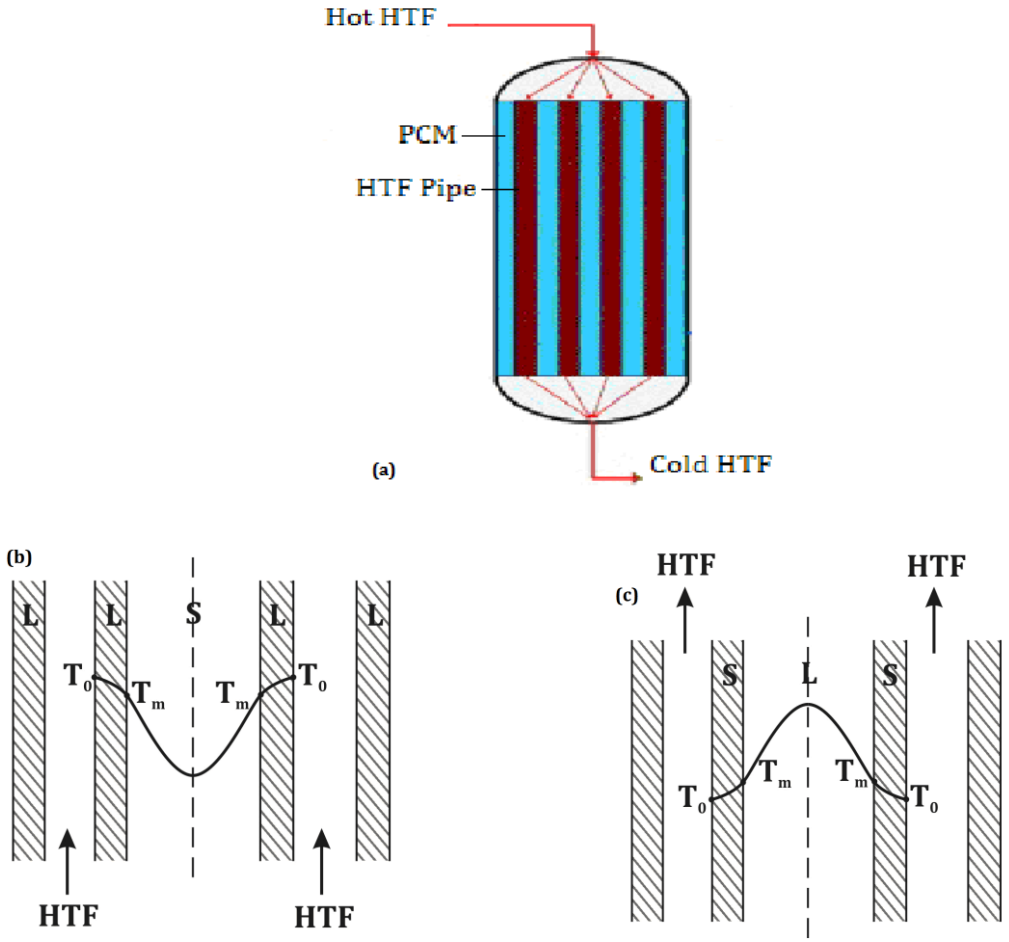

Fig. 2.3. (a) PCM and heat transfer fluid inside storage tank. (b) Temperature profile between two pipes during charging cycle, (c) Temperature profile between two pipes during discharging cycle.

During the charging cycle, the HTF that has been heated at solar collection tower, at the temperature above PCM melting point, starts to circulate through the pipes in the storage tank. As shown in Figure 2.4, the heat from the HTF starts to melt the salt. This cycle continues until all the PCM has melted and the molten PCM has heated up to the temperature required to store desirable sensible heat.

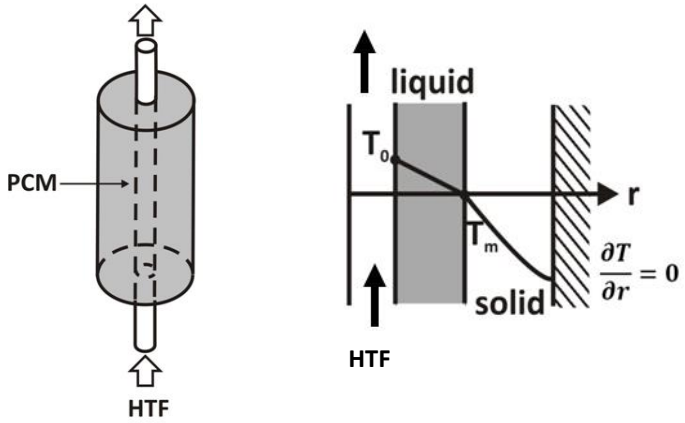

Fig.2.4. PCM charging cycle temperature profile.

During the discharging cycle, the HTF at the temperature below melting point of PCM circulates through the storage tank to transfer heat from the PCM to the boiler or heater or Rankin or Brayton cycles. As illustrated in Figure 2.5, first the sensible heat would be removed then the PCM starts to solidify and release the latent heat to HTF. The discharging cycle continues until all the PCM solidifies, or it might cool down farther to collect more sensible heat.

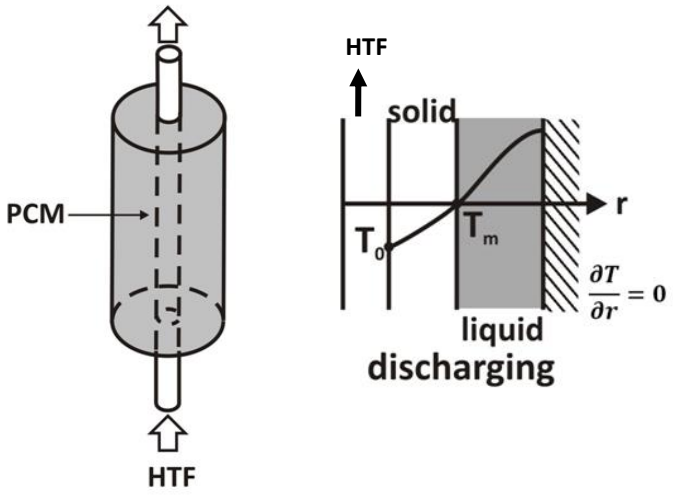

Fig. 2.5. PCM discharging cycle temperature profile.

Because during both charging and discharging cycle heat has to pass through the PCM thickness, the thermal conductivity of PCMs can become a critical factor on the thermal performance of the system. An analytical calculation was conducted to determine solidification time against thermal conductivity of PCMs based on Plank and Nesselmann solution [109].

2.2. **Solidification Time against Thermal Conductivity**

Cooling fluid at temperature T_0 is passing through a tube with radius r and wall thickness of Δr which cause solidified layers of PCM to develop on the outer surface of the tube, as illustrated in Figure 2.6.

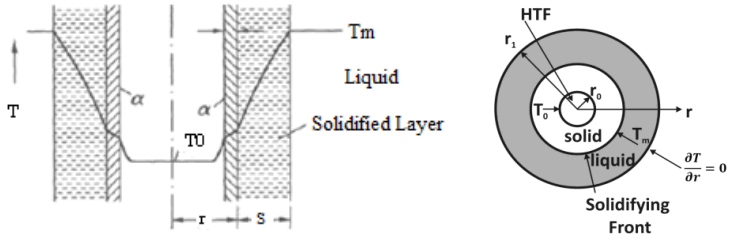

Fig. 2.6. Solidification on the outside of a tube from the inside.

During the time interval dt the phase interface moves a distance ds. This releases the heat of fusion of:

$$dQ = h_e \rho 2\pi (r+s) L ds \qquad (2.1)$$

where, h_e is the heat of fusion and L is the length of the tube. Also overall heat transfer can be written as:

$$dQ = Q' dt = \frac{T_m - T_0}{\frac{1}{2\pi L K_s} \ln \frac{r+s}{r} + \frac{1}{RA}} dt \qquad (2.2)$$

$$\frac{1}{RA} = \frac{1}{2\pi L K_w} \ln \frac{r}{r-\Delta r} + \frac{1}{2\pi L (r-\Delta r)\alpha} \qquad (2.3)$$

Where Q is the heat, Q' is the heat transfer rate, α is thermal difiusivity, t is time, K_s and K_w are the thermal conductivity of solidified layer and tube respectively. T_m and T_0 are solidification and HTF temperature, respectively.

Then from equations (2.1) and (2.2), such follows:

$$dt = \frac{h_e \rho}{K_s (T_m - T_0)} [(r+s)\ln\frac{r+s}{r} + (r+s)\beta] ds \qquad (2.4)$$

$$\beta = \frac{K_s}{K_w}\ln\frac{r}{r-\Delta r} + \frac{K_s}{(r-\Delta r)\alpha}$$

From (2.4) and the initial boundary condition s = 0 at t = 0 yields the solidification time as fallow:

$$t = \frac{h_e \rho s^2}{2K_s (T_m - T_0)} [(1+\frac{1}{s'})^2 \ln(1+s') - (1+\frac{2}{s'})(\frac{1}{2} - \beta)] \qquad (2.5)$$

$$s' = \frac{s}{r}$$

Equation 2.5 shows the effect of the thermal conductivity of PCM on discharging cycle time. Two PCMs with a latent heat of fusion of 100 kJ/kg and 300 kJ/kg were compared with the following assumptions:

At the beginning of both cases, the PCM is completely molten. The temperature inside the tube is set to 10° C below the solidification temperature. The tube has an outer diameter of 20mm and a wall thickness of 1mm. The thickness of the PCM layer for both PCMs is assumed to be 20mm. The heat capacity of the PCM is neglected, because in this case the latent heat of fusion is the main mechanism of energy storage.

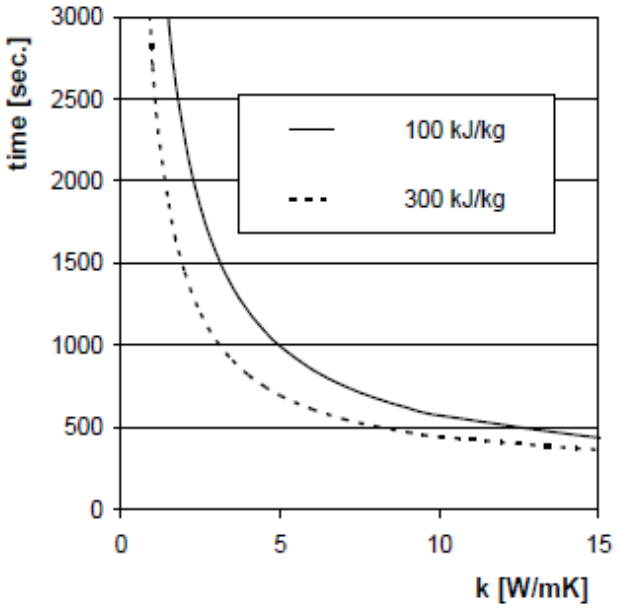

Fig. 2.7. Solidification time as a function of thermal conductivity on outside surface cylindrical tube for two different latent heat value.

Figure 2.7 presents the analytical solution for solidification time as a function of thermal conductivity. Results indicate solidification time decreases rapidly with increasing the thermal conductivity to about 5 W/K.m for PCM with 300KJ/Kg latent heat, and to 7 W/K.m for PCM with 100KJ/K.m latent heat. However, the improvement in solidification time is smaller for thermal conductivities above 5 W/K.m. Because the latent heat of most widely used PCMs for CSPP application is in the range of 100-300 KJ/Kg, for shorter charging/discharging cycles, the thermal conductivity of 7 W/K.m or higher is desirable.

Furthermore, from the above discussion one can conclude that thermal conductivity has a direct effect on the performance of latent-heat thermal energy

storages. In addition, the PCMs have to operate at wide ranges of temperature from above their melting point to below their solidification temperature, and during these ranges, the thermal conductivity of the PCM can vary because of changes in phonon vibration, crystal transformation, and phase change [110]. Thus to evaluate the thermal conductivity and understand the effect of temperature on PCMs, several medium- to high-(300-900°C) temperature salts were selected for thermal conductivity measurements with use of transient hot wire technique.

2.3. **Thermal Conductivity Measurements**

The transient hot wire technique was used to measure the thermal conductivity of several Alkali Nitrate and Chloride salts. The technique has been well developed and widely used for measurements of the thermal conductivity of solids, and in some cases, the thermal diffusivity of fluids with a high degree of accuracy [107-108, 111-114]. The most attractive advantage of the technique is the elimination of convective error in fluids and more accuracy compared to the data obtained using the steady-state method [115-121]. The steady-state method is based on constant, one-dimensional heat flow through two different materials (substrate and sample), and uses the known thermal conductivity of the substrate material as the reference for heat-flow measurement.

The transient hot-wire technique was first introduced by Carslaw and Jager [124], and it is based on one dimensional radial heat flow from a linear source with infinite length and very small diameter into the homogenous and isotropic substance. According to the theory of infinite long line heat source, the generated heat from the line source diffuses through the substance in the direction perpendicular to hot wire. For such an arrangement, the general Fourier equation can be used to calculate the thermal conductivity:

$$\frac{1}{\alpha_f}\frac{\partial \Delta T}{\partial t} = \frac{1}{r}\frac{\partial}{\partial r}\left(r\frac{\partial \Delta T}{\partial r}\right)$$

Boundary conditions:

$$t = 0 \;\&\; r = 0 \Rightarrow \underset{r\to 0}{Lim}[r(\frac{\partial T}{\partial r}) = -\frac{Q}{2\pi K}$$

$$t \geq 0 \;\&\; r = \infty \Rightarrow \underset{r\to \infty}{Lim}[\Delta T(r,t)] = 0$$

The temperature change at a radial distance r from the heat source conforms to a simple formula by applying boundary conditions:

$$\Delta T(r,t) = T(r,t) - T_0 = \frac{q}{4\pi k_f} Ei\left(\frac{r^2}{4\alpha_f t}\right)$$

Therefore, thermal conductivity can be calculated by the measure of temperature rise at a defined distance from the linear source by the following equation:

$$T(r,t) = \frac{Q}{4\pi K}[\ln(\frac{4\alpha.t}{r^2}) + \frac{r^2}{4\alpha t} - \frac{1}{4}(\frac{r^2}{4\alpha t}) - ... - \gamma] \qquad (2.8)$$

where K is the thermal conductivity, Q (W/m) is the power per unit length of the heating line source, α is the thermal diffusivity (m^2/s) of the sample, r is the radial position where the temperature is measured, and $\gamma = 0.5772156$is Euler's constant. At the significant large-value of time and small radial distance, the $(\frac{r^2}{4\alpha.t})$ term can be neglected, and equation 2.4 can be simplified to:

$$T(r,t) = \frac{Q}{4\pi K}[\ln t + \ln(\frac{4\alpha}{r^2}) - \gamma] \qquad (2.9)$$

By measuring the temperature at times t_1 and $t_2$at a specific point in the medium, the temperature gradient can be calculated using:

$$\Delta T = T_2 - T_1 = \frac{Q}{4\pi K}\ln(\frac{t_2}{t_1}) \qquad (2.10)$$

Based on this equation, the thermal conductivity is the slope of linear portion of temperature rise versus natural logarithm of time as shown in Figure.2.8, and can be calculated by:

$$K = \frac{Q}{4\pi[T(t_2) - T(t_1)]}\ln(\frac{t_2}{t_1}) \qquad (2.11)$$

The temperature history can be characterized into three stages as shown in Figure.2.5. The graph (a) indicates the theoretical curve from equation 2.7, graph (b) represents the general form of experimental measurement of temperature

rise versus the natural logarithm of time, and (c) shows an actual temperature rise versus time of sodium nitrate sample at room temperature. In graph (b), at the initial stage from $t = 0$ to t_{min}, the temperature will rapidly rise, then from t_{min} to t_{max} heat begins to dissipate into the surrounding material, the rate of temperature rise becomes constant, and finally at the third stage after t_{max}, the thermal front reaches the external boundary of the sample which causes the rate of temperature rise increases.

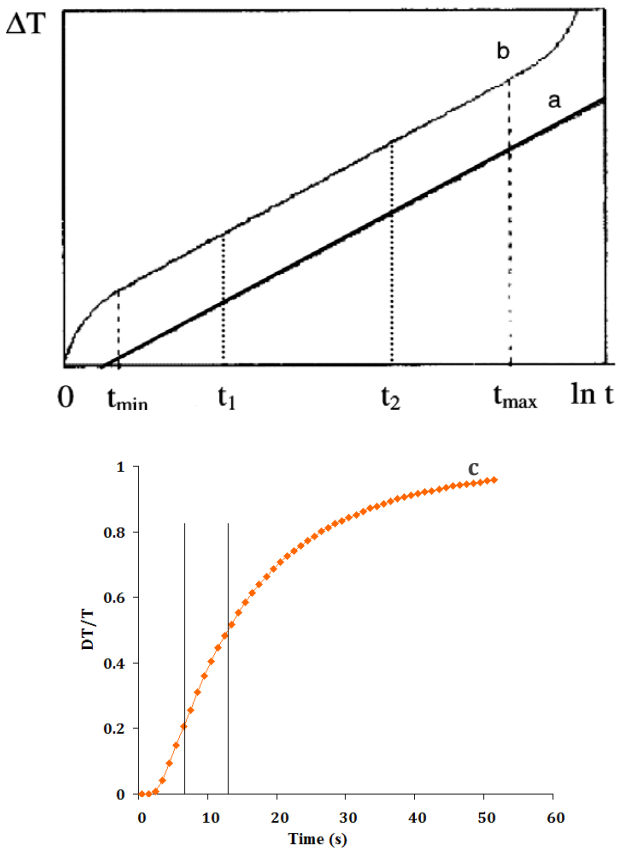

Fig. 2.8. Temperature rise vs. the natural logarithm of time dependence (a) Theoretical curve, (b) Typical experimental curve, (c) Actual experimental curve of sodium nitrate, and the two parallel lines indicate linear region for thermal conductivity calculation.

The schematic of the probe used in this investigation is shown in Figure 2.9. The probe was made of 15cm long close end quartz tube containing a two-hole, insulating ceramic tube and resistance wire. The resistance wire was passed through a two-hole, ceramic insulating tube with the OD 2mm, which was inserted into a quartz capillary with OD 3 mm. A thermocouple was passed through a quartz capillary with OD 1mm and was attached to heating probe at a small radial distance (0.5mm) from the heat source. The resistance wire used was 27-gauge nickel alloy (Karma wire) with specific resistance of 147.7 m Ohm/cm, and the thermocouple was 0.04 mm chromel-alumel. The two ends of the heater were welded to heavier copper wires, and then the joint was strengthened by epoxy resin. The copper wires were connected to a DC power supply to provide voltage for the probe.

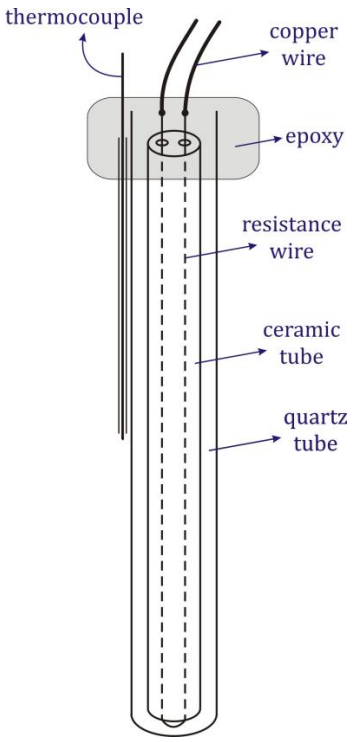

Fig. 2.9. Heating Probe

To ensure theoretical assumption has been satisfied the heating probe was designed to have length to diameter ratio of 50, which is sufficient to serve as line heat source. Also, the thermocouple was placed in quartz capillary at a fixed and short enough radial distance (0.5mm) from the heating source that would allow assuming $(\frac{r^2}{4\alpha.t})$ term in equation (2.4) is negligible. These two very important parameters led us to accurate measurements that are very close to measurements reported by others throughout literature.

2.4. **Experimental Procedure**

To measure the thermal conductivity of alkali salts which are presented in Table.2.1, first salt powder was poured into a ceramic crucible and was placed in a furnace to be heated to above its melting point. Then the molten PCM container was removed from the furnace and the preheated probe was placed at the center of the PCM container, as illustrated in Figure 2.10. The preheating of the probe was found to be necessary to avoid thermal shock and breakage of the quartz tube. For the ambient temperature measurements, the crucible containing the molten PCM and the heating probe was allowed to cool down to ambient temperature. For higher temperature measurements, the PCM crucible was placed inside a molten salt bath at a desired temperature. After the sample and its immediate environment reached thermal equilibrium as registered by a constant thermocouple reading, the current to the probe heater was switched on, the temperature rise of the sample was recorded for 100s, and the thermal conductivity was calculated using equation 2.11. Table 2.1 presents purity, melting point, specific heat, and latent heat of the salts used for thermal conductivity measurements.

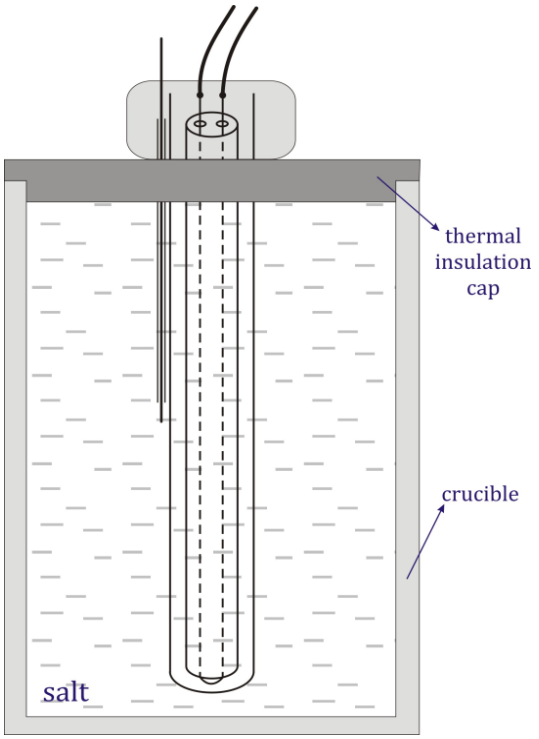

Fig. 2.10. Experimental apparatus.

Table 2.1. Thermal and Physical Properties of Experimental Salts

PCM	Density (gr/cm3)	Melting Point °C	Latent Heat (KJ/Kg)	Specific Heat (kJ/kg.K)	Purchased from
NaNO3 99.9%	2.26	306	172	1.1	Alfa Aesar
KNO3 99.9%	2.11	335	95.4	0.95	Alfa Aesar
LiNO3 99.9%	2.38	250	370	1.6	Alfa Aesar
NaCl 99.9%	2.16	801	466	0.51	Alfa Aesar
KCl 99.9%	1.98	771	-	0.69	Alfa Aesar
Na2CO3 99.9%	2.54	854	275	1	Alfa Aesar
K2CO3 99.9%	2.29	897	236	1.5	Alfa Aesar

2.5. Results and Discussion

The thermal conductivity of several 99.9% pure salts was measured at different temperatures using the heating probe described in section 2.2.1. For each thermal conductivity data point, at least three independent samples were prepared and measured for five times, and the average value of these measurements were listed and compared with the data from the literature in Table 2.2. The deviation of each sample measurement from the average value was less than 2.8%.

As the analytical results from section 2.1.1 of this chapter indicated, the thermal conductivity of PCM has to be at least 7 W/K.m or higher in order to maintain a feasible charging and discharging cycle. The experimental results reveal low (K<7 W/K.m) thermal conductivity for all selected PCM samples. Among the lowest are potassium and sodium nitrate, which are the most common nitrate salts that have been used in medium-temperature, latent-heat storages. For the higher melting temperature PCMs, chloride salts are much better thermal conductor compared to carbonate salts. Although chloride salts exhibit very high latent heat, and they have much higher thermal conductivity compared to other salts that have been presented here. Still, their thermal conductivity is not sufficient (K<7 W/K.m) to reduce charging and discharging cycle times to at least once a day. Therefore, further thermal conductivity improvement has to be done which will be explained in the next two chapters.

Table 2.2. Thermal conductivity of High Melting Point PCMs at Room Temperature

PCM	Melting point °C	Specific Heat (kJ/kh.K)	Latent Heat (KJ/Kg)	Measured Thermal Conductivity (W/k.m)	Literature Thermal Conductivity (W/k.m)
NaNO3	306	1.1	172	0.57	0.51
KNO3	335	0.95	95.4	0.62	0.5
LiNO3	250	1.6	370	0.42	0.59
NaCl	801	0.51	466	4.7	5
KCl	771	0.69	-	3.5	-
Na2CO3	854	1	275	1.44	1.8
K2CO3	897	1.5	236	1.52	1.7

Table 2.2 compares the thermal conductivity of salts measured by our heating probe to values reported in the literature. Although a small difference was recognized, the source of these variation was hard to identify because of lack of information regarding the purity of salt and measurements' temperature in regard to literature values.

Among the measured salts, nitrate salts have the lowest thermal conductivity; however, potassium nitrate and sodium nitrate are the only two salts with the melting temperature in (300-500°C) range, which make them suitable candidates for concentrating solar power plant heat storage application. Therefore, these two salts were selected for more in depth thermal conductivity measurements. To understand the effect of temperature on the thermal conductivity of potassium nitrate and sodium nitrate, thermal conductivity measurements were performed at different temperatures below and above their melting points. The

results as shown in Figure 2.11 indicate that the thermal conductivity of sodium nitrate is almost independent of temperature; however, the thermal conductivity of potassium nitrate decreases by 30% with increases of temperature to around 150°C. A significant decline of thermal conductivity was observed as temperature increased to 150°C.

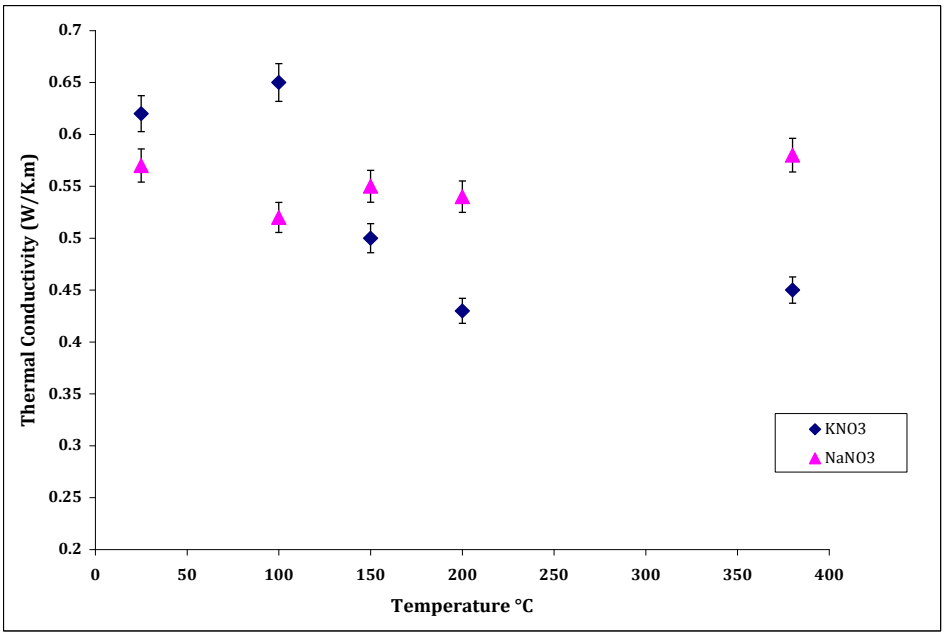

Fig. 2.11. Thermal conductivity of potassium and sodium nitrate as a function of temperature.

To understand the effect of temperature on thermal conductivity of potassium nitrate, a DSC test was done on potassium nitrate salt for 5 cycles from room temperature to 550 °C. The result is shown in Figure.2.12. In both endothermic and exothermic side at about 140°C a small peak was observed, which was reported by Freeman to be crystal transformation from the Orthorhombic to

Rhombohedral [122]. The evidence that the thermal conductivity of Potassium nitrate is decreased at temperature close to 150°C lead us to conclude this crystal transformation was the main reason for depletion of thermal conductivity of potassium nitrate.

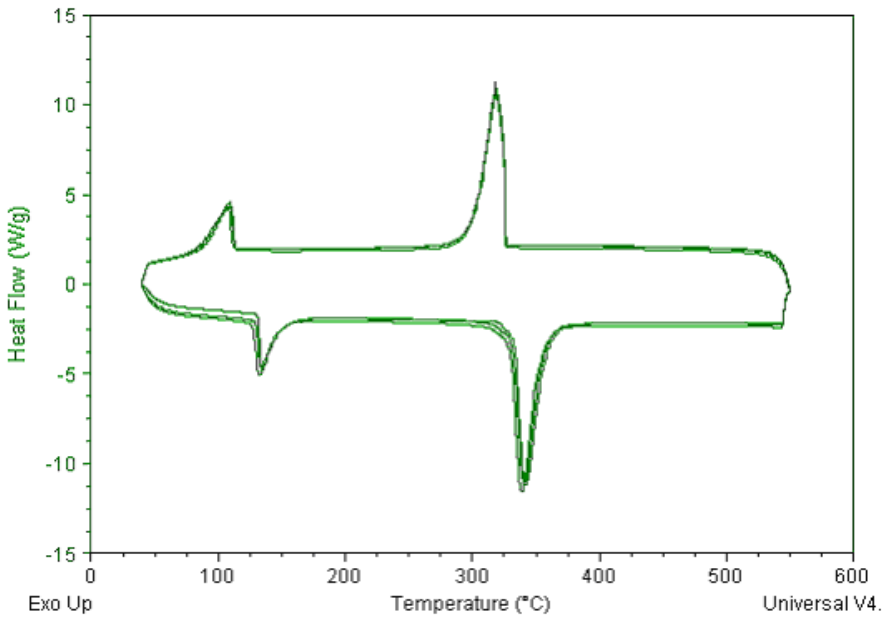

Fig. 2.12. DSC results of potassium nitrate heated up to 550°C and cooled down to 25°C.

Although the operating temperature of latent heat storages are close to melting points of PCMs, in many storages phase-change materials would be heated to much higher temperatures above their melting point to store sensible heat. These high temperature storages raise concerns about thermal stability especially for nitrate salts that contain large amount of oxygen. According to Paniccia [123], molten nitrate salts decompose to their nitrite salts at temperatures above their

melting point. This phenomenon was observed and studied by other scientists, and it was concluded that decomposition of the alkali metal nitrate salts happens in three stages, first negligible nitrite formation, then nitrate-nitrite equilibrium, and finally release of nitrogen oxide which is above 700 °C [122-127].

Kurt et al. [128] calculated the decomposition temperature and thermal behavior of nitrate and nitrite salts at high temperature. They also categorized the decomposition of potassium nitrate into three stages that are explained briefly as following.

I- At 530°C potassium nitrate starts to decompose to potassium nitrite and oxygen:

$$KNO_3 \rightarrow KNO_2 + \frac{1}{2}O_2$$

II- At 550-600 °C, very slowly the reaction starts to move toward the equilibrium, and finally at 650-750°C the reaction stays at equilibrium.

$$KNO_3 \Leftrightarrow KNO_2 + \frac{1}{2}O_2$$

III- At about 790°C, the second stage of decomposition has been observed in which the nitrite starts to decompose:

$$2KNO_3 \Leftrightarrow K_2O + 2NO_2 + \frac{1}{2}O_2$$

Freeman [122] has reported that potassium nitrate is stable at room temperature and starts to melt at 337°C and remain stable up to 530°C with the presence of nitrogen blanket. He also observed the decomposition temperature can be increased by increasing the oxygen pressure. Although there have been several studies on the thermal stability of potassium nitrate, they were all done with the presence of protecting gas. Therefore, several DSC experiment was done on 99.99% pure potassium nitrate without any gas blanket, and the results are presented in Figure2.13.

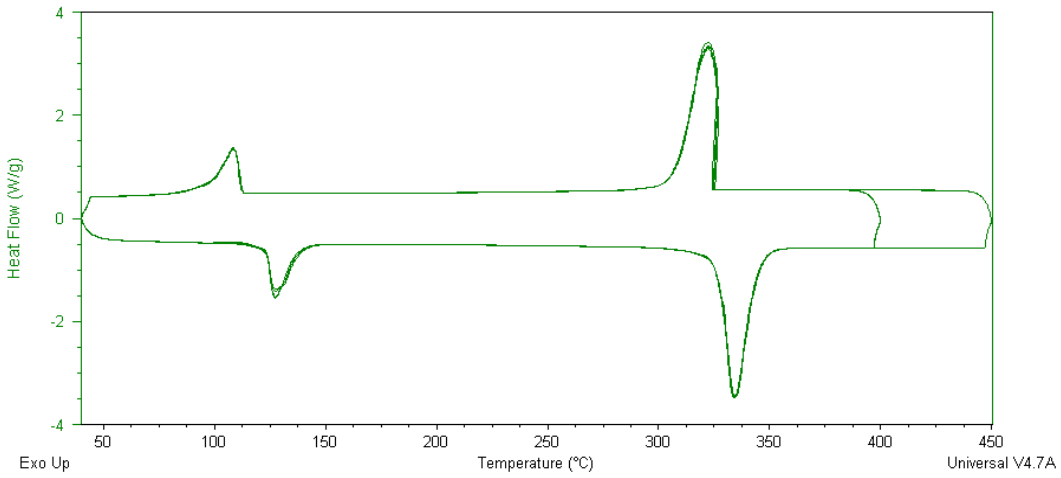

Fig. 2.13. DSC results of potassium nitrate heated up to 450°C.

The DSC curve shows a very smooth melting and solidification during the process and no decomposition up to 450° C is evident. In the endothermic side, the first small peak shows the crystal transformation of the salt from the orthorhombic to

rhombohedral at 143°C, which is consistent with the literature, and the second peak shows the melting point at 337°C which is the same as melting temperature that Freeman, et al. reported. In the exothermic side, the big peak indicates the solidification and the smaller peak shows the crystal transformation.

Because there was no sign of decomposition up to 450°C the experiment was repeated at higher temperatures. In this experiment, a KNO_3 sample was heated from 40°C to 550°C by heating rate of 10°C/Min and then cooled down to 40°C with the same cooling rate. This cycle was repeated 3 times, and the result is shown in Figure 2.14.

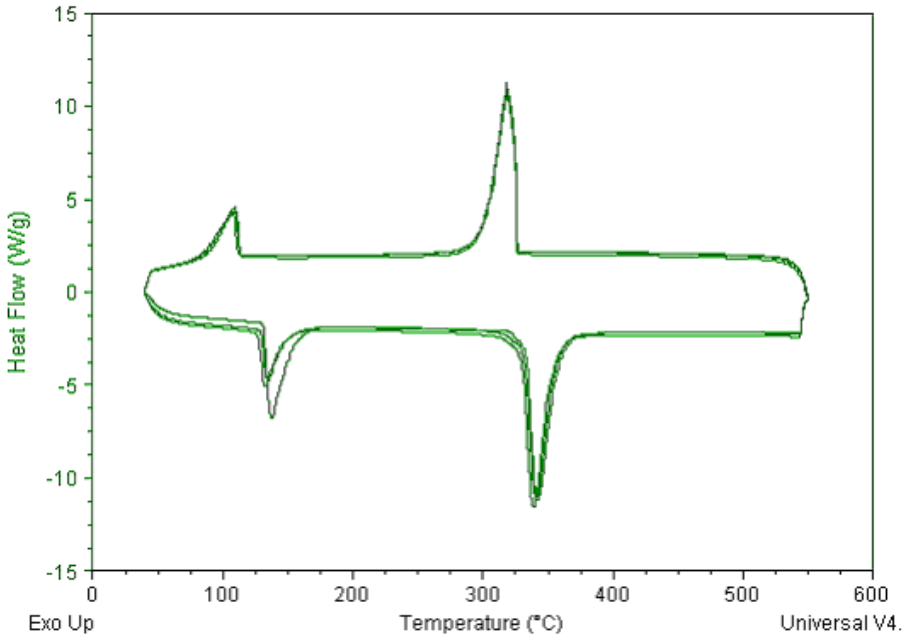

Fig. 2.14. DSC results of potassium nitrate heated up to 550°C.

The DSC result was very similar to the last experiment, except the melting point. The melting point appeared to deviate a little in each cycle from the previous cycle. The changes in melting point maybe due to the appearance of impurity into the sample. Since platinum pan was used in this experiment, there is no reaction between pan and the salt. In addition, the inside of the furnace was protected with high purity nitrogen, which eliminates the possibility of external impurities. Therefore, the impurities created during the process could be the amount of potassium nitrite that has been created from the decomposition of potassium nitrate in each cycle. To investigate this, the previous experiment was repeated for three cycles, and the amount of impurities was calculated using Van't Hoff's law, which is a known method for purity determination and the results are shown in Figure 2.15.

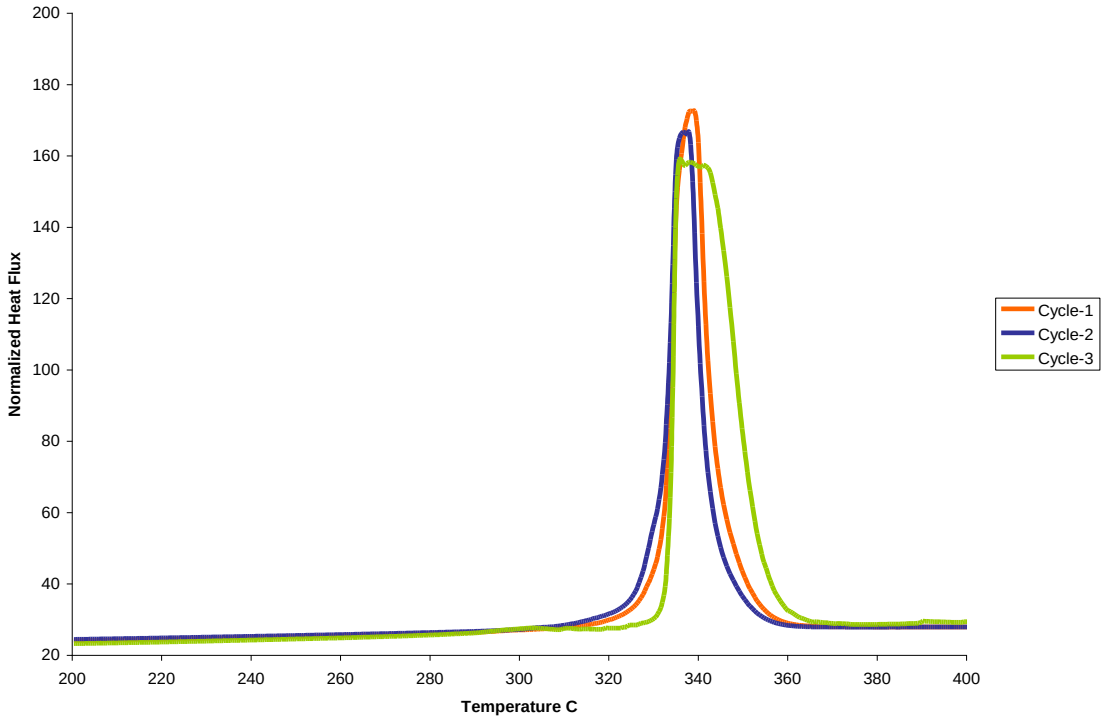

Fig. 2.15. DSC result of KNO_3 heated up to 550 for three cycles and the purity calculation after each cycle.

Van't Hoff's law describes the melting temperature reduction because of rise of impurities [104]. The molar fraction of impurities can be calculated by his equation:

$$X_{1(T)} = \frac{H_2}{R}\left(\frac{T_2 - T}{T_2}\right) \qquad (2.12)$$

where R=8.31441 J/(mol.K) is the molar gas constant, H_2 the melting enthalpy (J/mol) and T_2 the melting temperature of pure material, and T is the melting temperature of impure material. Figure 2.15 shows the melting ranges were

broadened and the melting temperature was reduced with each cycle. The calculated amount of impurities is shown on the graph as well. It is evident in each cycle that a fraction of nitrate salt has been decomposed to nitrite. To find out the optimum heating temperature of potassium nitrate without decomposition, more DSC tests were done, and the amount of impurities were calculated in relationship with temperature. Figures 2.16 and 2.17 presents the DSC results for 99.99% pure KNO_3 at 525°C and 510°C respectively. The decomposition of nitrate to nitrite was observed in both instances, therefore more experiments were done at lower temperature and the results are shown in Table 2.3.

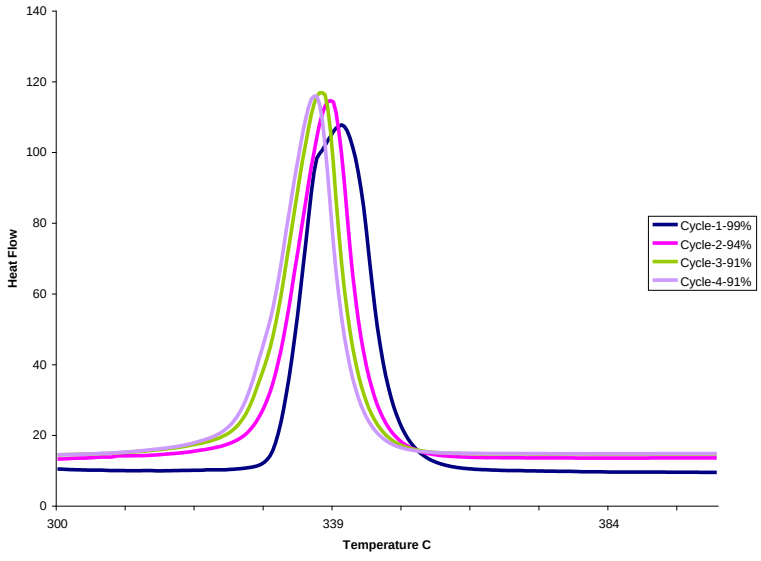

Fig.2.16. Potassium nitrate decomposition and appearance of impurity at 525°C.

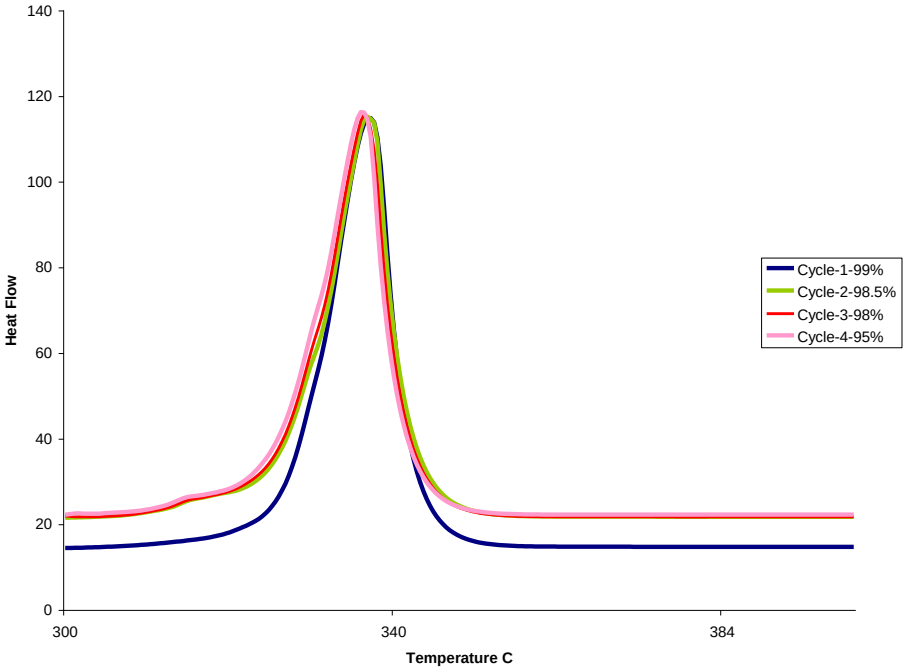

Fig. 2.17. Potassium nitrate decomposition and appearance of impurity at 510°C.

Table.2.3. Amount of Impurity Appearance in Potassium Nitrate Sample after Each Heating Cycle

Cycles	525°C		510°C		500°C		490°C		480°C	
	Temp	Impurity %	Temp	Impurity %	Temp	Impurity %	Temp	Impurity %	Temp	Impurity %
1	339.9	--	335.5	--	337.8	--	337.4	--	339.5	--
2	338	5.98	335	1.50	337.4	1.09	338.1	1.86	337.8	0.94
3	337	8.99	334.9	1.79	337.4	1.14	338.5	2.96	337.5	0
4	337	9.09	334	4.50	337	2.24	338.2	2.15	337.6	0.31
5		--	334	4.56		--		--		--

The experimental results indicated that potassium nitrate is relatively stable at 480°C; however; increases of storage temperature to above 480°C would change the melting behavior of potassium nitrate because of decomposition of nitrate to nitrite.

2.6. **Summary**

Thermal conductivities of several Alkali nitrate, chloride, and carbonate salt samples were measured using the transient, hot-wire method. Chloride salts have higher (3.5-4.7 W/K.m) thermal conductivity compared with nitrate (0.42-0.62 W/K.m) and carbonate salts (1.44-1.52 W/K.m). Furthermore, the studies on the effect of temperature on thermal conductivity of potassium nitrate and sodium nitrate indicated that thermal conductivity of potassium nitrate decreases by about 30% from 0.67 (W/K.m) at 100° C to 0. 48 (W/K.m) at 150° C, which was attributed to the crystal transformation from orthorhombic to rhombohedral at about 140°C. On the other hand, thermal conductivity of sodium nitrate was observed to be independent of temperature.

Also, the thermal stability of potassium nitrate was studied using DSC tests. Van't Hoff's law was used to calculate the amount of nitrate to nitrite decomposition at different temperatures. It was observed that potassium nitrate is stable up to 480°C and the decomposition rate increases with increasing the temperature.

Chapter 3

Enhancement of Thermal Conductivity of PCMs By Using Metal Foams

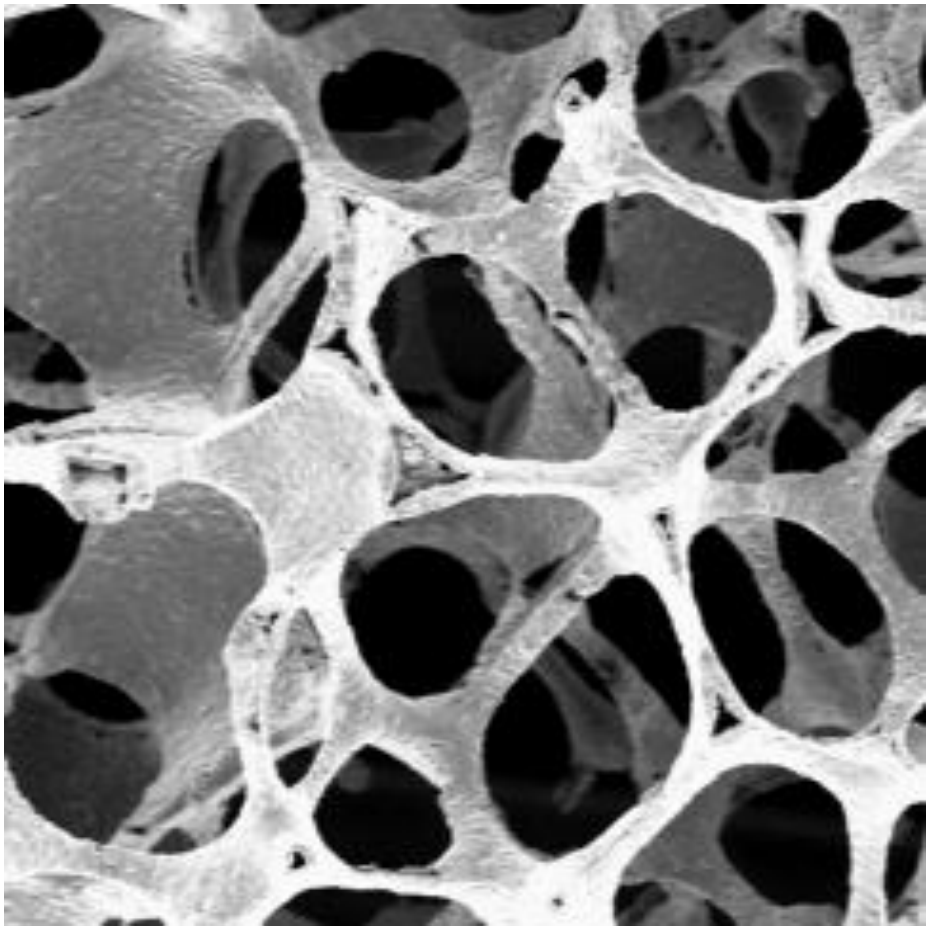

In the previous two chapters, alkali nitrate salts were shown to be more favorable compared to other PCMs for concentrating solar power plants' heat-storage applications. The suitable characteristics of alkali nitrates are their medium range melting temperature (300-500°C), high latent heat of fusion (~200 KJ/Kg), and low cost. Nevertheless, these salts like most of the known PCMs, exhibit low thermal conductivity, which leads to very long charging and discharging cycles. Therefore, to use alkali nitrate as a phase change material, it would be advantageous to enhance their thermal conductivity.

In this chapter, the enhancement of thermal conductivity by creating aluminum-PCM and copper-PCM composites was studied. These metal-PCM composites made by infiltration of PCMs into interconnected porous aluminum and copper foams. The chosen PCMs are potassium nitrate and sodium nitrate because of their moderate melting temperature (300-350°C), high latent heat (90-175 KJ/Kg) and low cost.

The improvement of thermal conductivity of many materials have been achieved by utilizing two major techniques. First is to increase the heat-transfer surface area, and the second is to create a composite by adding high thermally conductive particles into a material with low thermal conductivity. For instance, additions of fin structure, encapsulation methods, and using porous media have been shown to increase the thermal conduction rate by increasing the surface area [42-57].

Similarly for the second approach, adding copper, aluminum, or graphite particles to a low thermal conductivity material to create a composite with high effective thermal conductivity have also been reported [39, 129].

The influence of porous media on thermal conductivity enhancement of the materials has been studied since 1856 by Darcy, Maxwell, and others [130-131]. In recent years, open-cell, metal foam structures have been considered promising candidates for thermal conductivity enhancement in the latent heat storage area, because they have three desirable properties: low density, high strength to weigh ratio, and high surface-area-to-volume ratios. According to ERG (Metal Foam Producer Company). the specific surface area of these foams varies from 500 to 10000 m2/m3 depending on the foam porosity and number of pores per inch (PPI). Moreover, the position of pores and ligaments are closely repeatable and uniform through the material, which allows them to provide accurate density of metal per volume. In addition to the above qualities, the metal foam can be made from a very high thermally conducting metals such as aluminum (218 W/K.m) and Copper (400 W/K.m) [110].

The effects of metal foams on the thermal conductivity of potassium and sodium nitrate were experimentally and analytically investigated. Several analytical models of metal foams base on the pores morphology and their nodes are presented in the following section.

3.1. **Theory and Background**

The early works on the thermal conductivity enhancement of material with the use of porous media were done by Dul'nev, Calmidi, Boomsma, and Singh et al. [132-135]. Dul'nev [135] was among the first who modeled porous media as interconnected cubes; and later on Calmidi and Mahajn [132] modeled a metal foam as a two dimensional plane of hexagonal pores with square nodes, while Boomsma and Poulikakos [133] presented a three-dimensional conduction through a tetrakaidecahedron pores consisting of six squares and eight hexagon with cubic nodes.

3.1.1. **Simple Cube**

Dul'nev was one of the first to present an analytical model of heat conduction trough high-porosity materials [135]. The model considered metal foam as a simple cubic cell through which one-dimensional heat was conducted, as illustrated in Figure. 3.1.

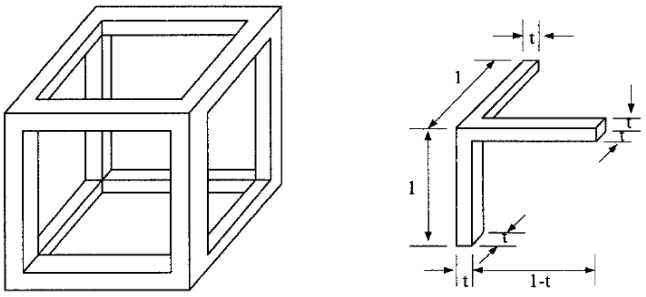

Fig.3.1. Dul'nev model of simple cube.

Where $\delta = \frac{t}{l}$ is the normalized thickness and can be expressed in terms of foam porosity:

$$\varepsilon = \frac{V_{void}}{V_{Cube}} \qquad (2.1)$$

$$\delta = \frac{1}{2} + \cos(\frac{1}{3}\cos^{-1}(2\varepsilon - 1) + \frac{4\pi}{3}) \qquad (2.2)$$

Under the assumptions of one-dimensional heat conduction through the cell without convective and radiation heat transfer in the void, the effective thermal conductivity of the metal foam was presented as:

$$K_e = K_s\delta^2 + K_f(1-\delta)^2 + \frac{2\delta(1-\delta)K_fK_s}{K_s(1-\delta) + \delta K_f} \qquad (2.3)$$

where K_e if the effective thermal conductivity of foam, K_s is thermal conductivity of solid (foam), and K_f is thermal conductivity of fluid.

3.1.2. **Hexagonal Cells with Circular Nodes**

This model presented by Bahttacharya [136], was based on one-dimensional heat conduction in a porous medium consisting of two dimensional array of hexagonal cell with circular lump at the intersection of ligaments. As shown in Figure.3.2.a,

Bahttachrya selected a representative unit cell-base on the symmetry of the foam; which furthermore was divided to five different layers in series as shown in Figure 3.2.b.

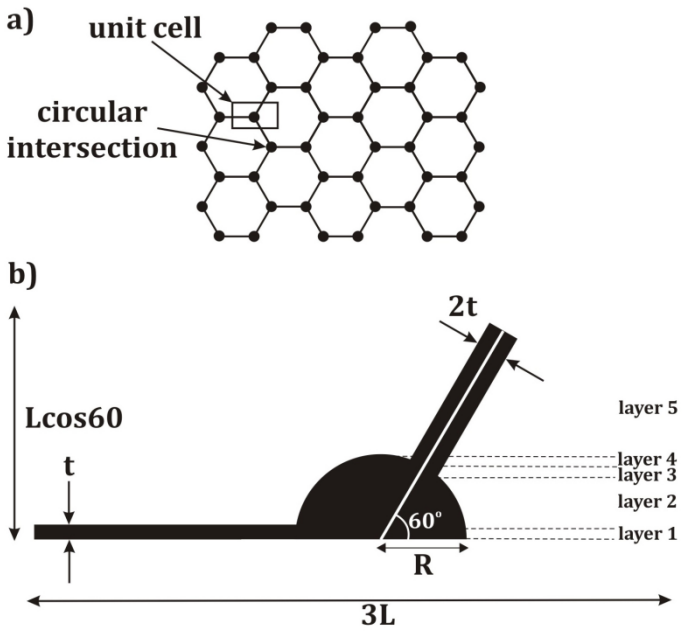

Fig. 3.2. a. Two-dimensional array of hexagonal cell with circular node, and the selected unit cell. b. Five layers in each unit cell [136].

This model considered five layers of foam and the void, which are in series, however, in each layer the foam and void are parallel. Therefore, to calculate the effective thermal conductivity of the unit cell, the thermal conductivity of each layer was calculated based on area fraction and thermal conductivity of each material, as follows:

$$K_n = \frac{A_{n,m}K_m + (A_n - A_{n,m})K_S}{A_n} \qquad (2.4)$$

$n = 1,2,3,4,5$

$$K_1 = K_s + \frac{(K_m - K_S)}{3Lt}(Lt + \frac{R^2}{2}(Sin^{-1}\frac{t}{R} + \frac{t}{R}\sqrt{1-\frac{t^2}{R^2}})) \qquad (2.5)$$

$$K_2 = K_f + \frac{(K_m - K_s)R^2}{\frac{3L}{2}(\sqrt{3(R^2 - t^2)} - 3t}[\sin^{-1}(\frac{1}{2R}(\sqrt{3(R^2 - t^2)} - t)) - \sin^{-1}(\frac{t}{R}) +$$
$$\frac{1}{2}\sin 2(\sin^{-1}(\frac{1}{2R}(\sqrt{3(R^2 - t^2)} - t))) - \frac{1}{2}\sin 2(\sin^{-1}(\frac{t}{R}))]$$

(2.6)

$$K_3 = K_s + \frac{(K_m - K_s)}{3Lt}(Rt + \frac{R^2}{2}(\sin^{-1}\frac{y_2}{R} - \sin^{-1}\frac{y_1}{R} + \frac{1}{2}\sin 2(\sin^{-1}\frac{y_2}{R}) - \frac{1}{2}(\sin 2(\sin^{-1}\frac{y_1}{R})) +$$
$$\frac{\sqrt{3}}{2}\frac{y_2^2 - y_1^2}{2} - \frac{\sqrt{3}}{2}y_1 t)$$

(2.7)

$$K_4 = K_s + \frac{(K_m - K_s)}{3L(R - y_2)}(R^2(\frac{\pi}{2} - \sin^{-1}\frac{y_2}{R}) - \frac{R^2}{2}\sin 2(\sin^{-1}\frac{y_2}{R}) + \frac{4t}{\sqrt{3}}(R - y_2))$$

$$K_5 = K_s + (K_m - K_s)\frac{4t}{3\sqrt{3}L}$$

(2.8)

Therefore, the thermal conductivity trough the selected unit-cell calculated based on heat conduction through a series of five layers using Fourier's law.

$$K_e = \frac{L_1 + L_2 + L_3 + L_4 + L_5}{\frac{L_1}{K_1} + \frac{L_2}{K_2} + \frac{L_3}{K_3} + \frac{L_4}{K_4} + \frac{L_5}{K_5}} \tag{2.9}$$

where L_n is the thickness of each layer, K_n is the thermal conductivity of each later, K_s is thermal conductivity of solid (foam), and K_f is thermal conductivity of fluid, R is the radius of lump.

3.1.3. **Tetrakaidecahedron Pores with Cubic Nodes**

One of the most recognized structures of high porosity foams is tetrakaidecahedron, which has been studied extensively [133]. In this structure, each pore consists of six squares and eight hexagons as has been illustrated in Figure.3.3. This analytical model is represented in three-dimensional tetrakaidecahedron pore by assuming cubical nods and cylindrical ligaments. The length of the cubic nod is shown by r, the ligament is defined by its length, L, and the cross-section radius of a, as presented in Figure.3.4.

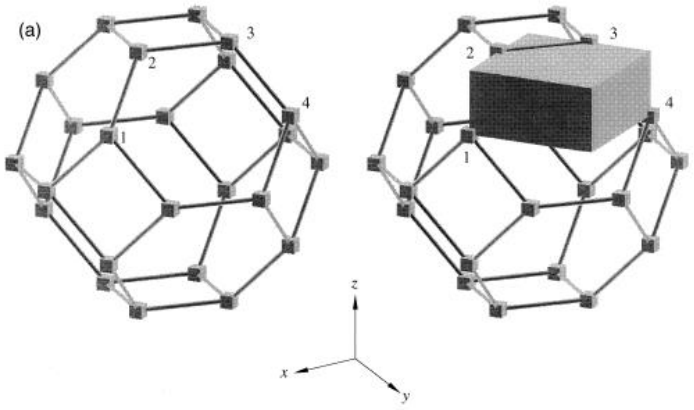

Fig. 3.3. The tetrakaidecahedron model with cylindrical ligaments and cubic nodes [133].

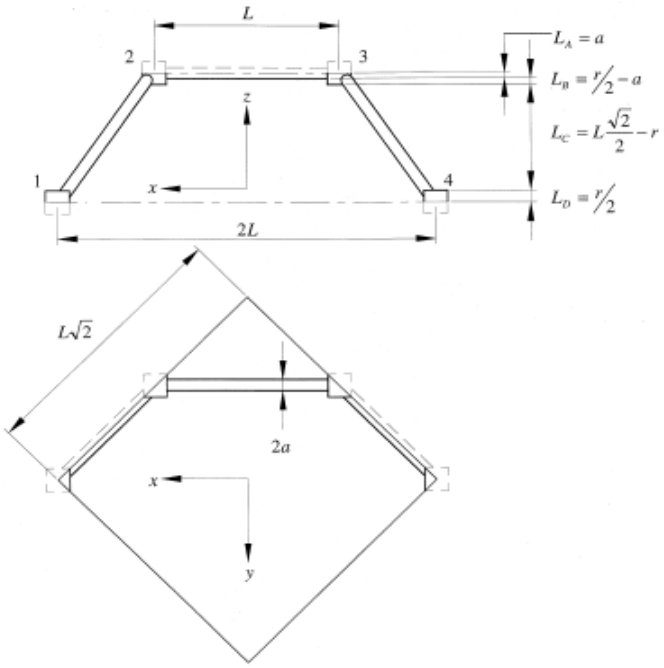

Fig. 3.4. . Rectangular cube sides.

The cubic representative section in Figure 3.3 was chosen based on the symmetry. This section covers one-sixteenth of a single tetrakaidecahedron pore.

As shown in Figure 3.4, the sides of the rectangular unit cell in x-y plane are $L\sqrt{2}$, and the height of the cell in z direction is $L\frac{\sqrt{2}}{2}$. Furthermore, the cubic cell was divided to four layers from top to bottom. In each layer, the volume of each rectangular section was calculated simply by multiplying the unit cell area in the x-y plane by the z, height of the individual sections. Knowing the volume of foam and void in each layer, the porosity was then calculated as:

$$\varepsilon = 1 - \frac{\sqrt{2}}{2}(de^2 + \frac{1}{2}d^2\pi(1-e) + (\frac{1}{2}e - d)e^2 + \pi d^2(1-2e\sqrt{2}) + \frac{1}{4}e^3)$$

(2.10)

where (e) and (d) are two non-dimensional relations $e = \frac{r}{L}$, $d = \frac{a}{L}$, which were used to simplify the equations. The values of d and e have to be determined to obtain the effective thermal conductivity as a function of porosity. Solving the above equation for an arbitrary porosity, ε, results in a quadratic solution for d. The amount of e should be estimated by experimental measurements of effective thermal conductivity based on porosity.

$$d = \sqrt{\frac{\sqrt{2}(2 - (5/8)e^3\sqrt{2} - 2\varepsilon)}{\pi(3 - 4e\sqrt{2} - e)}}$$

(2.11)

The effective thermal conductivity was calculated by averaging the thermal conductivity of each section based on the volume fraction and thermal conductivity of each material as follow:

$$K_n = \frac{V_{n,m}K_m + (V_n - V_{n,m})K_S}{V_n}$$

$$n = A, B, C.D$$

(2.12)

where A, B , C, and D are name of each layer.

Therefore, the thermal conductivity trough the selected cubic section is calculated based on heat conduction through a series of four levels using Fourier's law.

$$K_{eff} = \frac{L_A + L_B + L_C + L_D}{\left|\frac{L_A}{K_A}\right| + \left|\frac{L_B}{K_B}\right| + \left|\frac{L_C}{K_C}\right| + \left|\frac{L_D}{K_D}\right|} \qquad (2.13)$$

$$\frac{L_A}{K_A} = \frac{4d}{2e^2 + \pi d(1-e)K_m + (4 - 2e^2 - \pi d(1-e)K_s} \qquad (2.14)$$

$$\frac{L_B}{K_B} = \frac{(e-2d)^2}{(e-2d)e^2K_m + (2e - 4d - (e-2d)e^2)k_s} \qquad (2.15)$$

$$\frac{L_C}{K_C} = \frac{(\sqrt{2} - 2e^2)}{2\pi d^2(1-2e\sqrt{2})K_m + 2(\sqrt{2} - 2e - \pi d^2(1-2e\sqrt{2}))K_s} \quad (2.16)$$

$$\frac{L_D}{K_D} = \frac{2e}{e^2 Km + (4-e^2)K_s} \quad (2.17)$$

$$d = \sqrt{\frac{\sqrt{2}(2-(5/8)e^3\sqrt{2} - 2\varepsilon)}{\pi(3-4e\sqrt{2}-e)}} \quad (2.18)$$

$$K_{eff} = (\frac{\sqrt{2}}{2(R_A + R_B + R_C + R_D)}) \quad (2.19)$$

3.1.4. **Pentagonal Dodecahedron**

This model was presented by Truong et al. [137] based on perfect regular pentagonal dodecahedron geometry to estimate the characteristics of the solid foams and structural relationship. Depending on the porosity of the solid foam, the authors assume either ‘‘slim’’ foam, Figure 3.5.A, or ‘‘fat’’ foam, Figure 3.5.B [137]. Slim foams are foams with higher porosity and no ligament intersection lumps, while the fat foams are lower porosity foams with intersection lumps. In this model the main characteristic lengths used to describe the solid foam are the cell diameter (Φ), pore diameter (a), and strut diameter (d_s) as shown in Figure 3.5.

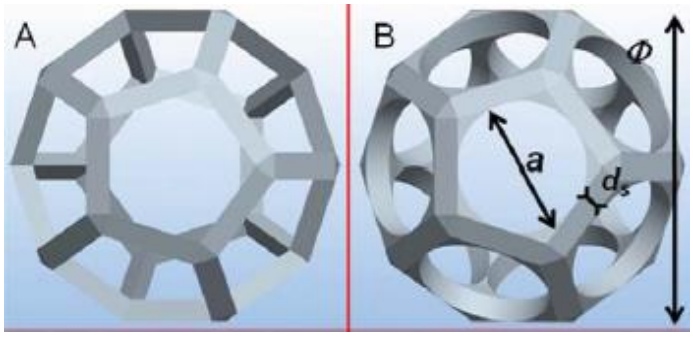

Fig. 3.5. Solid foam with pentagonal dodecahedron Structure A. Slim foam. B. Fat foam [137].

Based on the numerous similarities between solid foams and packed dodecahedron, this geometrical model is revealed to be quite close to the real structure of a unit cell constituting the solid foam. Moreover, this approach gives a very flexible representation that enables one to describe the specific surface area, pressure drop, and external solid-fluid mass transfer with a simple relationship that involves the porosity and the cell diameter. To determine the two limiting values of effective thermal conductivity for marginal cases (‘‘slim’’ or ‘‘fat’’ foam with triangular struts) was considered. Ratios of solid volume (V_{solid}) to the volume of unit cell ($V_{dodecahedron}$) for, respectively, ‘‘slim’’ and ‘‘fat” foam are given by:

$$(1-\varepsilon)=\frac{V_{S\,\lim,Solid}}{V_{dodecahedron}}=\frac{V_{Skeleton,S\,\lim}}{V_{dodecahedron}}=E_s{}^2\frac{\sqrt{15}}{\varphi^4}-E_s{}^3\frac{\sqrt{10}}{3\varphi^4} \qquad (2.20)$$

$$(1-\varepsilon)=\frac{V_{Fat,Solid}}{V_{dodecahedron}}=\frac{V_{Skeleton,Fat}}{V_{dodecahedron}}+\frac{V_{deadvol}}{V_{dodecahedron}} \qquad (2.21)$$

$$\frac{V_{Skeleton}}{V_{dodecahedron}} = E_f{}^2 \frac{\sqrt{15}}{\varphi^4} - E_f{}^3 \frac{\sqrt{10}}{3\varphi^4} \qquad (2.22)$$

$$\frac{V_{deadvol}}{V_{dodecahedron}} = \frac{40 \dfrac{\sin^2(\frac{\pi}{5})\varphi^2 (1-\frac{E_f}{2}\sqrt{\frac{2}{3}})^3}{32\sqrt{3}(3-\varphi)} \sqrt{(\frac{1}{4} - \frac{\sin^2(\frac{\pi}{5})\varphi^2}{9-3\varphi})}}{\sqrt{5}\varphi^4} +$$

$$\left(\frac{12E_f}{\sqrt{5}\varphi^4}\right)\left(\frac{5\varphi}{4\sqrt{3-\varphi}} - \frac{\pi}{4}\frac{\varphi^2}{(3-\varphi)}\right)\left(1-\frac{E_f}{2}\sqrt{\frac{2}{3}}\right)^2$$

(2.23)

where $V_{deadvol}$ is the volume of matter accumulates at the strut connection, and E_s or E_f are the ratio between d_s (strut side), and c (side of the perfect pentagon length).

Then, a thermal-conductivity averaging technique was used to estimate the effective thermal conductivity (K_{eff}) of the porous media considering only the porosity, the solid volume, and the unit-cell volume. In this technique, first, a unit cell based on the symmetry was chosen. Then the unit cell would be divided into its characteristic parts. Finally, thermal conductivity is calculated by averaging the thermal conductivity of each part (or layer) on the basis of the individual volume fractions and their respective thermal conductivities, which is given by the following relation:

$$K_n = \frac{V_{n,Solid} K_s + (V_{n,Cell} - V_{n,Solid}) K_f}{V_{n,Cell}} \qquad (2.24)$$

Afterward, the effective thermal conductivity of the cell is calculated by the method of electrothermal analogy [110], which consists of combining the different layers as series or parallels. In case of layers in series, K_{eff} of the unit cell can be written as:

$$\frac{\sum_{1}^{n} L_n}{K_{eff}} = \sum_{1}^{n} \left(\frac{L_n}{K_n}\right) \qquad (2.25)$$

where K_n is given by the relation to each layer, and L_n is the heights of each layer.

3.1.5. **Cubic Pore with Cubic Nodes:**

Edward [138] has presented a cubic-pore model based on the assumption of slim and fat foams which was introduced in the previous section. In this model, the modified cubic lattice, Figure 3.6, is divided into three layers in a series, namely, L_1, L_2, and L_3. In each cube, the solid volume consists of the contribution of the 12 cylindrical struts and 8 cubes at their meeting point. Moreover, in the unit-cell volume, each strut is shared by four cubic lattices and each cube is shared by eight cubic lattices. Consequently, only a quarter of each strut volume and an

eighth of each cube volume have to be considered for calculating the solid volume of each layer

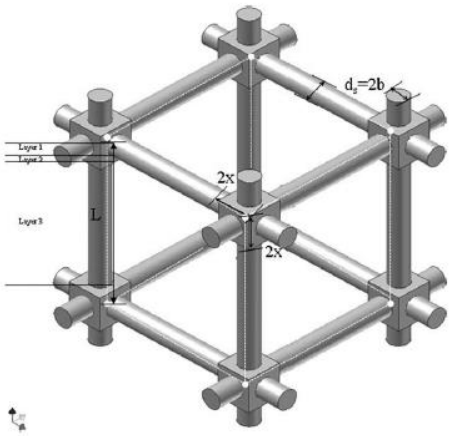

Fig. 3.6. Each cube layer [138].

Similar to previous models, the porosity was calculated based on the volume of each layer as follows:

$$(1-\varepsilon)=\frac{2V_{1,Solid}+2V_{2,Solid}+V_{3,solid}}{2V_{1,Cell}+2V_{2,Cell}+V_{3,Cell}}=\frac{3\pi b^2(L-2x)+8x^3}{L^3}$$
$$x=yb$$
$$y=1+\delta \qquad (2.26)$$
$$d=\frac{b}{L}$$

$$(1-\varepsilon)=3\pi d^2(1-2d)+8d^3+\delta d^3(8\delta^2+24\delta+24-6\pi) \qquad (2.27)$$

The next step would be to use the geometry of regular cube with the same porosity to develop a direct analogy between foam and the layered cubic lattice

model and, thus, estimate d and δ. When no matter accumulates at the strut connection (δ=0), we can use the ‘‘slim’’ foam model directly for estimating d as:

$$\frac{V_{\text{slim},Solid}}{V_{dodecahedron}} = 3\pi d^2(1-2d) + 8d^3 \qquad (2.28)$$

In contrast, when the matter at the strut connection cannot be neglected, the ‘‘fat’’ model is used to estimate the value of d and δ

$$\frac{V_{fat,solid}}{V_{dodecahedron}} \Rightarrow \frac{V_{skeleton,fat}}{V_{dodecahedron}} = 3\pi d^2(1-2d) = 8d^3 \qquad (2.29)$$

$$\frac{V_{fat,solid}}{V_{dodecahedron}} \Rightarrow \frac{V_{deadvol}}{V_{dodecahedron}} = \delta d^3(8\delta^2 + 24\delta + 24 - 6\pi) \qquad (2.30)$$

Knowing the value of porosity (ε), therefore E_s and E_f are known. d and δ can be calculated, and the thermal conductivity of each layer can be written as:.

$$K_1 = \frac{(\pi b^2(L-2x) + 4bx^2)K_s + (L^2 b - (\pi b^2(L-2x) + 4bx^2))K_f}{L^2 b} \qquad (2.31)$$

$$K_2 = (4y^2 d^2)K_s + (1-4y^2 d^2)K_f \qquad (2.32)$$

$$K_3 = (\pi d^2)K_s + (1-\pi d^2)K_f \qquad (2.33)$$

Therefore, the effective thermal conductivity trough a unit cell, is the thermal conductivities of the individual layers in series.

$$\frac{1}{K_{eff}} = \frac{2d}{(d^2(4y^2 - 2\pi y) + \pi d)K_s + (d^2(2\pi y - 4y^2) - \pi d + 1)K_f} + \frac{2d(y-1)}{(4y^2d^2)K_s + (1-4y^2d^2)K_f} + \frac{(1-2dy)}{(\pi d^2)K_s + (1-\pi d^2)K_f} \quad (2.34)$$

All the analytical models presented above reported that foam structure has a large effect on the effective thermal conductivity and can be used to improve heat conduction through low thermal conductivity materials. For instance, the hexagonal model by Battacharya et al. [136] showed the effective thermal conductivity depends strongly on the porosity and the ratio of the cross-section of the fiber and the intersection lump. Also, their experimental measure indicated the thermal conductivity of water was improved from 0.6 W/K.m to 2.7 W/K.m with the use of 90% porosity aluminum foam. The tetrakaidecahedron model by Boomsa [133] showed that despite the high porosity of the metal foam, the heat conductivity of metal controls the overall effective thermal conductivity to a large extent. This model predicted the effective thermal conductivity of aluminum-air and aluminum-water with the use of 95% porosity foam would be 3.82 W/K.m and 4.69 W/K.m, respectively, compared to the thermal conductivity of water (0.6 W/K.m) and air (0.2 W/K.m). Although the thermal conductivity of high porosity medium has been studied widely, there are not enough experimental and analytical studies on the effective thermal conductivity of high porosity material such as metal foams. The increasing demand for improving the thermal

conductivity of PCM has led us to study effect of aluminum and copper foam on thermal conductivity enhancement of potassium nitrate and sodium nitrate.

3.2. Aluminum-PCM and Copper-PCM Composite Samples Preparation

To improve the thermal conductivity of these salts, metal-PCM composites were designed consisting of aluminum or copper foam and potassium nitrate or sodium nitrate PCMs. The metal foams that were selected to be used as composite matrix were acquired from ERG (Address: 900 Stanford Avenue Oakland, CA 94608). The aluminum foam was constructed from 6101-T6 aluminum alloy with thermal conductivity of 218 (W/K.m), specific heat capacity of 0.895 (KJ/Kg.K), melting point of 621-654°C, and copper foam was constructed from C10100 copper with thermal conductivity of 391 (W/K.m), Specific heat capacity of 0.385 (KJ/Kg.K), melting point of 1083°C. The thermal properties of potassium nitrate and sodium nitrate used were presented in Table.2.1 of chapert.2.

The composites were prepared by infiltration of molten PCM into metal foams. To accomplish the infiltration process, first foam was submerged into a molten PCM crucible. Then the crucible was placed in an atmospheric controlled furnace, and heated up to 30° C above the PCM melting point. The furnace was then vacuumed to -1Psi, and then pressurized with pure argon to 15 Psi for 10 minutes to ensure

molten PCM infiltrated into the foam pores uniformly. After cooling down and PCM solidification, the sample was removed from the crucible with some excess PCM still surrounding. A 3mm diameter whole was then drilled at the center, and along the height of the sample to accommodate the heating probe. Figure.3.7 shows a schematic of a prepared Metal-PCM composite.

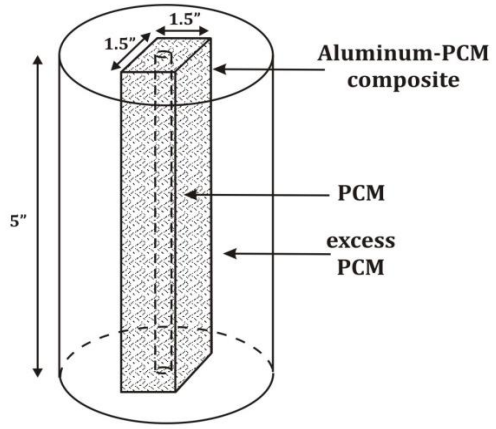

Fig.3.7. Aluminum-PCM composite specimen.

3.3. **Thermal Conductivity Measurements Using Hot Wire Technique:**

The transient hot-wire technique was applied to measure the thermal conductivity of the composite samples with the use of the heating probe described in the previous chapter. The design and details of this probe can be found in section 2.2.1 of chapter 2. For the ambient temperature measurement, the heating probe was inserted into the sample pre-drilled hole and powered. The rise of temperature as a function time was then recorded, and the thermal conductivity was determined using equation 2.11. Figure 3.8 presents a

temperature versus time for potassium nitrate and sodium nitrate composites. As was explained in chapter 2, to prevent measurement errors due to the required time to heat up the probe and the small gap between the probe and the sample, the linear portion of the temperature-time curve, shown by two black parallel lines in this graph, have to be used. For higher temperature measurements, the samples with the excess PCM and the heater were placed in a crucible and then was placed into constant temperature salt bath to reach the desired measurement temperature, as schematically shown in Figure.3.9. The temperature of the sample was measured trough the heating probe's thermocouple to ensure that sample has reached the equilibrium temperature with the salt bath. Then the thermal conductivity measurement was started by turning the heating probe on.

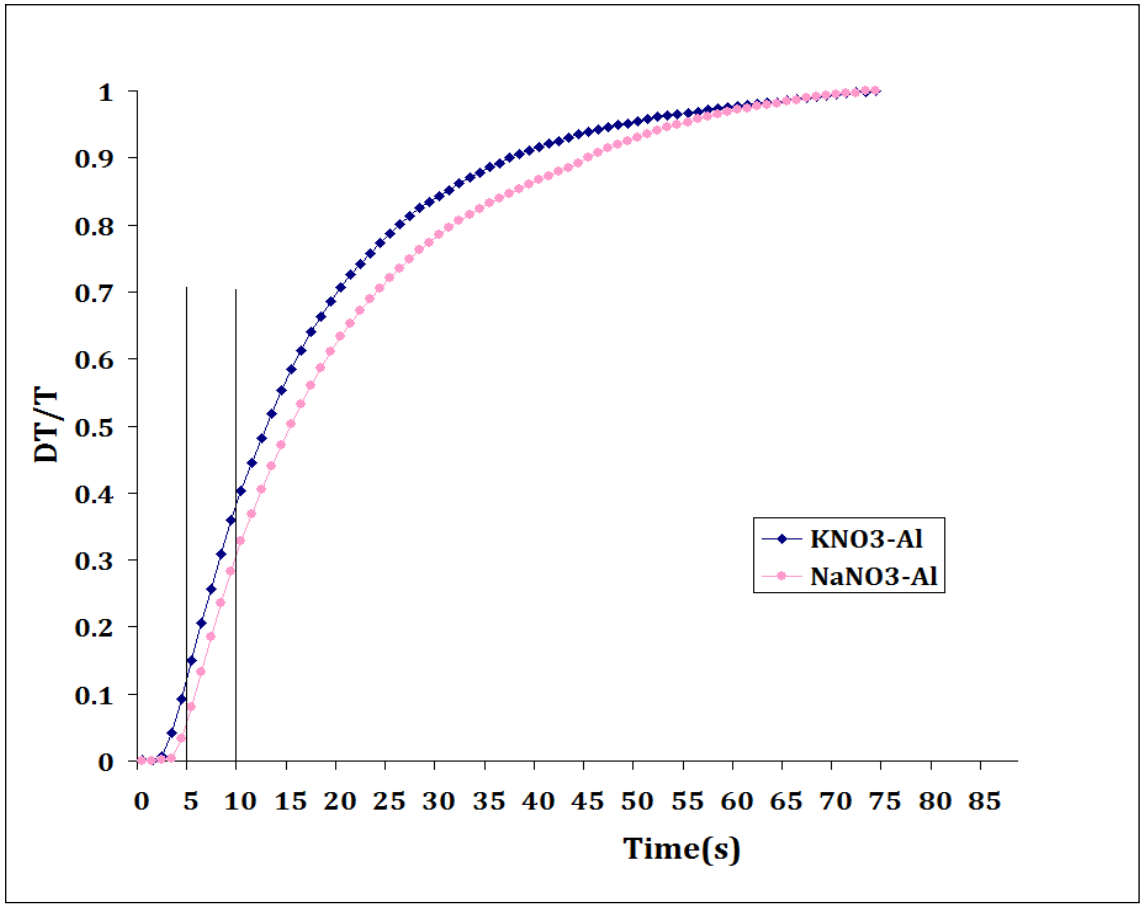

Fig. 3.8. Temperature rise versus time of $KNO_3 - Al$ and $NaNO_3 - Al$. The vertical lines indicate the region used for the thermal conductivity calculation.

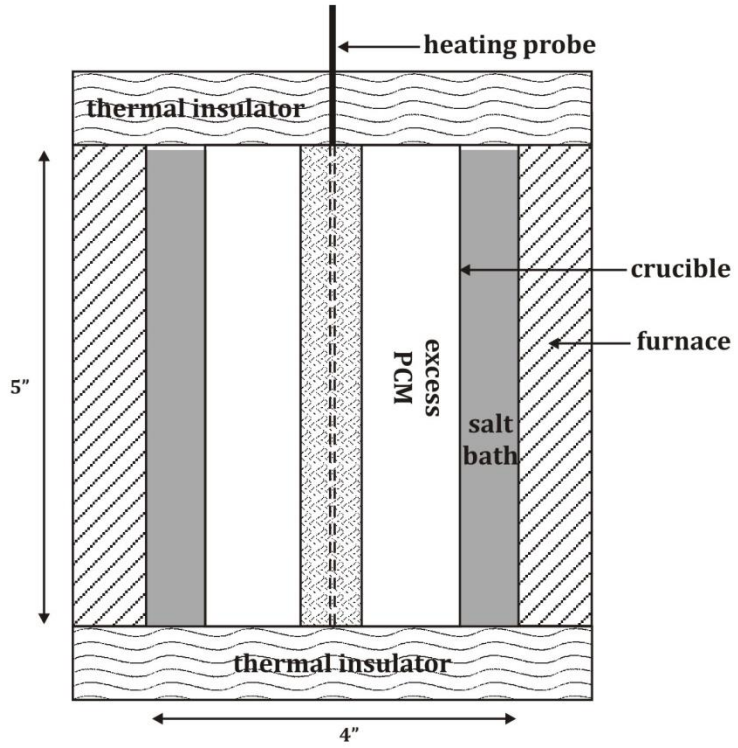

Fig.3.9. Experimental apparatus for high temperature thermal conductivity measurements.

3.4. **Results and Discussion**

Several aluminum-PCM and copper-PCM composites were prepared with the use of three different porosity foams. The thermal conductivities of the specimens were measured as a function of porosity and temperature using above apparatus. Table.3.2 presents volume percentage and weight percentage composition of each specimen. Each reported data represents an average value of three measurements for each specimen, and the standard deviation for each data point was less than 4%.

Table 3.1. Salt volume percentage and the composition of specimens by wt%.

Composite No.	Composite Type	Salt Volume%	Pore per Inch	Composition, wt%
1	Aluminum/ KNO_3	92	10	10%Al.-90% KNO_3
2	Aluminum/ KNO_3	75	10	30% Al.-70% KNO_3
3	Aluminum/ KNO_3	60	10	46%Al.-54% KNO_3
4	Aluminum/ $NaNO_3$	92	10	9%Al.-91% $NaNO_3$
5	Aluminum/ $NaNO_3$	75	10	28%Al.-72% $NaNO_3$
6	Aluminum/ $NaNO_3$	60	10	44%Al.-56% $NaNO_3$
7	Copper/ KNO_3	92	10	29% Cu-71% KNO_3
8	Copper/ KNO_3	75	10	59%Cu-41% KNO_3
9	Copper/ KNO_3	60	10	75% Cu-25% KNO_3
10	Copper/ $NaNO_3$	92	10	28%Cu-72% $NaNO_3$
9	Copper/ $NaNO_3$	75	10	57%Cu-43% $NaNO_3$
10	Copper/ $NaNO_3$	60	10	73%Cu-27% $NaNO_3$

The effective thermal conductivity is plotted as a function of PCM volume fraction for both aluminum and copper based composites in Figure.3.10. Potassium nitrate (k=0.62 W/K.m) and sodium nitrate (K=0.57 W/K.m) was used for PCM in both cases. The figure presents the measured effective thermal conductivity of

aluminum-PCM composites at solid and liquid states. The effective thermal conductivities are in the range of 1.7-7.2 (W/K.m) for potassium nitrate and are in the range of 1.9-4.9 (W/K.m) for sodium nitrate composites. As such, compared to the pure salts, the effective thermal conductivities of both salts were increased by factor of 2.7-11 depending on aluminum volume fractions.

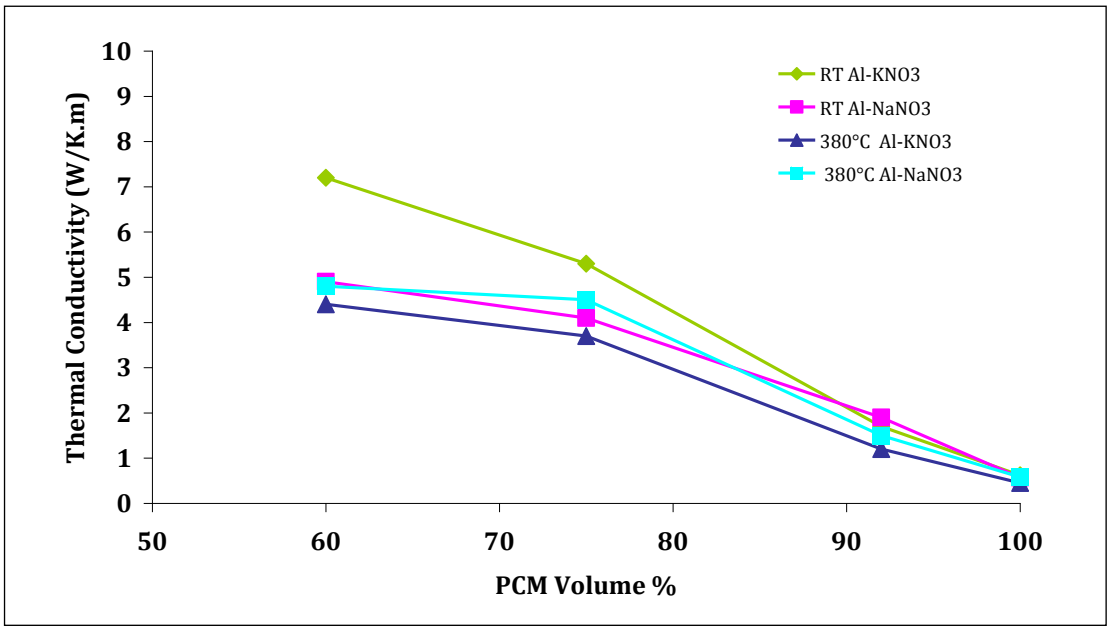

Fig. 3.10. The thermal conductivity of Al.-PCM composite as a function of PCM volume % .

Figure.3.11 illustrates the effective thermal conductivity of copper-PCM composites as a function of PCM volume fraction for both potassium nitrate and sodium nitrate composites. The effective thermal conductivities of potassium

nitrate composites were in between the range of 6.3 W/K.m to 19.5 W/K.m, and sodium nitrates were in the range of 5.9-18.7 W/K.m. Comparing the results of figure 3.10 and 3.11 reveals that the effect of copper foam on effective thermal conductivity of the composites are more pronounced because of higher thermal conductivity of copper (391 W/K.m). The effective thermal conductivity of Cu-KNO_3 was higher than pure potassium nitrate by factors of 10.1, 24.4, and 31.5 for 92%, 75%, and 60% salt volume fraction, respectively. Similar results were observed for Cu-$NaNO_3$ composites in which the effective thermal conductivities of composite were 10.3-32.8 times higher than pure sodium nitrate. It can be seen that the effective thermal conductivity of these composite are correlated with the volume fraction of the metal, an increase of metal volume fraction would result in higher effective thermal conductivity in metal foam-PCM composites. It can also be seen that in both aluminum and copper based composites the increase of effective thermal conductivity is slower from 25% to 40% metal volume fraction compared to 8% to25%.

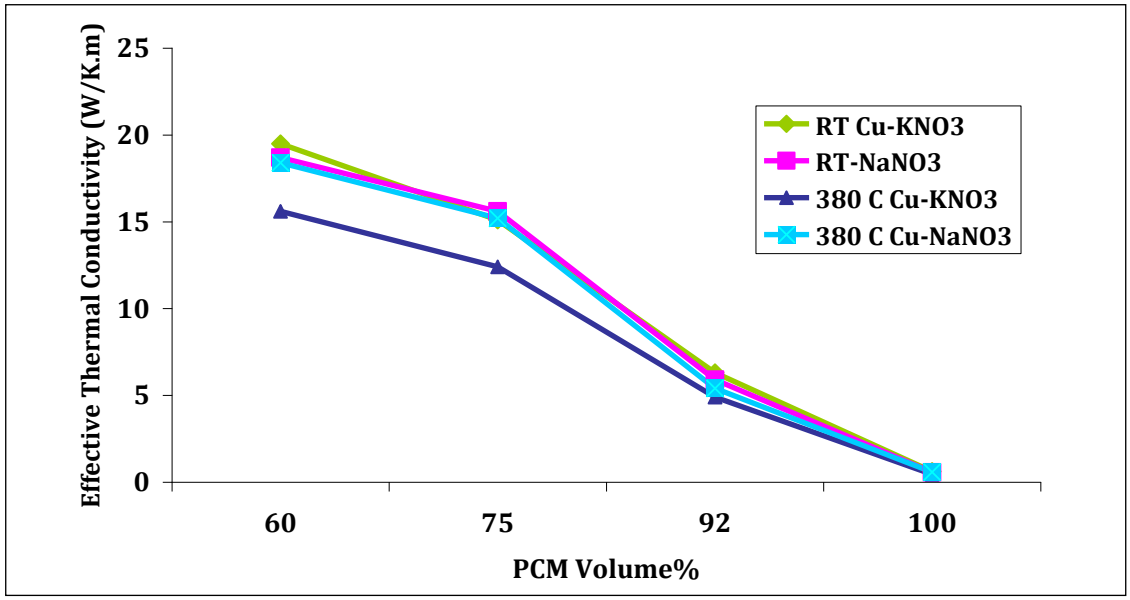

Fig. 3.11. The thermal conductivity of Cu-PCM composite as a function of PCM volume %.

Overall, the effective thermal conductivities of Cu-PCM composites were higher by a factor of 3-4 compared to Al-PCM composites for the same metal volume fractions. Although Cu-PCM composites are better thermal conductive materials, lower porosity copper foams might not be the best material for high capacity heat storages because of high density of copper, which results in lower PCM weight percent. Table 3.3 compares the PCM weight percentages, metal foam porosities, and the effective thermal conductivity improvement for all the composite samples. For example, the 92% aluminum and 92% copper foams resulted in a composite with 89wt% PCM and 71 wt% PCM respectively, and the effective thermal conductivity of Aluminum based composite is 1.7 W/K.m while copper based composite is 6.3 W/K.m. Thus 92% copper foam composites increase the

effective thermal conductivity about four times more than 92% aluminum composite, but 92% aluminum composite can store 18% more latent heat compared to 92% copper foams.

Table 3.2. Comparison of PCM wt% and Porosity on Thermal conductivity of Al-PCM Composite

PCM	Metal Foam & Porosity	PCM Wt%	K Enhancement Factor
KNO_3	Al-92%	90	2.7
KNO_3	Al-75%	69	8.5
KNO_3	Al-60%	53	11.6
$NaNO_3$	Al-92%	90	3.3
$NaNO_3$	Al-75%	71	7.2
$NaNO_3$	Al-60%	55	8.6
KNO_3	Cu-92%	71	10.1
KNO_3	Cu-75%	41	24.4
KNO_3	Cu-60%	25	31.5
$NaNO_3$	Cu-92%	72	10.4
$NaNO_3$	Cu-75%	43	27.4
$NaNO_3$	Cu-60%	27	32.8

Furthermore, the effective thermal conductivity of the same composites reported in Table 3.2 was measured as a function of temperature, and the results are presented in Figure 3.12 and Figure 3.13, along with thermal conductivity measurements of pure potassium nitrate and sodium nitrate from chapter 2.

Thermal conductivity of 99% pure potassium nitrate indicates a slight decrease with the increase of temperature as discussed in section 2.4 of chapter 2. A similar pattern is observed in the Al-KNO_3 composites (composite #1-3) and Cu-KNO_3 composites (composite7-9). However, the thermal conductivity of sodium nitrate is almost independent of temperature, and the same results are observed in sodium nitrate's composite (composite#3-6 and 9-12). In conclusion, potassium nitrate composites have higher thermal conductivity compared with sodium nitrate at lower temperatures, but their thermal conductivity decreases significantly (11-30%) at temperature above 150°C. On the other hand, sodium nitrate composites maintain relatively stable thermal conductivity across a wide range of temperatures.

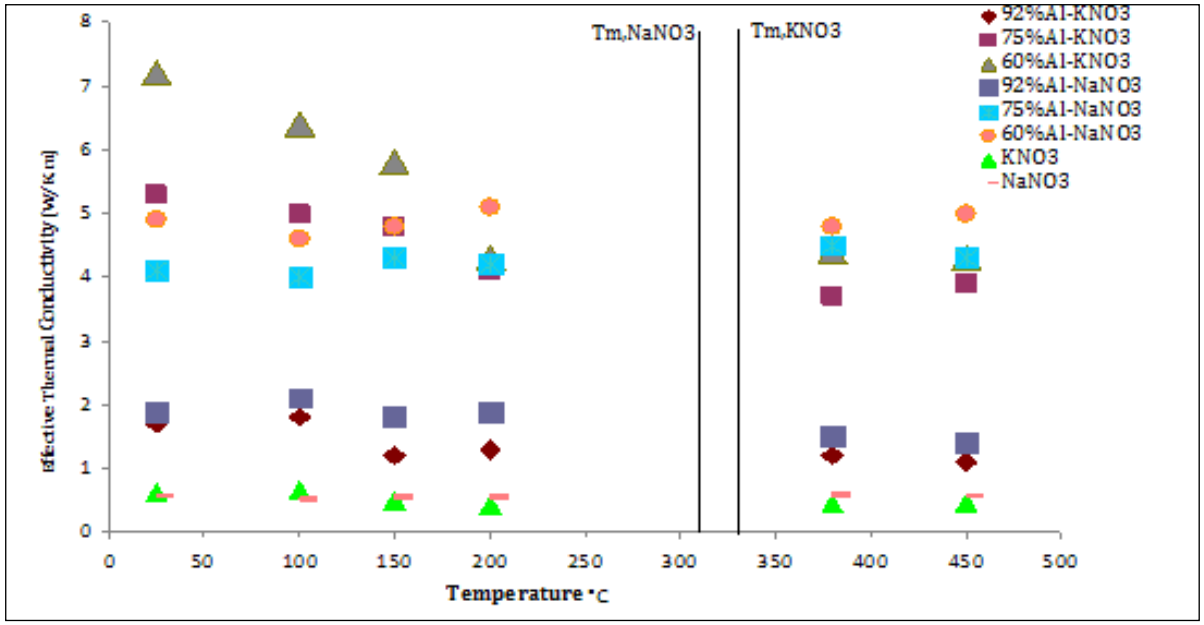

Fig.3.12. The effective thermal conductivity of aluminum-PCM composite as a function of temperature. The vertical lines presents the melting temperature of potassium and sodium nitrate.

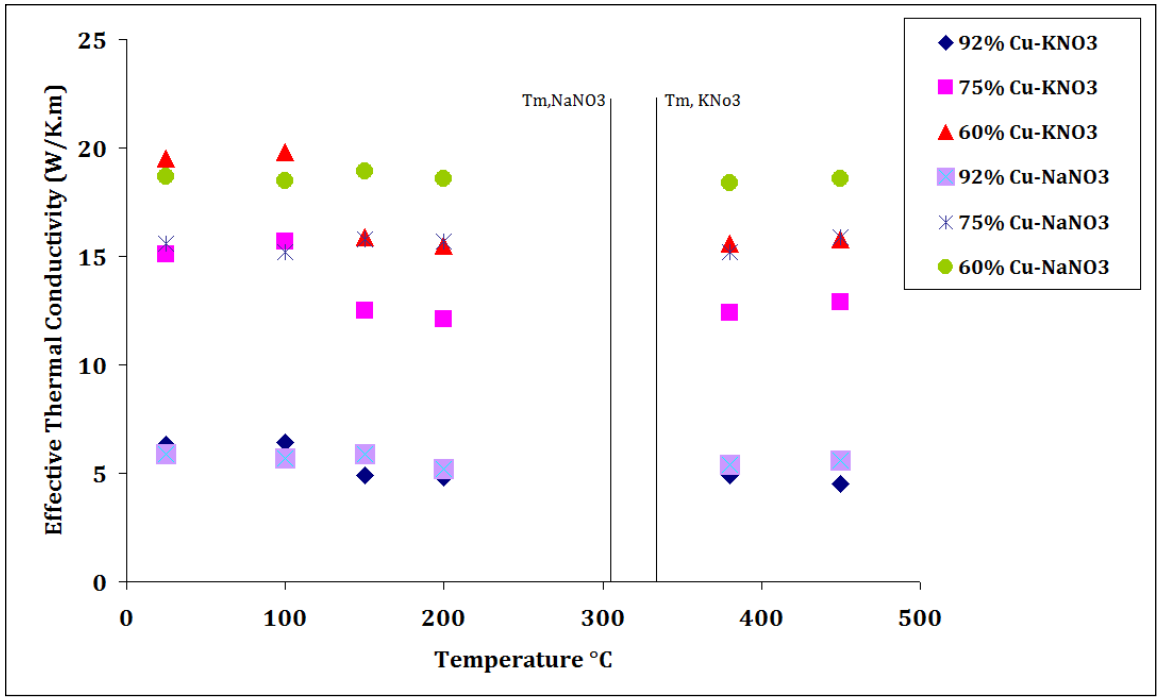

Fig.3.13. The effective thermal conductivity of copper-PCM composite as a function of temperature. The vertical lines present the melting temperature of potassium and sodium nitrate.

The experimental data were used against those from Bahttacharya model [136], which was introduced in section 3.1.2. This model was selected because of the close similarity of metal foam structure to presented model. Figure 3.14.(a) and (b) present pictures of 92% porosity aluminum and copper foams that were used in our experiments. An array of hexagonal cell with some circular lump at the intersection of ligaments can be observed. A few of the intersection lumps are shown by circles. Figure.3.15 illustrates aluminum-KNO_3 and copper-$NaNO_3$ composites.

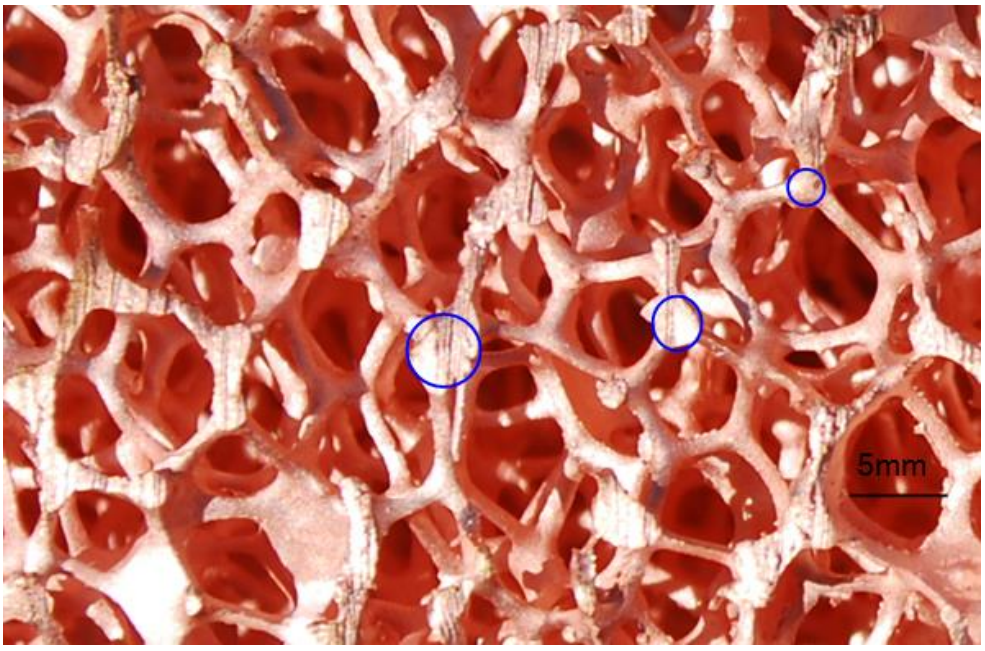

(a)

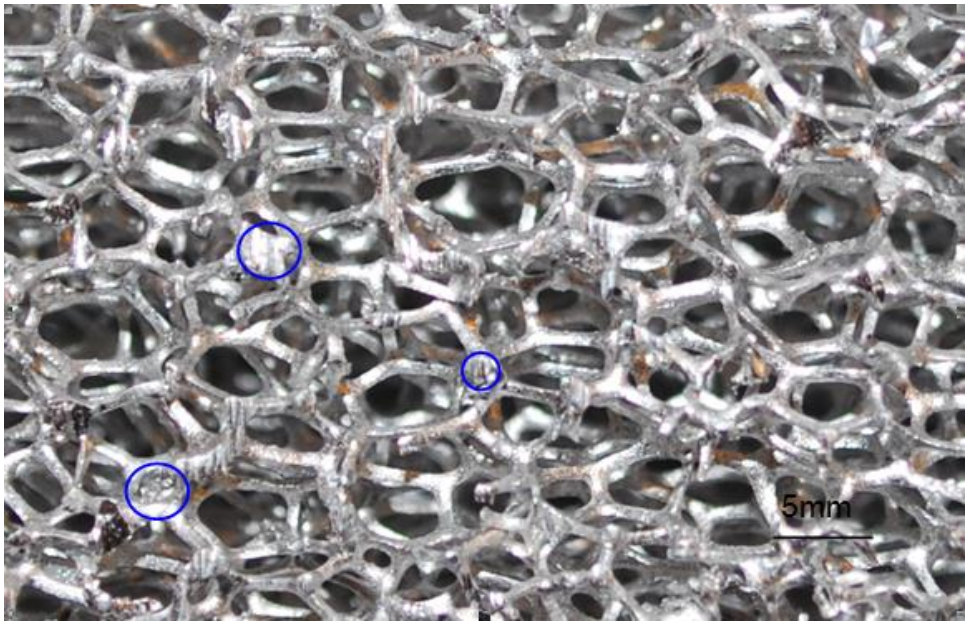

(b)

Fig.3.14. (a) 92% porosity Copper foam with circular intersection lump Aluminum foam, with circular lump intersection (b) 92% porosity Aluminum foam, with circular lump intersection.

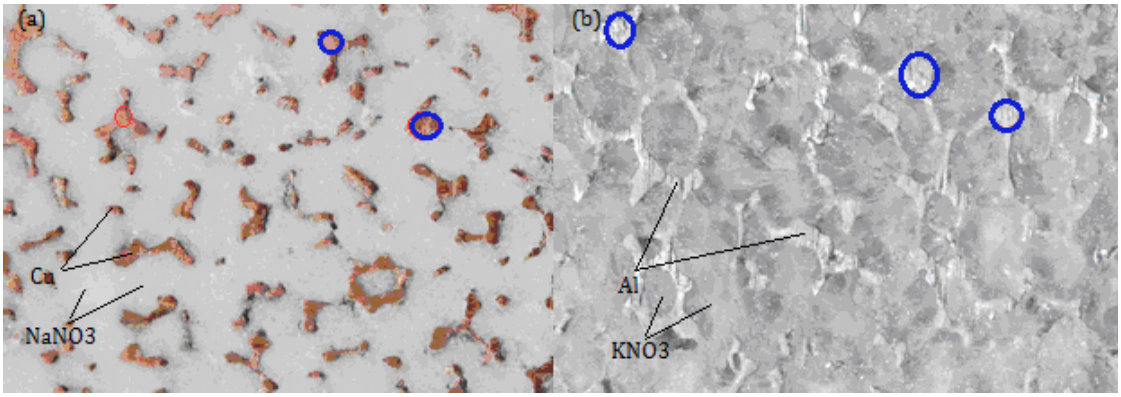

Fig.3.15. (a) Cu- $NaNO_3$ composite, (b) Al.- KNO_3 composite.

To use the Bahttacharya model, $r = \frac{t}{R}$ has to be known. In this work, r was determined by measuring the ligament thickness (t), and the diameter of lump intersection (2R) under microscope. Measurements were done at 10 different location of a 92% porosity metal foam sample, and the average measured value of r was determined to be at 0.34. The results of analytical and experimental data for Al- KNO_3 and Cu- KNO_3 are shown in Figure.3.16 and Figure3.17, respectively. Comparing the model to the experimental data shows that the model follows the curve of data points very well in both cases of aluminum and copper foams. However, the analytical model predicts higher thermal conductivities for both aluminum and copper composites. This gap is about 8-21% for aluminum- KNO_3 composites and about 10-20% for copper composites. This deficiency can be because of lower amount of intersection lump in the actual

sample, as shown in Figure 3.14, compared with the analytical model. It was concluded that assuming one r and uniform intersection lumps throughout the samples does not represent an actual metal foam structure. Thus, the model has to be modified to account for the variability of ligaments and shape of the pores.

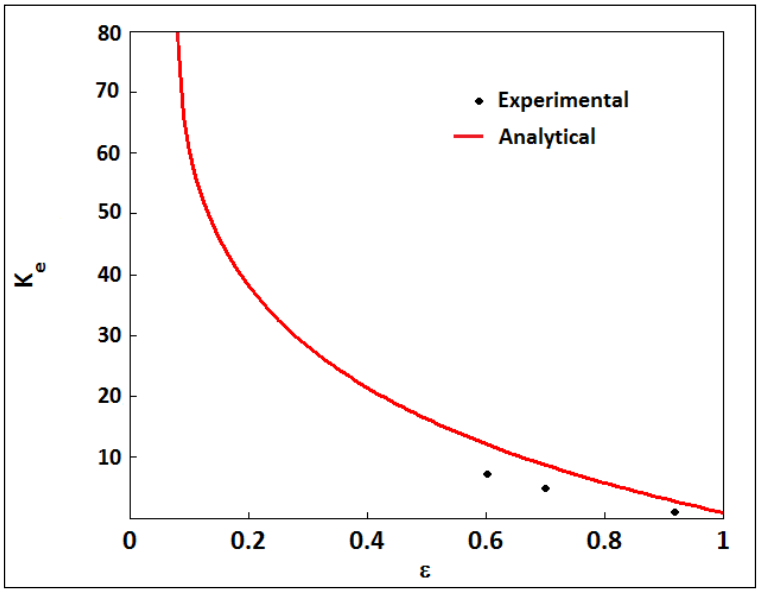

Fig.3.16. Analytical results of Al.- KNO_3 composite's effective thermal conductivity as a function of PCM volume fraction.

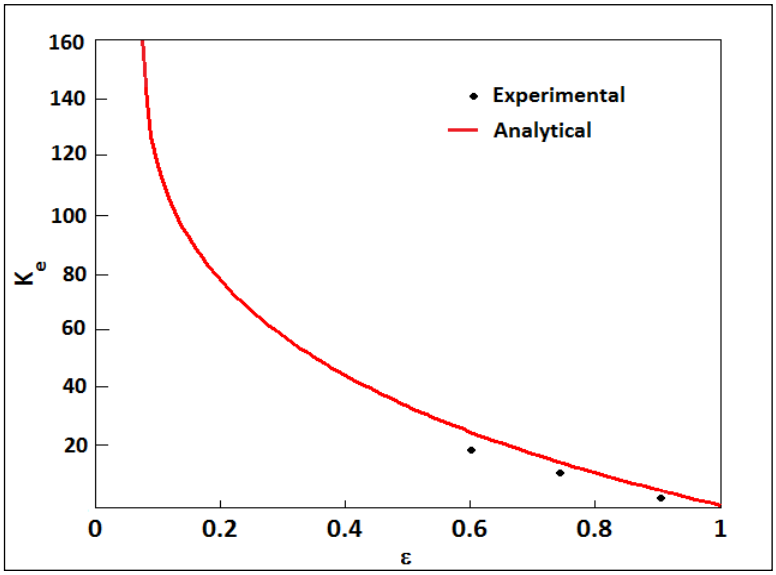

Fig. 3.17. Analytical results of Cu- KNO_3 composite's effective thermal conductivity as a function of PCM volume fraction.

3.5. **Summary**

To enhance the thermal conductivity of PCMs, metal foam-PCM composites were fabricated by infiltration of PCM into interconnected porous aluminum and copper foams. Composites were made from 92%, 75%, and 60% porosity foams, and potassium nitrate and sodium nitrate. The effective thermal conductivity of these composites were measured first as a function of porosity, then as a function of temperature. The thermal conductivity of potassium nitrate was increased from 0.62 W/K.m to 1.7 W/K.m, 5.3 W/K.m, and 7.2 W/K.m for 92%, 75%, and 60% porosity aluminum foam, respectively. The same pattern was observed for sodium nitrate, in which its thermal conductivity was improved from 0.57 W/K.m to 1.9 W/K.m, 4.1 W/K.m, and 4.9 W/K.m for 92%, 75%, and 60% porosity

aluminum foam, respectively. The measurement of the effective thermal conductivity of composites as a function of temperature indicated the thermal conductivity of all potassium nitrate composites would decrease by up to 30% at temperatures above 150°C, which is related to thermal conductivity depreciation of pure potassium nitrate at temperature above 150° because of crystal transformation. The effective thermal conductivity of sodium nitrate composites, on the other hand was independent of temperature.

In addition, several copper-PCM composites were made and their effective thermal conductivities were measured as a function of copper volume fraction and temperature. The effective thermal conductivity of potassium nitrate was increased from 0.62 to 6.3, 15.1, and 19.5 with use of 8%, 25%, and 40% copper volume fractions, respectively. The overall effect of copper foam on thermal conductivity enhancement of PCM was about 4 times higher than aluminum foam. Nevertheless, copper has much higher density compared with aluminum, which results in lower weight percentage of PCM in the copper composite for a given volume fraction of foam.

The experimental results were finally compared to an analytical model that was developed by Bahttacharya, based on one-dimensional heat flow through two-dimensional arrays of hexagonal pores with circular intersection lump. This model was selected because of geometrical similarities of actual metal foam to this model. The experimental and analytical results followed the same trend,

however, the experimental effective thermal conductivity data were about 8-21% lower than analytical results. This deficiency was because of lower amount of intersection lump in actual aluminum and copper foams compared to analytical model.

Chapter 4

Effect of Graphite Flakes and Metal Foam on Thermal Conductivity of PCMs

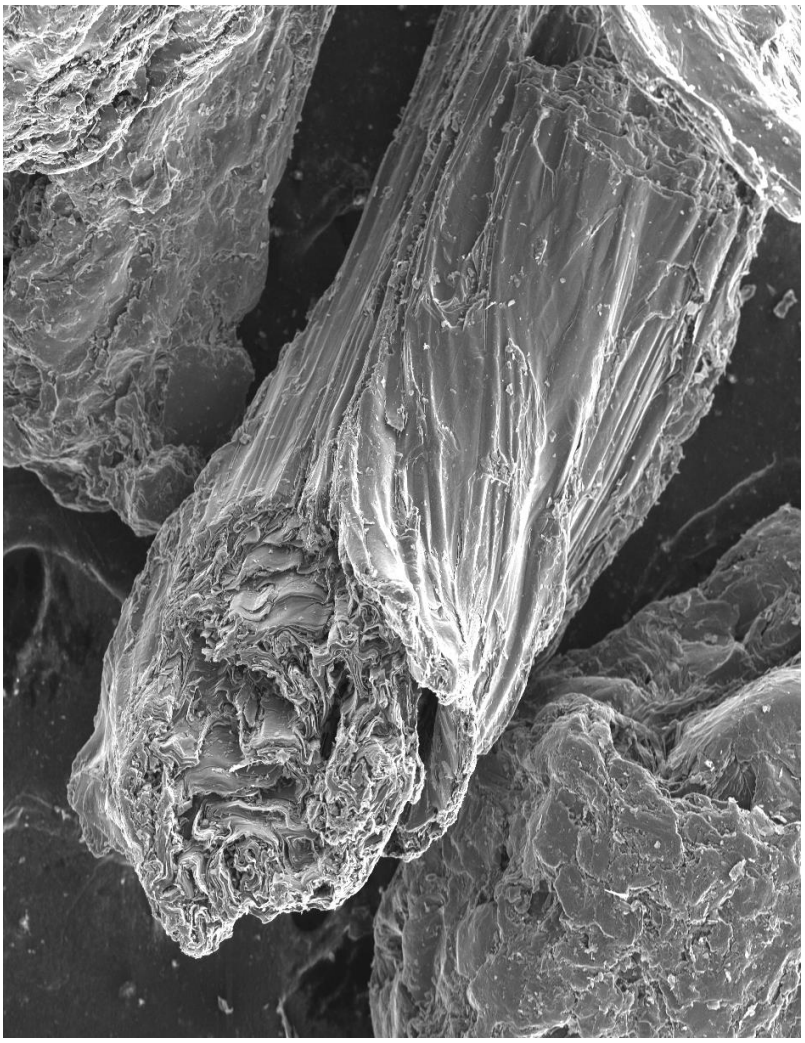

As discussed earlier in section 1.2 of chapter 2, there are two main methods to improve the heat conduction trough materials with low thermal conductivity. First, increasing the surface area, which can be done with the use of metal structures such as fins or metal foams or encapsulation techniques. Second, the addition of high thermally conductive particles such as graphite flakes, carbon nano tubes, aluminum or copper particles.

In chapter 3, the effect of aluminum and copper foam on effective thermal conductivities of potassium nitrate and sodium nitrate were studied. Although the achieved thermal conductivities were in the range of (1.7-7.2) for aluminum-PCM composites and (6.3-19.5) for copper composites, the effective thermal conductivity of high porosity (92%) metal foam composites were in the lower end of acceptable range (>7 W/K.m). The effect of PCM thermal conductivity on the effective thermal conductivity of composites was studied using the same analytical model that was used in chapter 3. The results shown in Figure 4.1 indicate improving the thermal conductivity of the PCM to above 1 W/K.m would increase the effective thermal conductivity of composite exponentially. Therefore, creating a composite with aluminum foam and a PCM with thermal conductivity of 1W/k.m or higher can lead to a composite with much higher thermal conductivity.

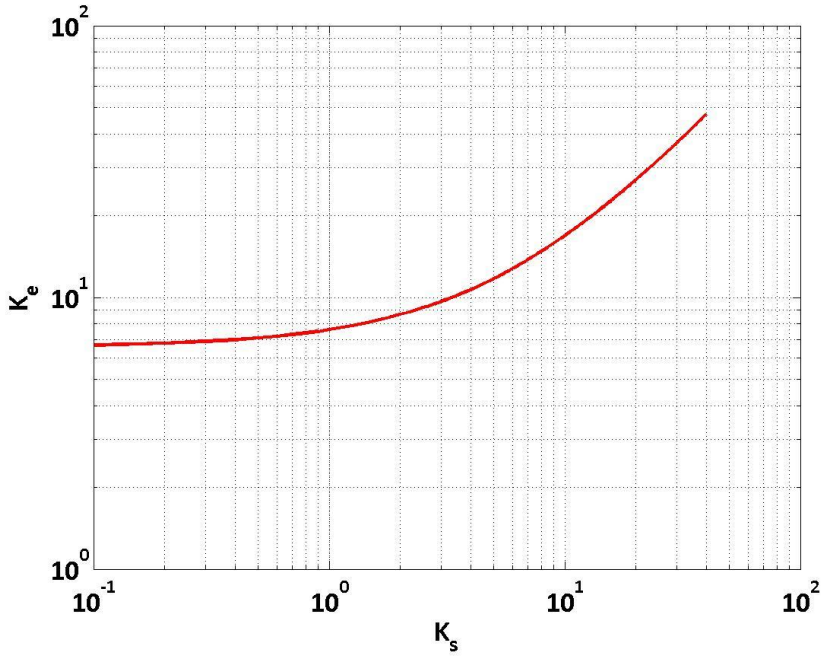

Fig. 4.1. Analytical model of Ke as a function of salt thermal conductivity for 92% porosity aluminum foam.

The use of graphite to improve the thermal conductivity of materials has been studied by several researchers. Aktay et al. [39] proposed infiltration of PCMs into expanded graphite to enhance the thermal conductivity. Their results indicated the thermal conductivity was improved 3 to 5 times, however, they observed thermal conductivity declines with the increase of temperature. Bauer et al. [139] also studied the effective thermal conductivity of several graphite-PCM composites, which were made with three different types of graphite; natural graphite flakes, ground expanded graphite particles, and compressed expanded graphite plates. They observed enhancement in the range of 3-30 times of single PCM thermal conductivity. It is therefore proposed to add graphite flakes to

metal-PCM composite and create aluminum-graphite-PCM composites and copper-graphite-PCM composites. The main approach was to improve the thermal conductivity of PCM to above (1W/K.m) with the use of graphite flakes. Then infiltrate PCM-graphite mixture into metal foams to increase the effect of metal foams on effective thermal conductivity of composites.

4.1. **Experiment**

The aluminum-graphite-PCM and copper-graphite-PCM composites were prepared by infiltration of molten PCM-graphite mixture into aluminum foams. The selected PCMs were potassium nitrate and sodium nitrate; some of their thermal and physical properties have been presented in chapter 2. The graphite used was in form of flakes, with an average size from 300-600 μm. Figure.4.2 shows the scanning electron microscope image of the flakes. The thermal conductivity of graphite flakes is highly anisotropic, with a thermal conductivity ranging from 140-500 W/K.m in and along the “a” and “b” axes (parallel to the layer planes) and from 3-10 W/k.m along the “c” axis (perpendicular to the planes) [140].

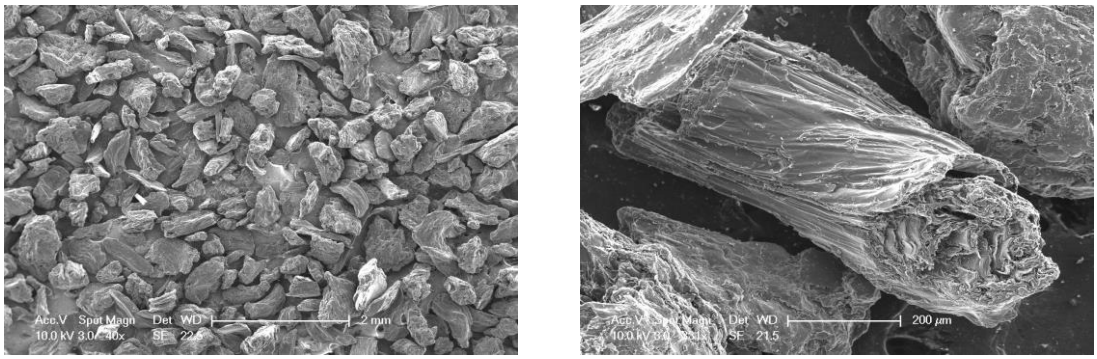

Fig. 4.2. Graphite flakes utilized in this study.

The 92% porosity aluminum and copper foams described in chapter 3 were used to prepare the samples. First salt powder and graphite flakes were mixed and heated up to temperature above melting point of PCM and stirred to create a homogenous mixture. Because the density of graphite (2.24 gr/m3) and both potassium nitrate (2.11 gr/m3) and sodium nitrate (2.26 gr/m3) are very close, no settling or floating of graphite flakes were observed during the process. The amount of graphite added varied from 3 to 15wt%. Then a procedure similar to that described in section 3.2, was used to prepare the composite samples and measure their thermal conductivities. Table.4.1 presents the PCM-graphite mixture composition and their metal-graphite-PCM wt% composition.

Table 4.1. Composition of Graphite-PCM and ternary Metal-Graphite-PCM Composites

PCM-Graphite Mix Composition Wt%	Metal-C-PCM Comp#	Metal Foam-Graphite-PCM Composite composition Wt%	Metal Foam-Graphite-PCM Composite composition V%
97% KNO3-3% Graphite	1	10.4%Aluminum-87% KNO3-2.6% Graphite	8%Aluminum-89% KNO3-3% Graphite
95% KNO3-5% Graphite	2	10.4%Aluminum-85.1% KNO3-4.5% Graphite	8%Aluminum-87% KNO3-5% Graphite
90% KNO3-10% Graphite	3	10.4%Aluminum-80.6% KNO3-9% Graphite	8%Aluminum-82% KNO3-10% Graphite
85% KNO3-15% Graphite	4	10.4%Aluminum-76.2% KNO3-13.4% Graphite	8%Aluminum-78% KNO3-14% Graphite
97% NaNO3-3% Graphite	5	9.7%Aluminum-87.6% NaNO3-2.7% Graphite	8%Aluminum-89.3% NaNO3-2.7% Graphite
95% NaNO3-5% Graphite	6	9.7%Aluminum-85.8% NaNO3-4.5% Graphite	8%Aluminum-87.5% NaNO3-4.5% Graphite
90% NaNO3-10% Graphite	7	9.7%Aluminum-81.3% NaNO3-9%Graphite	8%Aluminum-82.8% NaNO3-9.2%Graphite
85% NaNO3-15% Graphite	8	9.7%Aluminum-76.8% NaNO3-13.5% Graphite	8%Aluminum-78.2% NaNO3-13.8% Graphite
97% KNO3-3% Graphite	9	29%Copper-69%KNO3-2%Graphite	8%Copper-89% KNO3-3% Graphite
95% KNO3-5% Graphite	10	29%Copper-67%KNO3-4%Graphite	8%Copper-87% KNO3-5% Graphite
90% KNO3-10% Graphite	11	29%Copper-64%KNO3-7%Graphite	8%Copper-82% KNO3-10% Graphite
85% KNO3-15% Graphite	12	29%Copper-60%KNO3-11%Graphite	8%Copper-78% KNO3-14% Graphite
97% NaNO3-3% Graphite	13	28%Copper-70%NaNO3-2% Graphite	8%Copper-89.3% NaNO3-2.7% Graphite
95% NaNO3-5% Graphite	14	28%Copper-68%NaNO3-4% Graphite	8%Copper-87.5% NaNO3-4.5% Graphite
90% NaNO3-10% Graphite	15	28%Copper-65%NaNO3-7% Graphite	8%ACopper-82.8% NaNO3-9.2%Graphite
85% NaNO3-15% Graphite	16	28%Copper-61%NaNO3-11%Graphite	8%Copper-78.2% NaNO3-13.8% Graphite

4.2. **Results and Discussion**

The results of the thermal conductivity of graphite-PCM mixtures measured at room temperature are shown in Figure 4.2. As can be seen, the effective thermal conductivity of both potassium nitrate and sodium nitrate was improved with the addition of graphite flake from 1.6-1.8 W/K.m at 3 wt% graphite to 4.8-5.1 W/K.m at 15 wt% graphite. Therefore, the thermal conductivity was in direct relation with the weight percentage of graphite as was expected.

Nevertheless, the experimental data were substantially below those predicted from rule of mixture calculations. It was assumed in the rule of mixture calculations, the thermal conductivity of graphite flake to be 233 W/K.m based on the report by Smaic et al. [140]. As presented in Figure 4.3, the measured effective thermal conductivity is about 70-80% lower compared to effective thermal conductivity calculated by rule of mixture based on volume fraction. The rule of mixture indicates the maximum thermal conductivity that can be achieved by mixing two materials, because it assumes both materials are in parallel planes in the direction of heat flow, thus the heat can pass through the high thermal conductivity planes. However, in these samples the graphite particles are scattered throughout the samples and heat has to pass through parallel and

series layers of PCM and graphite flakes, which results in lower thermal conductivity.

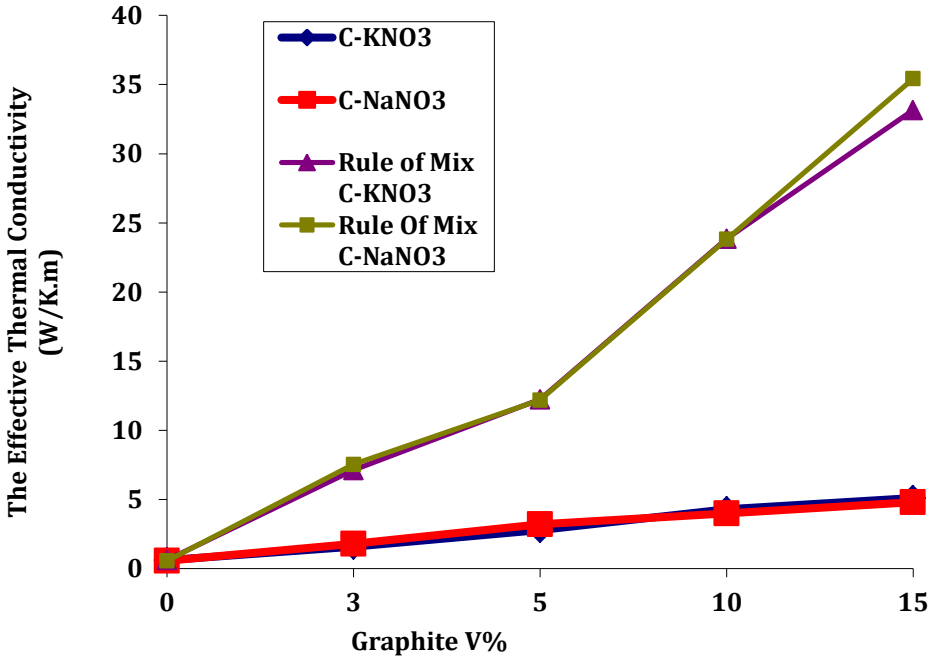

Fig.4.3. The effective thermal conductivity of graphite-PCM based on graphite V%.

As was mentioned earlier, the graphite-PCM composite described above was used to make aluminum-graphite-PCM and copper-graphite-PCM composite. The thermal conductivity of sixteen different composites as a function of temperature and composition are presented in Table.4.2. Each reported data represents an average value of three measurements for each specimen, and the standard deviation for each data point was less than 6.5%. The experimental data indicates

the positive effect of graphite flakes on metal foam-PCM composites' thermal conductivity. For example, the thermal conductivity of composite with composition of 8V% aluminum-89V% KNO_3 -3V% graphite was measured to be 3.1 which is 5 times higher than pure potassium nitrate and 1.8 times higher than 8V%Al-92V% KNO_3 composite. Also, it was observed that increasing the graphite percentage directly increases the thermal conductivity of the composite. As shown the effective thermal conductivity of Al-C- KNO_3 composites were measured to be 6.2 W/K.m and 13.3 W/K.m at 5V% and 10V% graphite, respectively. Similar results were observed for Al-C- $NaNO_3$ composites, for which effective thermal conductivity was improved by factor of 6.6-26.

The effect of graphite flake on effective thermal conductivity of Cu-PCM composites is shown in column 5 and 6 of Table 4.2. The results indicate that addition of graphite percentage improves the thermal conductivity of the composite significantly. For example, addition of only 3V% graphite enhances the thermal conductivity to 11.9 W/K.m, which is 19 times higher than thermal conductivity of pure potassium nitrate, 1.8 times higher than Cu- KNO_3 composites. This improvement was taken further with the increase of graphite percentage to 14 V%, which resulted on very high thermal conductivity of 78.1 W/K.m for 8V%Cu-78V% KNO_3 -14V%C, and 75.5 W/K.m for 8V%Cu-78.2V%

$NaNO_3$-13.8V%C. Although these composites provide very high thermal conductivity compared with pure potassium nitrate (K=0.62 W/K.m) and sodium nitrate (k=0.57 W/K.m), their latent heat capacity is lower because of addition of high thermal conductivity materials such as copper, aluminum and graphite. The three additive coppers provide the highest thermal enhancement, but also have the highest density (8.94 gr/m3) among the three, and thus it results to the lowest latent heat capacity composites.

Table 4.2. Thermal Conductivity Measurements of PCM Graphite mixture, and metal-Graphite-PCM Composite and their heat capacity.

PCM-Graphite Mix Composition Wt%	Ke of PCM-Graphite mix (W/K.m)	Al-PCM-C Comp #	Ke of Al-PCM-C Composite (W/K.m)	Latent Heat storage capacity %	Cu-KNO3-C Comp #	Ke of Cu-PCM-C Composite (W/K.m)	Latent Heat storage capacity %
97% KNO3-3% C	1.6	1	3.1	87	9	11.9	69
95% KNO3-5% C	2.8	2	6.2	85.1	10	29.6	67
90% KNO3-10% C	4.3	3	13.3	80.6	11	51.1	64
85% KNO3-15% C	5.1	4	11.7	76.2	12	78.1	60
97% NaNO3-3% C	1.8	5	3.8	87.6	13	12.4	70
95% NaNO3-5% C	3.2	6	7.2	85.8	14	26	68
90% NaNO3-10% C	4	7	11.2	81.3	15	54.2	65
85% NaNO3-15% C	4.8	8	14.9	76.8	16	75.5	61

As was explained in chapter 3, the weight percentage of PCM plays an important role in latent heat storage capacity; thus it is desired to achieve appropriate thermal conductivity with maximum PCM weight percent. Therefore, Figure 4.4 was plotted to compare the effective thermal conductivity and the PCM weight percentage of all composites made in this research. The effective thermal conductivity was increased in the order of PCM-graphite(~1.6-4.8 W/k.m), PCM-aluminum (~1.7-7.2 W/k.m), PCM-aluminum-graphite (~3.9-14.9 W/k.m), PCM-copper(~6.3-19.5 W/Km) and finally the PCM-copper-graphite (~11.9-78.1 W/K.M). On the other hand, the amount of latent heat storage capacity, which is based on PCM weight percentage, increases in the order of PCM-copper(27-70%), PCM-aluminum (55-80%), PCM-copper-graphite (60-70%), PCM-aluminum-graphite (78-87%), and finally the PCM-graphite composites (85-97%). All of these composites increase the effective thermal conductivity, but they all not suitable for one application. For instance, among these composites PCM-aluminum-graphite provide high enough (K>7 W/K.m) thermal conductivity for concentrating solar power plant application with losing about 20% of heat storage capacity per unit weight, while PCM-copper-graphite provides much higher thermal conductivity (~75-78 W/K.m), but lower heat capacity (40% PCM unit weight), which can be used in electronic applications with shorter charging and discharging cycles.

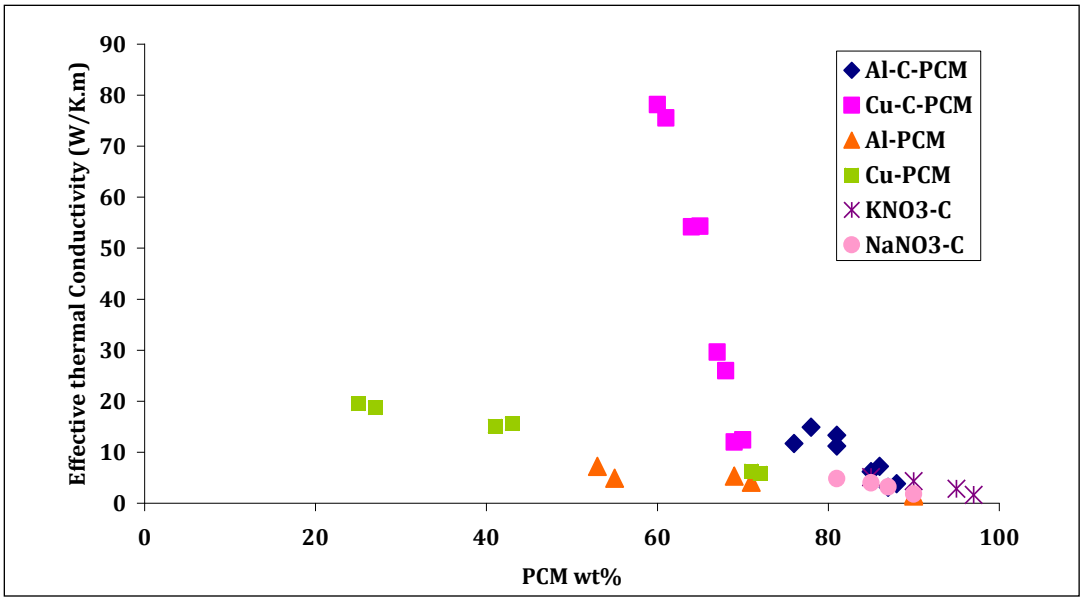

Fig. 4.4. Comparison of Effective thermal conductivity of all composites from chapter.3 and chapter.4 as a function of PCM wt%.

Furthermore, the effective thermal conductivity Al-C-KNO_3 and Cu-C-KNO_3 composites were measured as a function of temperature, and the results are presented in Figure.4.5. The effective thermal conductivity of these composites decreases by 11-25% with the increase of temperatures to above 150°C. As mentioned in chapter 2, this thermal conductivity depreciation is because of crystal transformation in potassium nitrate. However, experimental data indicate the depletion of thermal conductivity decreases with the increase of graphite percentage. For example, the thermal conductivity of composite made by 2-3wt% graphite decreases by 25% at temperature above 150° C, while this depreciation decreases to 4-10% with increase of graphite percentage to 10-13 wt%.

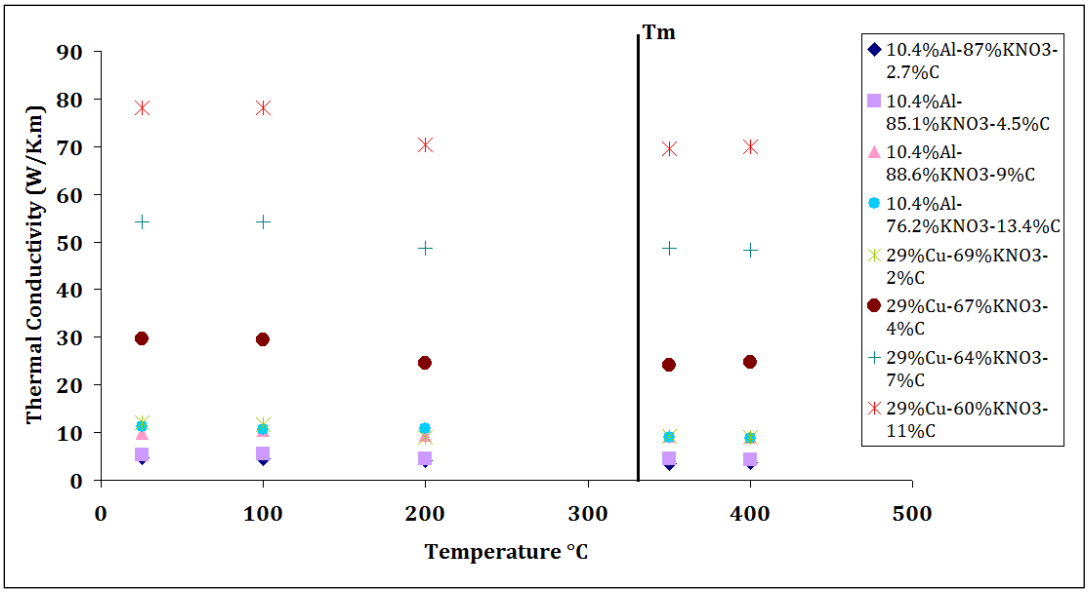

Fig. 4.5. The effective thermal conductivity of aluminum- graphite-potassium nitrate composite as a function of temperature.

4.3. **Summary**

To enhance the thermal conductivity of PCMs, aluminum-graphite-PCM composites were fabricated by infiltration of PCM-graphite mixture into interconnected porous aluminum and copper foams. A total of 16 composites were made with different compositions containing variable percentage of copper, aluminum, graphite, and potassium and sodium nitrate. The effective thermal conductivity of these composites were measured first as a function of graphite volume percentage composition. Addition of graphite improved the thermal conductivity of aluminum-PCM composites by factor of 5 at 3V% graphite and further increased up to 8 times with the increase of graphite to 14V%. Similar pattern was observed for sodium nitrate composite. The effective thermal conductivity of Al-C-$NaNO_3$ was 3.8, 7.2,

and 11.2 W/K.m at 2.7V%, 4.5V%, and 9.2V% graphite composition, respectively. The effective thermal conductivity comparison of Al-PCM and Al-C-PCM composites indicated, the thermal conductivities of Al-C-PCM composites are about 50% higher compared with Al-PCM composites at same PCM weight percent. In addition, the effective thermal conductivities of Cu-PCM-C composites were measured to be in the range of 11.9-78.1 W.K.m for potassium nitrate, and 12.4-75.5 W/K.m for sodium nitrate with increase of graphite volume percentage from 3 to 14.

The comparison of the effective thermal conductivity as a function of PCM weight percentage for all four types of composites showed, PCM-copper-graphite composites have the highest thermal conductivity (75.5-78.1 W/K.m) with low latent heat capacity (60%), while PCM-aluminum-graphite have moderate thermal conductivity (13.3-14.9 W/K.m) and moderate latent heat capacity (80%).

Finally, the effect of temperature on the thermal conductivity of Al-C-KNO_3 composites was studied. A small decline of effective thermal conductivity at 200°C was observed, which was concluded to be related to decrease of potassium nitrate thermal conductivity at temperature above 140°C because of its crystal transformation. Also it was observed that increase of graphite volume percent, reduces the decrease of potassium nitrate composites' thermal conductivity beyond 140° C. The thermal conductivity was decreased by 12% at 200°C in a sample with 3V% graphite, while this depletion was reduced to 4% in a sample with 10V% graphite composition.

Chapter 5

Latent heat storage has been shown to be suitable for concentrating solar power plants heat storage applications, because they can store 50% more heat compared to the same size sensible heat storages. More importantly, latent heat storages can supply heat at constant temperatures, which is an important factor for steam turbine applications. Latent heat storage operates with the use of phase change material (PCM), which can store and release heat by going through phase transformation. A brief survey on categories of phase change materials and their thermal properties were conducted. Among PCMs, alkali salts are suitable for high temperature concentrating solar power plant (CSPP) applications because of their melting temperature (290°-900°C), moderate latent heat of fusion (180-450 KJ/Kg), durability for 5000 cycles of melt and freeze, and their low cost. Nevertheless, alkali nitrates, similar to other PCMs candidates, exhibit low (K<1 W/K.M) thermal conductivity, while PCMs' thermal conductivity for medium to high temperature heat storages is required to be above 7 W/K.m for appropriate charging and discharging cycle times. In order to be able to use alkali nitrate salts as PCMs in heat storages, their thermal conductivity needs to be improved.

In this research, the thermal conductivity of several alkali salts was measured using transient hot wire technique. The experimental data indicated the thermal conductivity decreases in the order of Chloride (~5 W/K.m), Carbonate (1.5<K<2W/K.m), and Nitrate (K<1 W/K.m). Although chloride salts have much higher thermal conductivity compared to the other two categories, they have shown not suitable as PCM materials because they are corrosive. On the other hand,

carbonate salts have higher thermal conductivity compared to nitrate salts, but their very high (T>800°C) melting temperature make them only applicable for very high temperature heat storages. Therefore, nitrate salts were the most viable candidates with PCM requirement for CSPP application. Among alkali, nitrate potassium nitrate and sodium nitrate were the main focus of this research.

The thermal conductivity of sodium nitrate was measured to be 0.57 W/K.M, 0.54 W/K.m, and 0.58 W/K.m at room temperature, 200, and 380°C, respectively. It was observed that the thermal conductivity of sodium nitrate is independent of temperature. However, the thermal conductivity of potassium nitrate decreased by 30% with the increase of temperature beyond 150°C. Further DSC experiments indicated a crystal transformation from orthorhombic to rhombohedral at around 140° C, which is believed to be the source of thermal conductivity depreciation.

In the third chapter, it was proposed to improve the thermal conductivity of potassium nitrate and sodium nitrate by application of metal foams. Several aluminum-PCM and copper-PCM composites were designed with use of three different porosity aluminum and copper foams (60%, 75%, and 92%). Each composite was created by infiltration of molten PCM into metal foams. Then their effective thermal conductivities were measured.

The experimental results indicated the use of metal foams improved the effective thermal conductivity of salts. The conductivity of Al-KNO_3 composites was measured to be at 1.7, 5.3, and 7.2 W/K.m with use of 92%, 75%, and 60% porosity

aluminum foam, respectively. Similar results were observed for aluminum-$NaNO_3$ composites. The thermal conductivity of sodium nitrate was improved by factors of 3.3, 7.2, and 8.5 for 92%, 75%, 60% porosity aluminum foams, respectively. Use of copper foams enhanced the effective thermal conductivity 3 to 4 times higher compared to aluminum foam. The effective thermal conductivity of copper-PCM composites were measured to be in the range of 6.3-19.5 W/K.m for potassium nitrate and 5.9-18.7 W/K.m for sodium nitrate composites.

Furthermore, the effective thermal conductivity of Al-PCM and Cu-PCM composites as a function of temperature was measured. Similar to potassium nitrate (KNO_3), thermal conductivity of Al-KNO_3 and Cu-KNO_3 composites decreased with the rise of temperature. The thermal conductivity of 10wt%Aluminum-90wt%PCM composites decreased from 1.7 at room temperature to 1.3 at 150° C, while the thermal conductivity of 29wt%Cu- 71wt%KNO_3 decreased from 6.3 W/K.m at room temperature to 4.9 W/K.m at 150°C. The effective thermal conductivity of all potassium nitrate composites decreased by about 11-31% with increases of temperature to 150°C. This decrease was related to thermal conductivity depreciation of pure potassium nitrate by about 30% at 140°C due to crystal transformation. The thermal conductivity of sodium nitrate composites were stable with increase of temperature, and no temperature dependence was observed.

To further improve thermal enhancement with use of metal foams and reduce metal fraction, the addition of graphite flakes into the composite were studied. Aluminum-

graphite-PCM and copper-graphite-PCM composites were designed by infiltration of a graphite flake-PCM mixture into aluminum and copper foams. First ,the effective thermal conductivity of these composite were measured as a function of graphite volume percentage. The thermal conductivity of 8V%Al-3V%C-89% KNO_3 was measured to be 3.1W/K.m, which is 5 times higher than pure potassium nitrate (0.62W/K.m), at room temperature. The thermal conductivity of 8v%Cu-89V% KNO_3 -3V%C at room temperature was measured to be 11.9 W/K.m. Furthermore, increasing the percentage of graphite from 3V% to 10V% increased the effective thermal conductivity of Al-C- KNO_3 composite to 13.3 W/K.m, which is 21 times higher than the thermal conductivity of pure potassium nitrate. The addition of graphite improved the thermal conductivity of Cu-C- KNO_3 to 54.2 W/K.m.

Among the created composites, Cu-PCM-C composite was determined to have the highest thermal conductivity, in the range of 11.9-78.1 W/K.m, however, their latent heat capacity is in the range of 70-60% compared to pure salt. The next category is Al-PCM-C composites with moderate thermal conductivity of 3.5-13.1W/K.m and high-heat capacity of 80-89%. Then they are followed by Cu-PCM, Al-PCM, and PCM-C composites, respectively. Therefore, it can be concluded that Al-C-PCM composites are more suitable composites for concentrating solar power plant applications because of their moderate thermal conductivity and higher latent heat storage capacities. On the other hand, Cu-PCM-C composites are suitable candidates

for lower capacity heat storages with shorter charging and discharging cycles because of their high thermal conductivities.

The thermal conductivity of Al-C-KNO_3 and Cu-C-KNO_3 as a function of temperature indicated the effective thermal conductivity of these composites decreases with increase of temperature due to decrease of potassium nitrate thermal conductivity. However, the addition of graphite reduced the percentage of conductivity depreciation from 25% to 12%. Also, it was observed that increasing the amount of graphite in the composite decreased the thermal conductivity depreciation of potassium nitrate composites by increase of temperature.

The main objective of this work was to design a phase-change material with melting temperature of (300°-500°C), latent heat of fusion of (100-200 KJ/Kg), thermal conductivity of (K>7 W/K.m), and low cost. After studying and designing several PCM composites, it can be concluded (10.4%Aluminum-80.6% KNO_3-9% Graphite) and (9.7%Aluminum-81.3% $NaNO_3$-9%Graphite) composites are the two best PCM candidates that meet most of the requirements with maximum heat storage capacity.

References

1- Mills, D.R., Morrison, G.L., 2000. Compact linear Fresnel reflector solar thermal power plants. Solar Energ. 68 (3), 263–283.

2- http://www.torresolenergy.com

3- www.terrafore.com

4- Baylin F. Low temperature thermal energy storage: a state of the art survey. Report no. SERI/RR/-54-164. Golden, Colorado, USA: Solar Energy Research Institute; 1979.

5-Sharma, A., V.V. Tyagi,. 2007. Review on Thermal Energy Storage With Phase Change Materials and Applications. J.J.rser.2007.10.005

6- Mehling,H., Cazbah, L.,Heat and Cold Storage with PCM, Heat and Mass Transfer, 2008

7- Hauer A.: Sorption theory for thermal energy storage. In: Paksoy H.Ö. (ed.): Thermal energy storage for sustainable energy consumption – fundamentals, case studies and design, pp. 393-408. Springer, (2007), NATO Science series II. Mathematics, Physics and Chemistry – Vol. 234, ISBN 978–1–4020–5289–7

8- Hoshi, A., Saitoh, T.S., 2004 . Screaning of high melting point phase change materials (PCM) in solar thermal concentrating technology based on CFLR.J.Solener.2004.04.023

9- Hoshi, A., Saitoh, T.S., 2001a. A study of solar steam accumulator with high temperature latent heat thermal energy storage (1st Report; High melting point phase change material). J. JSES 27 (5), 34–40.

10- Lane GA. Solar heat storage—latent heat materials, vol. I. Boca Raton, FL: CRC Press, Inc.; 1983.

11- Zalba, B. Marin, J. Review on thermal energy storage with phase change: materials, heat transfer analysis and applications. J. Applied Thermal Engineering 23(2003) 251-283

12- Abhat, A., Low temperature latent heat thermal energy storage: heat storage materials, Solar Energy 30 (1983) 313–332

13- Lane, G.A. Solar Heat Storage: Latent Heat Material, vol. I, Background and Scientific Principles, CRC Press, Florida, 1983.

14-Lane, G.A. Solar Heat Storage: Latent Heat Material, vol. II, Technology, CRC Press, Florida, 1986.

15-Dincer, I. Rosen,M.A,. Thermal energy storage, Systems and Applications, John Wiley & Sons, Chichester (England), 2002.

16- Farid, M., Khudhair, A., A review on phase change energy storage: materials and applications. J.enconman.2003.09.015

17- Abhat A. Low temperature latent heat thermal energy storage. In: Beghi C, editor. Thermal energy storage. Dordrect, Holland: D. Reidel Publication Co.; 1981.

18- Farid, M.M, Husian, R.M. An electrical storage heater using phase change method of heat storage. Energy Convers Mgmt 1990;30:219–30.

19- Farid, M.M, Kim, Y, Kanzawa, A. Thermal performance of heat storage module using PCM_s with different melting temperatures-experimental. Trans ASME, J Solar Energy Eng 1990;112:125–31.

20- Pillai, K.K, Brinkwarth, B.J. The storage of low grade thermal energy using phase change materials. Appl Energy 1976;2:205–16.

21- Hale, DV. Hoover, MJ, O'Neill, MJ. Phase change materials hand book. Alabaa: Marshal Space Flight Center; 1971.

22- Lane, GA, Glew, DN. Heat of fusion system for solar energy storage. In: Proceedings of the workshop on solar energy storage subsystems for the heating and cooling of buildings. Virginia: Charlothensville; 1975. p. 43– 55.

23- Herrick ,S, Golibersuch, DC. Quantitative behavior of a new latent heat storage device for solar heating/cooling systems. In: General International Solar Energy Society Conference; 1978.

24- Abhat, A. et al.., Development of a modular heat exchanger with an integrated latent heat storage. Report no. BMFT FBT 81-050. Germany Ministry of Science and Technology Bonn; 1981.

25- Buddhi, D, Sawhney, RL.In: Proceedings on thermal energy storage and energy conversion; 1994.

26- Lane, G.A. et al.. Macro-encapsulation of PCM. Report no. ORO/5117-8. Midland, Michigan: Dow Chemical Company; 1978. p. 152.

27- Herrick, S. A rolling cylinder latent heat storage device for solar heating/ cooling. ASHRAE Tans 1979;85:512–5.

28- Lane, GA. Low temperature heat storage with phase change materials. Int J Ambient Energy 1980;1:155 68.

29- Stark, P. PCM-impregnated polymer microcomposites for thermal energy storage. SAE Soc Automotive Eng) Trans 1990;99:571–88.

30- Costello, YA, Melsheimer SS, Edie DD. Heat transfer and calorimetric studies of a direct contact-latent heat energy storage system; thermal storage and heat transfer in solar energy system. ASME Meeting, San Francisco, USA, 1978. p. 10–5.

31- Telkes, M. Nucleation of super saturated inorganic salt solution. Indust Eng Chem 1952;44:1308.

32- Telkes, M. Thermal storage for solar heating and cooling. In: Proceedings of the workshop on solar energy storage sub-systems for heating and cooling of buildings. University of Virginia, Charlottesville; 1975.

33- Biswas, DR. Thermal energy storage using sodium sulphate decahydrate and water. Solar Energy 1977;19:99–100.

34- Farid, M.M, Hamad, F.A, Abu-Arabi, M. Phase change cool storage using dimethyl sulfoxide. Energy Convers Mgmt1998;39:819–26.

35- Cristopia Energy System Web Site [www.cristopia.com].

36- Ryu ,HW, Woo, SW, Shin, BC, Kim, SD. Prevention of subcooling and stabilization of inorganic salt hydrates aslatent heat storage materials. Solar Energy Mater Solar Sells 1992;27:161–72.

37- Lane GA. Phase change materials for energy storage nucleation to prevent subcooling. Solar Energy Mater Solar Sells 1991;27:135–60.

38- Buschle, J., Steinmann, W.-D., Tamme, R. (2006) Latent Heat Storage for Process Heat Applications, The Tenth International Conference on Thermal Energy Storage, Atlantic City, New Jersey, 31. May – 2. June.

39- do Couto Aktay K.S., Tamme R., Müller-Steinhagen H. (2005) PCM-Graphite Storage Materials for the Temperature Range 100-300°C, Proc. 2nd Phase Change Material and Slurry Conference, Yverdon-les-Bains, Switzerland, 15. – 17. June, 89-97.

40- George, A. Hand book of thermal design. In: Guyer C, editor. Phase change thermal storage materials. McGraw Hill Book Co.; 1989 [chapter 1].

41- http://www.crct.polymtl.ca/fact/documentation/FTsalt/FTsalt_Figs.htm

42- Velraj R, Seeniraj RV, Hafner B, Faber C, Schwarzer K. Heat transfer enhancement in a latent heat storage system. Solar Energy 1999;65:171–80.

43- Hasnain SM. Review on sustainable thermal energy storage technologies, Part 1: Heat storage materials and techniques. Energy Convers Mgmt 1998;39:1127–38.

44- Morcos VH. Investigation of a latent heat thermal energy storage system. Solar Wind Technol 1990;7:197–202.

45- Sadasuke I, Naokatsu M. Heat transfer enhancement by fins in latent heat thermal energy devices. Solar Eng, ASME 1991:223–8.

46- Costa M, Buddhi D, Oliva A. Numerical simulation of a latent heat thermal energy storage system with enhanced heat conduction. Energy Convers Mgmt 1998;39:319–30.

47- Padmanabhan PV, Murthy MV. Outward phase change in a cylindrical annulus with axial fins on the inner tube. Int J Heat Mass Transfer 1986;29:1855–68.

48-Bauer C, Wirtz R. Thermal characteristics of a compact, passive thermal energy storage device. In: Proceedings of the 2000 ASME IMECE, Orlando, USA, 2000.

49-Kamimoto M, Abe Y, Kanari K, Swata S, Tani T, Ozawa, T. Heat transfer in latent heat thermal storage units using pentarythritol slurry, thermal energy storage. World Congress of Chemical Engineering, Tokyo, Japan, 1986.

50-Mehling H, Hiebler S, Ziegler F. Latent heat storage using a PCM-graphite composite material: advantages and potential applications. In: Proceedings of the 4th Workshop of IEA ECES IA Annex 10, Bendiktbeuern, Germany, 1999.

51-Fukai J, Morozumi Y, Hamada Y, Miyatake O. Transient response of thermal energy storage unit using carbon fibers as thermal conductivity promoter. In: Proceedings of the 3rd European Thermal Science Conference, Pisa, Italy, 2000.

52-Py X, Olives S, Mauran S. Paraffin/porous graphite matrix composite as a high and constant power thermal storage material. Int J Heat Mass Transfer 2001;44:2727–37.

53- Lane GA. Encapsulation of heat of fusion storage materials. In: Proceedings of 2nd Southeastern Conference on Application of Solar Energy, 1976. p. 442–50.

54-Lane GA. Low temperature heat storage with phase change materials. Int J Ambient Energy 1980;1:155 68.

55-Wood RJ, Gladwell SD, Callahar PWO, Probert SD. Low temperature thermal energy storage using packed beds of encapsulated phase-change materials. In: Proceedings of the International Conference on Energy Storage, Brighton, UK, 1981. p. 145–58.

56- Saitoh T, Hirose K. High-performance of phase change thermal energy storage using spherical capsules. Chem Eng Commun 1986;41:39–58.

57- Farid MM, Kanzawa A. Thermal performance of a heat storage module using PCM_s with different melting temperatures-mathematical modeling. Trans ASME, J Solar Energy Eng 1989;111:152–7.

58-De Jong AG, Hoogendoorn CJ. Improved of heat transport in paraffin for latent heat storage systems. In: Proceedings of TNO Symposium on Thermal Storage of Solar Energy, Amsterdam, Holland, 1980. p. 99–110.

59- Ageynim F, Eammes P, A comparison of heat transfer enhancement of medium temperature energy storage heat exchanger using fins. J.Solar energy, 2009.

60- Velraj R, Seeniraj RV, Hafner B, Faber C, Schwarzer K. Experimental analysis and numerical modeling of inward solidification on a finned vertical tube for a latent heat storage unit. Solar Energy 1997;60:281–90.

61- Telkes M , Thermal storage for solar heating and cooling, Proceedings of the Workshop on Solar Energy StorageSubsystems for the Heating and Cooling of Buildings, Charlottesville (Virginia, USA), 1975.

62-Li H.J, Zhang G.E, Wang J.Y, Investigation of a eutectic mixture of sodium acetate trihydrate and urea as latent heat storage, Solar Energy 47 (6) (1991) 443–445.

63- Kamimoto M., Abe M , Sawata S, Tani T, Ozawa T, Latent heat storage unit using form stable high density polyethylene for solar thermal applications, Proceedings of the International Symposium on Thermal Application of Solar Energy, Hakone (Kanagawa, Japan), 1985.

64- Cassedy E.S, Prospects for Sustainable Energy, Cambridge University Press, 2000.

65- Dermott A.M, Frysinger G.R, Storage assisted air-conditioning using a new low-cost PCM packaging concept, Proceedings of the Conference of Peak-load Pricing and Thermal Energy Storage, Chicago, Illinois, 1979.

66- Hawes DW, Feldman D, Banu D, Latent heat storage in building materials, Energy Buildings 20 (1993) 77–86.

67- Barkmann H.G, Wessling F.C, Use of buildings structural components for thermal storage, Proceedings of the Workshop on Solar Energy Storage Subsystems for the Heating and Cooling of Buildings, Charlottesville (Virginia, USA), 1975.

68- Peippo K, Kauranen P, Lund P.D, A multicomponent PCM wall optimized for passive solar heating, Energy Buildings 17 (1991) 259–270.

69- Merker O, Hepp F, Beck A, A new solar shading system with phase change material (PCM), Proceedings of the World Renewable Energy Congress WII, Cologne (Germany), 2002.

70- Sasaguchi, R. Viskanta, Phase change heat transfer during melting and resolidification of melt aroung cylindrical heat source(s)/sink(s), J. Energy Resources Technol. 111 (1989) 43–49.

71- Ismail K, Batista de Jesus A, Parametric study of solidification of PCM around a cylinder for ice-bank applications, Int. J. Refrig. 24 (2001) 809–822.

72- Vakilaltojjar S.M, Saman W, Analysis and modelling of a phase change storage system for air conditioning applications, Appl. Thermal Eng. 21 (2001) 249–263.

73- Safarik. M, Gramlich K, Schammler.G, Solar absorption cooling system with 90 _C latent heat storage, Proceedings of the World Renewable Energy Congress WII, Cologne (Germany), 2002.

74- Bedecarrats J.P, Strub F, Falcon B, Dumas J.P, Phase-change thermal energy storage using spherical capsules: performance of a test plant, Int. J. Refrig. 19 (1996) 187–196.

75- Espeau, Mondieig D, Haget Y, Cuevas-Diarte M.A, _Active_ package for thermal protection of food products, Packag. Technol. Sci. 10 (1997) 253–260.

76- Farid M.M , Husian R.M, An electrical storage heater using the phase change method of heat storage, Energy Convers. Mgmt. 30 (3) (1990) 219–230.

77- Costa.M, Buddhi.D , Oliva.A , Numerical Simulation of a latent heat thermal energy storage system with enhanced heat conduction, Energy Convers. Mgmt. 39 (3/4) (1998) 319–330.

78- Sharma SD, Buddhi D, Sawhney RL, Sharma A. Design, development and performance evaluation of a latent heat unit for evening cooking in a solar cooker. Energy Convers Manage 1997;38(5):493–8.

79-Cabeza L.F, Roca J, Nogu_es M, , Transportation and conservation of temperature sensitive materials with phase change materials: state of the art, IEA ECES IA Annex 17 2nd Workshop, Ljubljana (Slovenia), 2002.

80- Sharma SD, Iwata T, Kitano H, Sagara K. Thermal performance of a solar cooker based on an evacuated tube solar collector with a PCM storage unit. Solar Energy 2005;78:416–26.

81- Pal D, Joshi Y, Application of phase change materials for passive thermal control of plastic quad flat packages: a computational study, Numer. Heat Transfer, Part A 30 (1996) 19–34.

82- Mulligan J.C, Colvin D.P, Microencapsulated phase-change material suspensions for heat transfer in spacecraft thermal systems, J. Spacecraft and Rockets 33 (1996) 278–284.

83- Bilgen E, Bourquin J.P. Solar power plants hand book. Renewable Alternatives, Volume 1, 1978.

84- Winter CJ, Sizmann RL, Vant-Hull LL. Solar power plants: fundamentals, technology, systems, economics. Springer-Verlag, 2002,02

85- Morikama Y, Suzuki H, Okagawa F, A development of building elements using PCM, Proceedings of the International Symposium on Thermal Application of Solar Energy, Hakone (Kanagawa, Japan), 1985.

86- Lee C, Choi H.K, Crystalline Morphology in High-Density Polyethylene/Paraffin Blend for Thermal Energy Storage, Polym. Composites 19 (6) (1998) 704–708.

87- Mehling H, Krippner R, Research project on PCM in wood–light weight concrete, Proceedings of the 2nd Workshop of IEA ECES IA Annex 17, Ljubljana (Slovenia), 2002.

88- Haussmann T, Henning M, Schossig P, Phase change materials in wall integrated systems, Proceedings of the 2nd Workshop of IEA ECES IA Annex 17, Ljubljana (Slovenia), 2002.

89- Shapiro M.M, Feldman D, Hawes D, PCM thermal storage in wallboard, Proceedings of the 12thPassive Solar Conference, Portland (Oregon, USA), 1987, pp. 48–58.

90- Omer S.A, Riffat S.B, Ma X, Experimental investigation of a thermoelectric refrigeration system employing a phase change material integrated with thermal diode (thermosyphons), Appl. Thermal Eng. 21 (2001) 1265–1271.

91- Riffat S.B, Omer S.A , A novel thermoelectric refrigeration system employing heat pipes and a phase change material: an experimental investigation, Renew. Energy 23(2001) 313–323.

92- Ismail K, Henr_ıquez J.R, Thermally effective windows with moving phase change material curtains, Appl. Thermal Eng. 21 (2001) 1909–1923.

93- Ismail K, Henr_ıquez J.R, Parametric study on composite and PCM glass systems, Energy Convers. Mgmt. 43 (2002) 973–993.

94- Merker O, Hepp V, Beck A, Fricke J, A new PCM-shading system: a study of the thermal charging and discharging process, Proceedings of Eurosun 2002, Bologna 2002.

95- Merker O, Hepp V, Beck A, Fricke J, A new solar shading system with phase change material (PCM), Proceedings of the World Renewable Energy Congress WII, Cologne, 2002.

96- I.O. Salyer, A.K. Sircar, Phase change materials for heating and cooling of residential buildings and other applications, Proceedings of the 25th Intersociety Energy Conversion Engineering Conference––IECEC_90, 1990.

97- Revankar S.T, Croy.T , Void distribution in phase-change material capsule of solar latent heat energy storage system, Proceedings of the 35th National Heat Transfer Conference, Anaheim (California, USA), 2001.

98- Esen M, Durmus A, Geometric design of solar-aided latent heat store depending on various parameters and phase change materials, Solar Energy 62 (1998) 19–28

99- Saitoh T, Hirose K, Spherical capsule-type latent heat thermal energy storage/heat pump system with application to solar system, Proceedings of the International Symposium on Thermal Application of Solar Energy, Hakone (Kanagawa, Japan), 1985.

100- Paek,Jw., Kang,BH., Effective thermal conductivity and permeability of Aluminum foams,J,Thermodynamics, Vol,2.2000.

101- Cassedy E, Prospects for Sustainable Energy, Cambridge University Press, 2000.

102- Mehling H, Hippeli S, Improvement of stratified hot water heat stores using a PCMmodule, Proceedings of EuroSun 2002, Bologna (Italy), 2002.

103- Mehling H, Cabeza L.F, PCM-module to improve hot water heat stores with stratification, Renewable Energy 28 (2003) 699–711.

104- Janz, G.J., 1967. Molten Salts Handbook. Academic Press,New York.

105- Seki, N., 1995. Thermal Storage Engineering. Morikita Publ. Co., Ltd., Chiyoda-ku, Tokyo, Japan.

106- Pilkington Solar International, Survey of thermal storage for parabolic trough power plants, Report NREL1EC24 (2002).274

107- Castro C A N, Calado J C G, Wakeham W A and Dix M 1976An apparatus to measure the thermal conductivity of liquids *J. Phys. E: Sci. Instrum.* **9** 1073–80

108- Nagasaka Y and Nagashima A 1981 Simultaneous measurements of the thermal conductivity and thermal diffusivity of liquids by the transient hot-wire method *Rev. Sci. Instrum.* **52** 229–32

109- Baehr H. D., Stephan K. (2004). Wärme- und Stoffübertragung. 4 ed. Berlin, Heidelberg: Springer. ISBN 3-540-40130-X

110- Bejan, Heat transfer hand book

111- Gurova A N and Nieto de Castro C A 1995 The thermal conductivity of halo carbon *Proc. 4th Asian Thermophysical Properties Conf. (Tokyo)* ed A Nagashima pp 129–32

112- Assael M J, Karagiannidis L, Malamataris N and Wakeham W A 1992 The transient hot wire technique: a numerical approach *Int. J. Thermophys.* **19** 379–89

113- Xie H Q, Lee H, Youn W and Choi M 2003 Nanofluids containing multiwalled carbon nanotubes and their enhanced thermal conductivities *J. Appl. Phys.* **94** 4967–71

114- Gustafsson S E 1991 Transient plane source techniques for thermal conductivity and thermal diffusivity measurements of solid materials *Rev. Sci. Instrum.* **62** 797–804

115- Log, T and Metallinou M M 1992 *Rev. Sci. Instrum.* **63** 3966–71

116-Log, T 1991 Transient hot-strip method for simultaneous determination of thermal conductivity and thermal diffusivity of refractory materials *J. Am. Ceram*

117- Mathis N 2000 Transient thermal conductivity measurements: comparison of destructive and nondestructive techniques *High Temp.–High Pressures* **32** 321–7

118- Liang X G, Ge X S, Zhang Y P and Wang G J 1991 A convenient method of measuring the thermal conductivity of biological tissue *Phys. Med. Biol.* **36** 1599–605

119-Xie H Q and Cheng S X 2001 A fine needle probe for determining the thermal conductivity of penetrable materials *Meas. Sci. Technol.* **12** 58–62

120- Fujii M, Zhang X, Imaishi N, Fujiwara S and Sakamoto T 1997 Simultaneous measurements of thermal conductivity and thermal diffusivity of liquids under microgravity conditions *Int. J. Thermophys.* **18** 327–39

121- Zhang X, Wicaksono H, Fujiwara S and Fujii M 2002 Accurate measurements of thermal conductivity and thermal diffusivity of molten carbonates *High Temp.–High*

122- Freeman E.S., J. Phys.Chem. 60.1487

123- Paniccia F. et al.. (1973) The Journal of Physical Chemistry, 77(14), pp.1810-

124- Carsla H.S, Jager J.C, Conduction of heat in Solids, 2ed ed.

125- Sirotkin G.D, (1959) Russian Journal of Inorganic Chemistry, 4(11), pp.1180-1182.

126- Plambeck J.A. (1976) Encyclopedia of electrochemistry of the elements, Vol. X, Marcel Dekker, pp. 189-232.

127- Bader R.G. et al.. (1993) Thermo-chemical Acta, 229, pp. 85-96.

128- Kust R.N. et al.. (1970) Inorganic and Nuclear Chemistry Letters, 6, pp. 333-335.

129- A. Mills, M. Farid, J.R. Selman, S. Al.-Hallaj, Thermal conductivity enhancement of phase change materials using a graphite matrix, Appl. Therm. Eng. 26 (2006) 1652–1661.

130- D'Arcy Thompson, On Growth and Form, Canto, Cambridge, 1995, p. 121.

131- Maxwell J.C , A Treatise on Electricity and Magnetism, Clarendon Press, Oxford, 1873, p. 365.

132-Calmidi V.V, Mahajan R.L, The effective thermal conductility of high porosity metal foams, J. Heat Transfer 121 (1999) 466±471.

133-Boomsma K, Poulikakos D, On the effective thermal conductivity of a three dimensionally structured fluid saturated metal foams, Int. J. Heat Mass Transfer 44 (2001) 827–836.

134-Singh R, Kasana H.S, Computational aspects of effective thermal conductivity of highly porous metal foams, Applied Thermal Engineering 24 (2004) 1841–1849

135-Dul'nev G.N, J. Eng. Phys. 9:275 (1965).

136-Bhattacharya A, Calmidi V.V, Mahajan R.L, Thermophysical properties of high porosity metal foams, Int. J.Heat Mass Transfer 45 (2002) 1017–1031

137-Truong Huu T, Lacroix M, Pham Huu C, Schweich D, Edouard D. Towards a more realistic modeling of solid foam: use of the pentagonal dodecahedron geometry. Chem Eng Sci. 2009;64:5131–5142.

138- Edouard D, The effective thermal conductivity for Slim" and "Fat" foams.,J,AICHE, 2011.

139- Bauer.T, Tamme.R; PCM-Graphite Composites for High Temperature Thermal Energy Storage,SGL Tech, Ger.

140- Smaic.M, Thermal performance of natural graphite heat spreads., Interpack,2005.

Appendix:

1- Tetrakaidecahedron Pores with Cubic Nodes

This figure presents the side of selected cubic cell in tetrakaidecahedron pores. The cubic cell is divided into four layers.

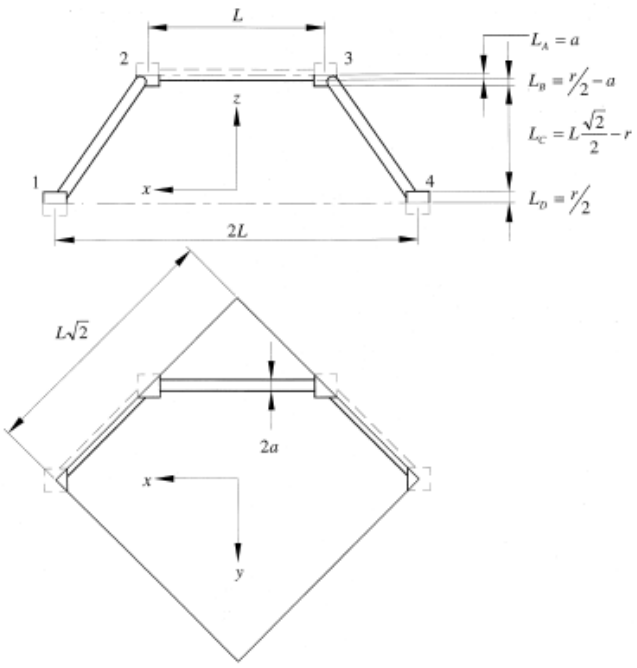

Volume of each layer can be calculated by multiplying the area in x-y plane by heigh of each layer in z direction as follow;

$$V_A = 2aL^2$$

$$V_B = (r - 2a)L^2$$

$$V_C = 2(\frac{1}{2}L\sqrt{2} - r)L^2$$

$$V_D = rL^2$$

Metal volume fraction of each layer, then calculated;

$$d = \frac{a}{L}$$

$$e = \frac{r}{L}$$

$$V_{A,m} = (e^2 + \frac{1}{2} d\pi(1-e) dL^3$$

$$V_{B,m} = (\frac{1}{2} e - d) e^2 L^3$$

$$V_{C,m} = (1 - 2e\sqrt{2})\pi d^2 L^3$$

$$V_{D,m} = \frac{1}{4} e^3 L^3$$

With knowing the volume of foam and void in each layer, the porosity was calculated to be:

$$\varepsilon = 1 - \frac{\sqrt{2}}{2}(de^2 + \frac{1}{2} d^2 \pi(1-e) + (\frac{1}{2} e - d) e^2 + \pi d^2 (1 - 2e\sqrt{2}) + \frac{1}{4} e^3)$$

$$d = \sqrt{\frac{\sqrt{2}(2 - (5/8)e^3\sqrt{2} - 2\varepsilon)}{\pi(3 - 4e\sqrt{2} - e)}}$$

Thermal conductivity of each layer was calculated by averaging the thermal conductivity of each section based on volume fraction, as follow

$$K_n = \frac{V_{n,m} K_m + (V_n - V_{n,m}) K_S}{V_n}$$

$$n = A, B, C.D$$

$$R_A = \frac{4d}{2e^2 + \pi d(1-e)K_m + (4 - 2e^2 - \pi d(1-e)K_s}$$

$$R_B = \frac{(e-2d)^2}{(e-2d)e^2 K_m + (2e - 4d - (e-2d)e^2)k_s}$$

$$R_C = \frac{(\sqrt{2} - 2e^2)}{2\pi d^2(1-2e\sqrt{2})K_m + 2(\sqrt{2} - 2e - \pi d^2(1-2e\sqrt{2}))K_s}$$

$$R_D = \frac{2e}{e^2 Km + (4-e^2)K_s}$$

$$d = \sqrt{\frac{\sqrt{2}(2 - (5/8)e^3\sqrt{2} - 2\varepsilon)}{\pi(3 - 4e\sqrt{2} - e)}}$$

Therefore the effective thermal conductivity of cubic cell is calculated based on heat conduction through a series of four layers using following equation:

$$K_{eff} = (\frac{\sqrt{2}}{2(R_A + R_B + R_C + R_D)})$$

2- Hexagonal cells with circular nodes

This figure presents the selected unit cell in hexagonal pores which is divided to five layers of foam and void which are in series.

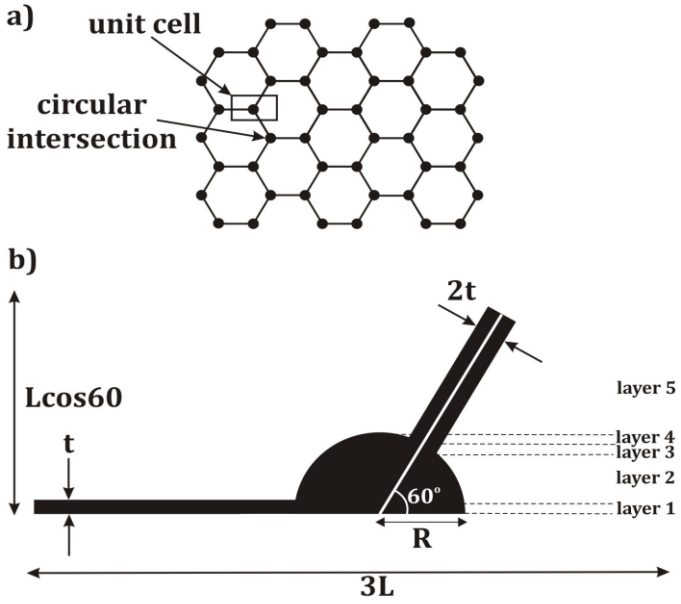

Thermal conductivity of each layer was calculated based on the area fraction of foam and void in each layer, which presented with following equations:

$$K_1 = K_s + \frac{(K_m - K_S)}{3Lt}(Lt + \frac{R^2}{2}(Sin^{-1}\frac{t}{R} + \frac{t}{R}\sqrt{1-\frac{t^2}{R^2}}))$$

$$K_2 = K_f + \frac{(K_m - K_s)R^2}{\frac{3L}{2}(\sqrt{3(R^2-t^2)}-3t}[\sin^{-1}(\frac{1}{2R}(\sqrt{3(R^2-t^2)}-t)) - \sin^{-1}(\frac{t}{R}) +$$

$$\frac{1}{2}\sin 2(\sin^{-1}(\frac{1}{2R}(\sqrt{3(R^2-t^2)}-t))) - \frac{1}{2}\sin 2(\sin^{-1}(\frac{t}{R}))]$$

$$K_4 = K_s + \frac{(K_m - K_s)}{3L(R - y_2)}(R^2(\frac{\pi}{2} - \sin^{-1}\frac{y_2}{R}) - \frac{R^2}{2}\sin 2(\sin^{-1}\frac{y_2}{R}) + \frac{4t}{\sqrt{3}}(R - y_2))$$

$$K_5 = K_s + (K_m - K_s)\frac{4t}{3\sqrt{3}L}$$

$$y_1 = \frac{1}{2}(\sqrt{3(R^2 - t^2)} - t)$$

$$y_2 = \frac{1}{2}(\sqrt{3(R^2 - t^2)} + t)$$

Therefore the thermal conductivity trough the selected unit cell calculated based on heat conduction trough five layers in series using Fourier's law.

$$K_e = \frac{L_1 + L_2 + L_3 + L_4 + L_5}{\frac{L_1}{K_1} + \frac{L_2}{K_2} + \frac{L_3}{K_3} + \frac{L_4}{K_4} + \frac{L_5}{K_5}}$$

3- Pentagonal dodecahedron

This figure presents pentagonal dodecahedron pores, which are categorized as slim, and fat foams.

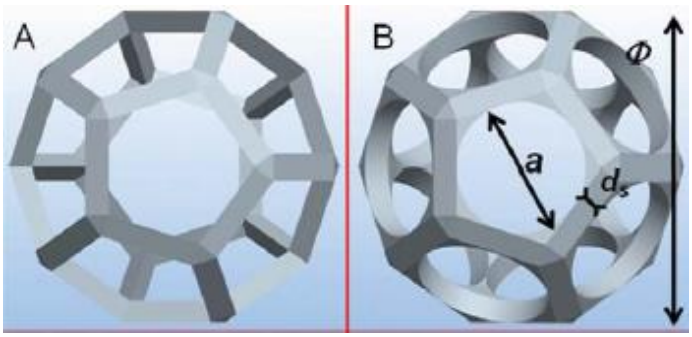

First, the porosity was calculated based on the volume fravtion of void and foam as fallow:

$$(1-\varepsilon)=\frac{V_{S\lim,Solid}}{V_{dodecahedron}}=\frac{V_{Skeleton,S\lim}}{V_{dodecahedron}}=Es^{2}\frac{\sqrt{15}}{\varphi^{4}}-Es^{3}\frac{\sqrt{10}}{3\varphi^{4}}$$

$$(1-\varepsilon)=\frac{V_{Fat,Solid}}{V_{dodecahedron}}=\frac{V_{Skeleton,Fat}}{V_{dodecahedron}}+\frac{V_{deadvol}}{V_{dodecahedron}}$$

$$\frac{V_{Skeleton}}{V_{dodecahedron}}=Ef^{2}\frac{\sqrt{15}}{\varphi^{4}}-Ef^{3}\frac{\sqrt{10}}{3\varphi^{4}}$$

$$\frac{V_{deadvol}}{V_{dodecahedron}}=\frac{40\dfrac{\sin^{2}(\frac{\pi}{5})\varphi^{2}(1-\frac{Ef}{2}\sqrt{\frac{2}{3}})^{3}}{32\sqrt{3}(3-\varphi)}\sqrt{(\frac{1}{4}-\frac{\sin^{2}(\frac{\pi}{5})\varphi^{2}}{9-3\varphi})}}{\sqrt{5}\varphi^{4}}+$$

$$\left(\frac{12Ef}{\sqrt{5}\varphi^{4}}\right)\left(\frac{5\varphi}{4\sqrt{3-\varphi}}-\frac{\pi}{4}\frac{\varphi^{2}}{(3-\varphi)}\right)\left(1-\frac{Ef}{2}\sqrt{\frac{2}{3}}\right)^{2}$$

Thermal conductivity of each layer was calculated based on volume fraction and thermal conductivity of each material.

$$K_n = \frac{V_{n,Solid} K_s + (V_{n,Cell} - V_{n,Solid}) K_f}{V_{n,Cell}}$$

Then the thermal averaging based on volume fraction was used to calculate the effective thermal conductivity of the pore, with using following equation:

$$\frac{\sum_{1}^{n} L_n}{K_{eff}} = \sum_{1}^{n} \left(\frac{L_n}{K_n}\right)$$

4- Cubic pore with cubic nodes

This figure presents the cubic pore witch is divided to three layers in series. The thickness of each layer was presented as :

$$L_1 = b$$
$$L_2 = x - b$$
$$L_3 = (L - 2x)$$

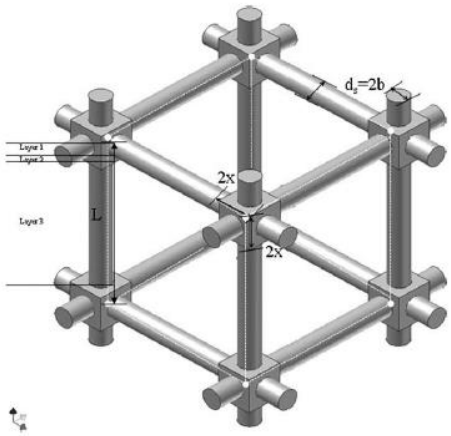

This model assumes each ligament is shared by four cubic lattice, and each cubic intersection lump is shared by eight cubic latice, therefore only a quarter of each ligament volume, and an eighth of each intersection lump have to be consired for volume calculation. Knowing this, the volume of each layer was calculated as:

$$V_{1,cell} = L^2 b$$
$$V_{2,Cell} = L^2 (x - b)$$
$$V_{3,Cell} = L^2 (L - 2x)$$

Layers volume fraction of solid;

$$V_{1,Solid} = \pi b^2 (L - 2x) + 4bx^2$$
$$V_{2,Solid} = 4(x - b)x^2$$
$$V_{3,Solid} = \pi b^2 (L - 2x)$$

Then the porosity is calculated based on volume fraction as follow:

$$(1-\varepsilon)=\frac{2V_{1,Solid}+2V_{2,Solid}+V_{3,solid}}{2V_{1,Cell}+2V_{2,Cell}+V_{3,Cell}}=\frac{3\pi b^2(L-2x)+8x^3}{L^3}$$

$$x=yb$$

$$y=1+\delta$$

$$d=\frac{b}{L}$$

$$(1-\varepsilon)=3\pi d^2(1-2d)+8d^3+\delta d^3(8\delta^2+24\delta+24-6\pi)$$

$$\frac{V_{s\lim,Solid}}{V_{dodecahedron}}=3\pi d^2(1-2d)+8d^3$$

$$\frac{V_{fat,solid}}{V_{dodecahedron}}\Rightarrow\frac{V_{skeleton,fat}}{V_{dodecahedron}}=3\pi d^2(1-2d)=8d^3$$

$$\frac{V_{fat,solid}}{V_{dodecahedron}}\Rightarrow\frac{V_{deadvol}}{V_{dodecahedron}}=\delta d^3(8\delta^2+24\delta+24-6\pi)$$

With knowing the value of porosity, the thermal conductivity of each layer is calculated as:

$$K_1=\frac{(\pi b^2(L-2x)+4bx^2)K_s+(L^2b-(\pi b^2(L-2x)+4bx^2))K_f}{L^2b}$$

$$K_2=(4y^2d^2)K_s+(1-4y^2d^2)K_f$$

$$K_3=(\pi d^2)K_s+(1-\pi d^2)K_f$$

Therefore the thermal conductivity trough the selected unit cell calculated based on heat conduction trough three layers in series:

$$\frac{1}{K_{eff}} = \frac{2d}{(d^2(4y^2 - 2\pi y) + \pi d)K_s + (d^2(2\pi y - 4y^2) - \pi d + 1)K_f} +$$

$$\frac{2d(y-1)}{(4y^2d^2)K_s + (1-4y^2d^2)K_f} + \frac{(1-2dy)}{(\pi d^2)K_s + (1-\pi d^2)K_f}$$